UNIVERSITY OF CALIFORNIA SAN DIEGO

The role of alpha oscillations in visual information processing

A dissertation submitted in partial satisfaction
of the requirements for the Doctor of Philosophy

in

Neurosciences with a Specialization in Computational Neurosciences

by

Stephanie Nelli

Committee in charge:

Professor, John Serences, Chair
Professor Eric Halgren
Professor Eran Mukamel
Professor Lara Rangel
Professor Bradley Voytek

2019

The Thesis of Stephanie Nelli is approved, and it is acceptable in quality and form for publication on microfilm and electronically:

_____

_____

_____

_____

_____

Chair

University of California San Diego

2019

TABLE OF CONTENTS

LIST OF FIGURES

LIST OF TABLES

ACKNOWLEDGEMENTS

First, thank you to my family and friends for the unconditional support and love. Additionally, thank you to Sue Goodman, Jason Cook, Jan Smith, Leslie Morrow, Paul Voss, Michael Neelon and Carolina Perez Heydrich – my teachers and mentors during my undergraduate mathematics degree and scientific research experiences - for starting me on this path.

My scientific path would be radically different without the input from all members of the Perception and Cognition lab at UC San Diego over the last five to six years. I have learned an incredible amount about experimental psychology, computing and academia from various lab members over the years. Importantly, I'd like to thank my advisor John Serences for his interesting discussion, nearly flawless mentorship, and for collecting an amazing group of scientists to form a nurturing, fun, diverse and enriching lab environment. I thank former lab member Sirawaj Itthipuripat for his endless well of ideas, I have learned deeply from his experimental prowess during our scientific collaborations and have benefitted immensely from his unwavering friendship. Former lab members Tommy Sprague, Mary Smith, Javier Garcia, and Kim Kaye were invaluable in the early years of my PhD, helping to introduce me into the lab and smooth my move to the west coast by being great scientists and friends. Thanks to all current members - including Vy Vo, Margaret Henderson, Chaipat Chunharas and Rosanne Rademaker - for the scientific collaboration, insightful suggestions and steadfast comradery you have provided me over the years. A special nod goes to Nuttida Rungratsameetaweemana and Edward Ester for sharing a work space with me in the lab – you are brave! Finally, this thesis would have been impossible without the undergraduate researchers that helped run experiments included this thesis: Sarah Fraley, Rachel Chen, Aayushi Malpani and Max Boonjindasup. I thank and congratulate you all.

Outside of the lab, I extend special thanks to fellow neuroscience graduate student and good friend Chris Gonzalez for teaching me a lot about dynamical systems and neural

oscillations, this thesis wouldn't be the same without our late-night conversations on everything from the philosophy of consciousness to abstract topology. Finally, I thank my committee Eric Halgren, Eran Mukamel, Brad Voytek and Lara Rangel and Professors Stefan Leutgeb, Ramesh Srinivasan and Timothy Gentner deeply for scientific feedback, invaluable mentorship and especially for letters of recommendation.

I would also like to acknowledge generous funding from the Department of Defense through the National Defense Science and Engineering Graduate (NDSEG) Fellowship program. Additional support was provided by NEI R21-EY024733, NEI R01-EY025872, and James S. McDonnell Foundation awards to J.T.S

Chapter 1, in full, is in preparation for publication of the material at it currently appears in: Nelli S, Chen R, Serences J. (2019) Behavioral rhythmicity in alpha and theta bands differentially characterize precision of spatial attention. *In Prep*. The dissertation author was the primary investigator and author of this paper.

Chapter 2, in full, is a reprint of the material as it appears in: Nelli, S., Itthipuripat, S., Srinivasan, R., & Serences, J. T. (2017). Fluctuations in instantaneous frequency predict alpha amplitude during visual perception. *Nature communications*, *8* (1), 2071. The dissertation author was the primary investigator and author of this paper.

Chapter 3, in full, is in preparation for publication of the material at it currently appears in: Nelli S, Serences J. (2019). The efficiency of visual processing depends on deviations of alpha rhythms from their endogenous peak frequency. *In Prep*. The dissertation author was the primary investigator and author of this paper.

VITA

Education

University of California - San Diego. 2013 - 2019
Doctor of Philosophy in Neurosciences with a Specialization in Computational Neurosciences 2019

University of North Carolina - Chapel Hill. 2011-2013
Bachelor of Arts in Mathematics with Highest Distinction 2013

Research Experience & Projects

Perception and Cognition Lab. Advisor: Dr. John Serences 2014 - 2019
The role of neural synchrony in selective visual information processing
Experimental skills: EEG, SSVEP, Psychophysics, Eye-tracking
Analysis skills: Time-frequency analyses, Machine Learning, Behavioral Modeling
Proficiencies: MatLab, Adobe Illustrator, EEGlab

Computational and Cognitive Neuroscience Summer Course, NYU Shanghai 2016
Convolutional Neural Networks and the Visual Hierarchy - Advisor: Dr. Dan Yamins
Skills: TensorFlow, Python

Multimodal Imaging Lab. Advisor: Dr. Eric Halgren. 2014
Skills: Signal Processing, Sleep and epileptiform activity identification

Molecular Neuropharmacology Lab. Advisors: Drs. L Morrow & J Cook 2012 - 2013

Carolina Population Center. Advisors: Drs. C Perez-Heydrich & P Voss 2012
Skills: Topological data analysis, longitudinal data analysis, SAS, R

Awards

National Defense Science and Engineering Grant, Tuition + Stipend 2015 - 2018
Awarded by DoD and ASEE for doctorate work
Scholarship, LWTech Summit, San Francisco, CA 2017
Travel Award, Cold Spring Harbor Computational Neuroscience course 2016
Paid Attendance, Communicating Science Conference, San Diego CA 2016
San Diego Fellowship, Tuition + Stipend 2013 - 2014
Awarded by UCSD's Institute for Temporal Dynamics for graduate studies

Publications

SM Nelli, RW Chen, JT Serences. *Behavioral rhythmicity in alpha and theta bands differentially characterize precision of spatial attention* In prep

SM Nelli, JT Serences. *The efficiency of visual processing depends on deviations of alpha rhythms from their endogenous peak frequency* In prep

SM Nelli*, S Itthipuripat*, N Rungratsmeetaweemana, JT Serences. *Flexible access to evidence accumulation during speed-accuracy tradeoff. Biorxiv. *=co-first authors* 2018

SM Nelli, S Itthipuripat, R Srivansian, JT Serences. *The interacting influence of alpha amplitude and instantaneous frequency on visual perception*, Nature Communications 2017

JB Cook, **SM Nelli**, MR Neighbors, DH Morrow, TK, O'Buckley, AM Maldonado-Devincci, AM, AL Morrow. *Ethanol alters local cellular levels of 3α, 5α-THP independent of the adrenals in subcortical brain regions,* Neuropsychopharmacology 2014

Talks & Presentations

Invited Talk: Human Info Processing Lab - PI: Dr. Christopher Summerfield 2018

Invited Talk: Neuro of Attention & Perception Lab - PI: Dr. Sabine Kastner 2018

SM Nelli, A Malpani, M Boonjindasup, J Serences. The joint impact of alpha amplitude and frequency on visual detection, Society for Neuroscience 2017

SM Nelli, S Itthipuripat, R Srivansian, JT Serences. The interacting influence of alpha amplitude and frequency on visual perception, European Conference on Visual Perception 2017

SM Nelli, MS Boonjindasup, A Malpani, JT Serences, *Alpha entrainment of posterior visual cortex impacts visual detection.* Vision Sciences Society 2017

S Itthipuripat, **SM Nelli**, JT Serences, *Flexible access to evidence accumulation during speed-accuracy tradeoff*. Society for Neuroscience 2016

SM Nelli, R Chen and JT Serences**.** *Alpha band fluctuations in iconic memory recall.* Vision Sciences Society 2016

SM Nelli & JT Serences**.** *Modulation of visual perception by low frequency oscillations.* Society for Neuroscience 2015

SM Nelli, S Fraley and JT Serences**.** *Post-stimulus alpha oscillations influence visual discrimination performance.* Vision Sciences Society 2015

SM Nelli. *The topology of depression in adolescent social networks: A case study.* Southern Demographic Association Conference. 2012

Teaching and Leadership Experience

Diversity Admissions Committee, UCSD Neuroscience Doctorate Program 2013 - current
Read, rate and discuss applications, attended ABRACAMs 2014, SACNAS 2017

Teaching Certification, Associate level Spring 2016
Center for Integration of Research Teaching and Learning

Invited Lecture "Is Perception Continuous?", History of Art and Technology (VIS 159) Winter 2016

Research Mentorship, Perception and Cognition Lab
Max Boonjindasup - Biology Undergraduate 2016 - 2018
Sunandha Srikanth - Biology PhD Student Winter 2016
Aayushi Malpani - Psychology Undergraduate 2015 - 2018

Rachel Chen - Honors Student Research Thesis 2015 - 2016
Sarah Fraley - Psych 199 Research Thesis 2014 - 2015

TA, Psychology of Sleep **-** Tim Rickard (Psych 191) Spring 2015 & 2016
"Excellent" rating from instructor and "Excellent" average rating from students
Wrote exams, held weekly office hours, lectured

Graduate Training Program Assistant, Carolina Population Center 2012 - 2013
Authored sections of NIH grant proposal

GRE mathematics teacher, UNC MURAP research diversity program, 2012
Lead weekly GRE Mathematics courses and individual tutoring students

ABSTRACT OF THE DISSERTATION

The role of alpha oscillations in visual information processing

by

Stephanie Nelli

Doctor of Philosophy in Neurosciences with a Specialization in Computational Neurosciences

University of California San Diego, 2019

Professor John Serences, Chair

Neural oscillations are one the most prominent features of electrical brain recordings, involving the synchronized activity of large populations of neurons, and have been linked to a variety of important functions over the past century. Existing theories propose these oscillations allow the brain to dynamically switch between functional neural circuits, allowing computational flexibility on time scales too fast for the slow structural changes that characterize long-term cortical plasticity. In particular, alpha oscillations (~8-13 Hz) are often visible in raw scalp electroencephalography (EEG) recordings over visual and parietal cortex and seem to regulate the waxing and waning of visual attention and perception across time. However, many previous

results focus specifically on the phase, power or frequency of the alpha oscillation, neglecting the common dynamical systems that simultaneously generate all these metrics and impact visual information processing. In this dissertation, I begin by reviewing relevant literature about alpha oscillations, and then aim to link together disparate measures of the alpha oscillations in both behavior and the brain to address how dynamical alpha state regulates visual information processing. First, in C1 I find that both phase locked and purely power based analyses of imprecise attentional selection display alpha rhythms, suggesting a common impact on behavior. Indeed, in C2 I show that alpha frequency, which governs phase and amplitude are linked mathematically in simple models of harmonic oscillators, which I confirm in neural recordings. Thus, the impact of alpha oscillations on perception depend on circuit interactions with top-down driving oscillators, and in C3 I find that optimal oscillatory drive for visual perception depends intimately on each subject's particular dynamical system and resultant peak alpha frequency. Together, this thesis challenges core assumptions underlying current theories of the role that alpha oscillations play in regulating visual information processing using both mathematical models and empirical data. I then propose a more unified theoretical framework in which alpha frequency, phase and amplitude should not be viewed as independent metrics to be correlated with behavior, but instead as the result of a common dynamical system that impacts visual perception.

INTRODUCTION

A seemingly simple string of behaviors such visually searching for an apple, allocating visual attention to that apple and finally reaching for the apple is really quite a feat that a narrow focus on the brain's anatomical structures and pathways cannot entirely account for. The fact that humans easily accomplish these behaviors confirms the *existence* of these anatomical pathways through which early sensory representations are available for use by multiple downstream cognitive and motor processes, but the mere existence of these pathways cannot account for how the *right* representation is coordinated with the *right* downstream process. From allocating attention on a moment's notice to flexibly switching between cognitive tasks, humans are constantly faced with situations in which different neural circuits must be dynamically coordinated. Neural oscillations are theorized to support this rapid, selective communication necessary to effectively coordinate networks at time scales too fast for structural changes in neural connectivity to be involved (Akam & Kullmann, 2014; Pascal Fries, 2005; Voytek et al., 2015; Womelsdorf et al., 2007). Indeed, neural ensembles appear to shift easily between interference-prone complexity and robust oscillatory synchrony, a potentially efficient way for the brain to detect environmental changes all while preserving structural internal organization (Buzsáki, 2006). These neural oscillations are a prominent feature of macroscale electrophysiological recordings, and have been implicated across various temporal and spatial scales in virtually every behavior (Draguhn, Buzsáki, Andreas, & Draguhn, 2004).

Generally, neural oscillations in human scalp and intracranial electroencephalography (EEG) are divided into several canonical frequency bands: delta (<1-4 Hz), theta (4-8 Hz), alpha (8-12 Hz), beta (15-30 Hz), gamma (30-70 Hz), and high gamma (>70 Hz; note the precise boundaries between these bands can vary between sources). While invasive studies in rodent and macaques have shown promise for the importance of various brain rhythms (Blatow et al., 2003; Fiebelkorn, Pinsk, & Kastner, 2018; P Fries, Reynolds, Rorie, & Desimone, 2001; Mann & Mody, 2010), precisely characterizing the mechanistic roles of neural oscillations in the human

brain has proven elusive due to limitations in the available recording and stimulation techniques and conventional analysis approaches.

The alpha oscillation is a particularly prominent neural oscillation maximal over visual regions in human scalp EEG that was first described nearly a century ago by Hans Berger (Haas, 2003). This discovery of rhythmic neural activity in the alpha band has since inspired well over 18,000 papers speculating about its function in cortical information processing (a conservative estimate obtained via Google Scholar). Part of the fascination with alpha oscillations stems from their pervasiveness – they are nearly always present and are often large enough in magnitude to be easily seen in raw EEG traces, in contrast to more transient responses in other oscillatory bands that are often only visible after filtering. Indeed, much has been observed about alpha physiology since their discovery. The generation of alpha rhythms is distributed throughout cortex and thalamus, and alpha oscillations have been observed both in intrinsically oscillating single neurons and in field potentials that result from network interactions in neural populations (F. Lopes da Silva, 1991; F. H. Lopes da Silva, Vos, Mooibroek, & van Rotterdam, 1980; Silva & Leeuwen, 1977), and it has since then been observed that the same macroscopic field potential can be brought about by various intrinsic cellular and network mechanisms (Buzsáki, 2006)s. Furthermore, the spectral parameters of alpha oscillations were noted to have the highest test-retest reliability of all EEG bands in 1985 - subjects showed similar alpha power and peak frequency in two recordings separated by nearly a year (Gasser, Bächer, & Steinberg, 1985), and since that observation, peak alpha frequency has been confirmed as a stable neurophysiological trait (Grandy et al., n.d.). However, although the physiology underling alpha oscillations was studied after the oscillations were discovered (from roughly the 1950s-1980), these rhythms were thought to reflect an “idling” of the brain and to have no causal involvement in brain functions (Adey, 1988).

Since the 1980s, oscillations in general have begun to receive traction as being causally involved in brain function, with alpha oscillations being linked to the waxing and waning of visual

perception over time (Başar, 2012). Specifically, many reports have linked changes in various aspects of ongoing alpha oscillations, i.e. amplitude, phase, and frequency, with concurrent modulations in visually dependent behaviors (Klimesch, Sauseng, & Hanslmayr, 2007; Mathewson et al., 2011; Mierau, Klimesch, & Lefebvre, 2017; Palva & Palva, 2007). However, previous results measuring the impact of alpha amplitude, phase and frequency have led to distinct theories about the role of alpha oscillations in visual information processing.

I begin by reviewing the central hypotheses of this thesis, along with relevant literature. Then, in **Chapter 1:** *Alpha and theta band behavioral rhythms characterize low and high-fidelity visual information processing***,** I address whether there is rhythmicity in visual behaviors. I ask whether behaviors along the continuum from visual perception and attentional selection to the short-term retention of information wax and wane in the alpha range, and if the precision of behavioral performance modulates the frequency of this rhythmicity. In **Chapter 2:** *Fluctuations in instantaneous frequency predict alpha amplitude during visual perception*, I address the perceptual impact of the resonant alpha system. Specifically, I address whether fluctuations in alpha frequency and amplitude interact to impact early visual information processing. In **Chapter 3:** *The efficiency of visual processing depends on deviations of alpha rhythms from their endogenous peak frequency,* I drive alpha oscillations to determine how circuit interactions with endogenous oscillations determine behavior. Specifically, I determine how alpha oscillations in early visual populations interact with the endogenous alpha oscillation to impact behavior by clamping, through SSVEP entrainment, the frequency of early visual alpha oscillations. Finally, I make concluding remarks on the nature of the dynamical system that generates alpha oscillations, and their role in visual information processing.

Central Hypothesis:

While decades of work have focused on measuring how the amplitude, phase and frequency of the alpha oscillations change with visual stimulation and task demands, the mechanisms underlying the metrics described above and how they relate are still unknown.

First, a large literature has focused on how changes in amplitude impact perception, leading to the conception of alpha oscillations as an inhibitory process (the “tonic inhibition” account). This account proposes that the relatively large default alpha amplitude in visual cortex reflects suppression of visual information processing due to population-level synchronization. In contrast, when processing visual input, the E/I balance in certain circuits shifts, leading to a desynchronization from the default rhythm and a subsequent reduction in alpha amplitude (Pascal Fries, Womelsdorf, Oostenveld, & Desimone, 2008; Klimesch, 1996; Klimesch et al., 2007; Pfurtscheller, 2001; Salinas & Sejnowski, 2001; Shao & Burkhalter, 1996; von Stein, Chiang, & König, 2000). Consistent with this framework, high alpha amplitude is associated with reduced perceptual sensitivity, presumably owing to a failure of circuits that process relevant information to desynchronize from the default rhythm (Foxe, Simpson, & Ahlfors, 1998). Furthermore, alpha amplitude modulations have also been shown to be topographically selective: spatial attention decreases alpha amplitude in areas of visual cortex encoding attended regions of the visual field and increases alpha amplitude in areas encoding task-irrelevant regions (Händel, Haarmeier, & Jensen, 2011; Kelly, Gomez-Ramirez, & Foxe, 2009; Meeuwissen, Takashima, Fernández, & Jensen, 2011; Rihs, Michel, & Thut, 2007; Sauseng et al., 2005). Finally, the relatively slow time-scale of these amplitude modulations (> 100 ms) suggests correspondingly slow alterations between periods of efficient and inefficient visual information processing (Figure 0.2B; for review see (Klimesch et al., 2007)). Thus, according to this framework, visual perception is more efficient when local circuits are operating independently of the widespread “inhibitory” alpha.

In addition to the tonic inhibition hypothesis, which focuses on relatively slow changes in alpha amplitude, rapid, cycle-by-cycle fluctuations in alpha oscillations are also thought to reflect alterations in the E/I balance and hence the efficiency of visual information processing (Atallah & Scanziani, 2009; Busch, Dubois, & VanRullen, 2009; Dugue, Marque, & VanRullen, 2011; Hasenstaub et al., 2005; Lakatos et al., 2009; Mathewson, Gratton, Fabiani, Beck, & Ro, 2009; Samaha & Postle, 2015; Womelsdorf et al., 2007). This account, referred to here as the phasic inhibition account, posits that epochs of neural excitability and efficient visual information processing are associated with a particular phase of ongoing alpha oscillations (Lorincz, Kékesi, Juhász, Crunelli, & Hughes, 2009). These shorter and more rapidly occurring alternations in the E/I balance are thought to enhance perception both by sharpening feature tuning to stimuli and by temporally concentrating neural activity, thereby increasing the probability that activity is propagated to downstream areas (Draguhn et al., 2004; Isaacson & Scanziani, 2011; E.M. Izhikevich, 2003; Kayser, Montemurro, Logothetis, & Panzeri, 2009; Wehr & Zador, 2003). Building off these previous results concerning alpha phase, it is useful to note that frequency is simply the first derivative of phase: specifically, at time t, $\omega(t) = \frac{1}{2\pi}\frac{d\varphi}{dt}(t)$, where ω= frequency and φ= phase (pipeline for calculating frequency shown in Figure 0.1). This means that modulations in frequency reflect the temporal density of periods of maximal perceptual sensitivity and the rate at which visual information is sampled and processed, supported by results associating faster alpha oscillations with enhanced perceptual performance (Nelli, Itthipuripat, Srinivasan, & Serences, 2017; Osaka, 1984; Samaha & Postle, 2015). For example, an increase from 10Hz to 10.5Hz should enhance visual perception by increasing the amount of visual information sampled in a fixed length of time. Thus, similar to the tonic inhibition account, the phasic inhibition account also holds that alpha oscillations index changes in the E/I balance and the efficiency of information processing. However, the transitions between information processing states indexed by alpha phase/frequency occur on a finer temporal scale than the

alpha amplitude modulations, and are linked theoretically to changes in the sampling rate of the visual system (Figure 0.2 B).

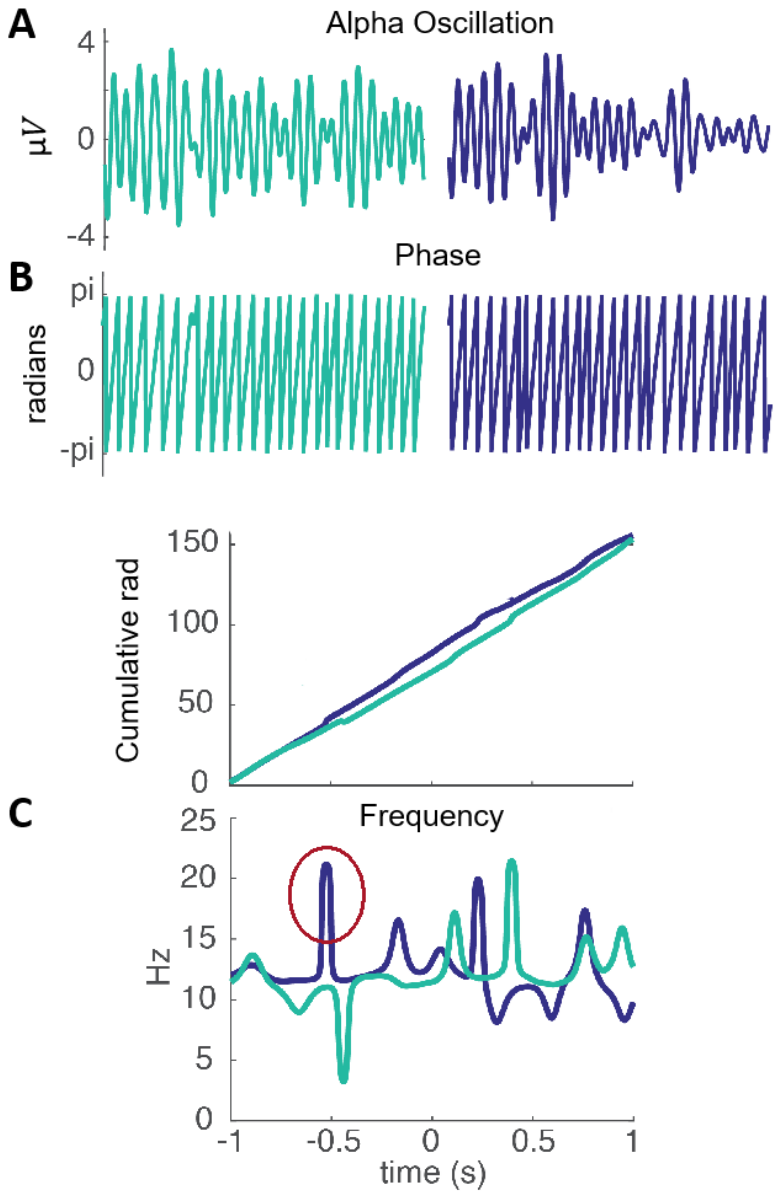

Figure 0.1: Calculation of frequency from the alpha oscillation. **A:** Two different epochs of time of data bandpassed from ±2.5 Hz around each subject's peak alpha frequency using a third order Butterworth filter are shown. From this, one can calculate the analytic signal using a Hilbert transform. Two seconds worth of data are shown for each timecourse, EEG data recorded for experiment in Chapter 2. **B:** Phase angle from –π to π is calculated from the analytic signal, from which cumulative phase is calculated by ignoring each reset from π to –π. Note the timepoints in which there are local discontinuities in phase that propagate to unwrapped phase (sudden bumps in the generally smooth line). All timecourses show two seconds worth of data. **C:** Frequency is calculated from unwrapped phase. Red circle indicates a timepoint with a sudden phase jump, leading to a discontinuity in the frequency calculation. Phenomena like these jumps often motivate post-processing frequency using median filters.

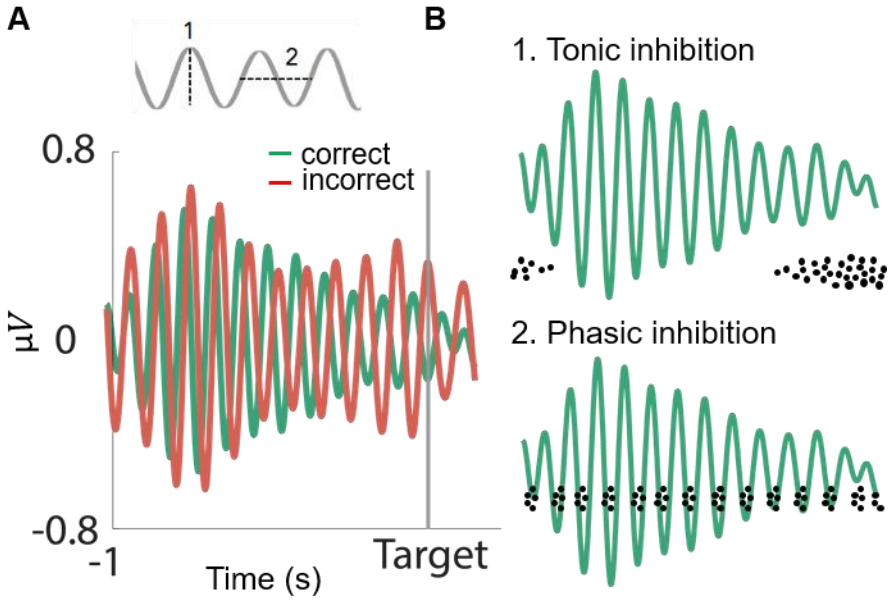

Figure 0.2: Tonic vs Phasic Inhibition. **A:** Top Inset- Amplitude (1.) and phase/frequency (2.) are plotted in reference to an oscillation to display each metric. 1 indicates alpha amplitude, which has been implicated in theories on tonic inhibition, while 2 indicates alpha phase or frequency, which is implicated in theories on phasic inhibition. For illustration purposes, over one second of data from one subject is shown, averaged over red (undetected) and green (detected) trials. Note that these traces show how it is possible that two oscillations can go from in-phase to anti-phase through frequency shifts (target presentation occurred at gray vertical line at 1 second). **B:** The average oscillation over correct trials is replotted with cartoon neural action potentials (black dots) plotted to show how tonic (top) and phasic (bottom) inhibition are theorized to work.

Thus, despite the abundance of data, a common unified theoretical framework has not been articulated. Instead, the key tenant of the above theories is that the amplitude and phase/frequency of ongoing alpha oscillations reflect the operation of *independent* mechanisms that uniquely contribute to the overall efficiency of cortical information processing. The assumption that these metrics are independent is intuitively appealing. For example, the most common way of describing a simple oscillation explicitly writes the amplitude and frequency as separable factors (e.g. the voltage (*V*) of a sinusoidal wave at time *t* is often expressed with the familiar equation V(t) = amplitude * sin(frequency * t)). . However, reduced neuronal spiking has been associated with both alpha power and alpha phase in sensorimotor cortices of macaques performing somatosensory discrimination tasks,

suggesting alpha phase/frequency and power are describing a similar underlying generative dynamical system (Haegens, Nácher, Luna, Romo, & Jensen, 2011).

Importantly, physiological experiments that measure inter-regional connectivity have shown that alpha operates as a “feedback” or “top town” signal(Bastos et al., 2015). Specifically, while attention decreases the amplitude of alpha oscillations in visual areas, connectivity between visual regions like the thalamus & V1(Saalmann, Pinsk, Wang, Li, & Kastner, 2012) and circuits representing overlapping receptive fields in V1 and V4(Bosman et al., 2012) actually increases with attention. Additionally, while visual alpha amplitude is negatively correlated with behavioral performance in the macaque, the opposite is true in higher order region IT (Bollimunta, Chen, Schroeder, & Ding, 2008), and alpha enhancement has also been observed in LGN and hippocampus(Başar, 2012). Together, these observations suggest alpha is not simply an inhibitory signal that completely shuts down all information processing, but instead may control the routing of visual information (Pascal Fries, 2015). Thus, whether metrics measured at the scalp concerning the alpha rhythm reflect changes in the same or different underlying oscillatory dynamical systems is unknown.

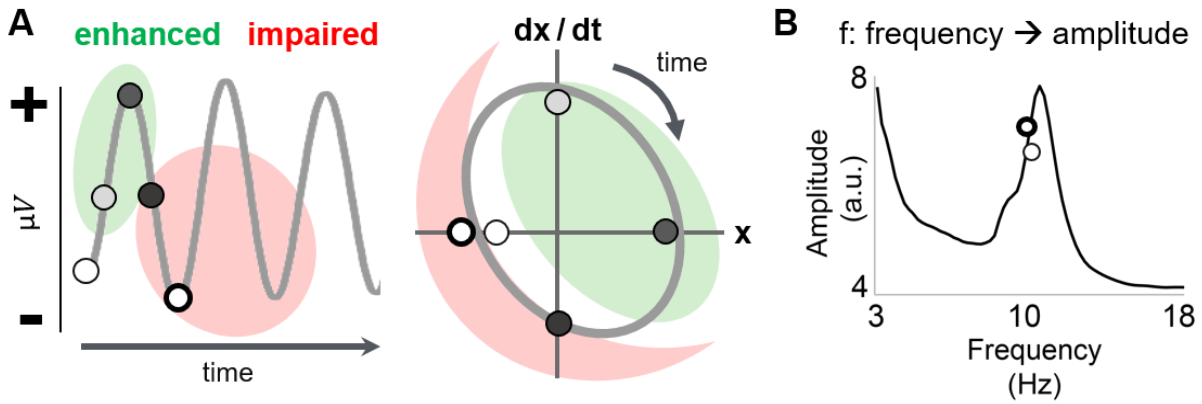

Figure 0.3: Attractor cycle perspective on alpha oscillations. **A:** Left panel: A few cycles of an oscillation is plotted, with four distinct phases indicated with different shades of gray. These points are replotted in the right panel, but instead visualized as a cyclic process by plotting the signal against its derivative. Right panel: the signal "x" is plotted against its temporal derivative "dx/dt". The same points from the left panel are replotted. The dark black oval is the average attractor cycle (shape drawn arbitrarily), note that particular points may fall off this average due to variations in amplitude at a specific phase. In both plots, green and red shaded regions are cartoons indicating potential regions where information processing is enhanced or impaired, and gray arrows indicate the direction along which time increases. Note that amplitudes at the same phase but different times along the oscillation may be different, as outlined by differentially bolded white dots. Thus, the radius of the limit cycle (amplitude) is modulated by how fast it is traversed (frequency) **B:** I propose that complex neural interactions result in the link between the radius of the limit cycle in A (amplitude) and how fast it is traversed (frequency). This relationship, equations for which are in Chapter 2, results in the average amplitude spectrum, plotted for one subject here in black. This amplitude spectrum provides a general mapping from frequency to amplitude that is defined by each subject's idiosyncratic dynamical alpha system.

This problem is difficult, as oscillations in the brain are "metastable", meaning they are perpetually in a state of transient stable phase synchrony due to the presence of multiple coupled oscillators continuously engaging and disengaging each other (Buzsáki, 2006). One popular model holds that weakly coupled limit cycle oscillators are desynchronizied until coupling strength K exceeds critical value K_c, and as K continues to increase more and more oscillators are recruited into the synchronized group (The Kuramoto model) (Kuramoto, 2003). As the brain is composed of non-identical oscillators with complex topology, metastable neural synchronization is even more complex than the original Kuramoto model suggests, further emphasizing the fact that interactions between neural oscillators lead to off-cycle timepoints by constant adjustments in amplitude (limit cycle radius), phase (location along limit cycle) and frequency (speed of limit cycle traversal; specific timepoints marked with circles in cartoon

Figure 0.3A) (Strogatz, 2001). Perturbation by outside events and dynamic coupling with other oscillators will accumulate as these dynamical systems continue to operate in time (Buzsáki, 2006) to form the distribution of amplitudes at each alpha frequency commonly referred to as a spectra (Figure 0.3B). Hence, amplitudes at the same phase but at different *times* along the oscillation may be different due to coupled oscillatory interactions that lead to deviations from the limit cycle in the phase space – inherently linking the radius of the limit cycle (amplitude) to its traversal (frequency).

Thus, perhaps the tonic and phasic inhibition accounts describe enhancements and impairments in visual perception that depend on oscillatory location in the alpha phase space at a particular time with respect to the limit cycle (Figure 0.3A: green/red shaded regions are cartoons of enhanced/impaired performance). Along these lines, I propose that tonic and phasic inhibition reflect a common dynamical system generated by complex circuit interactions that support efficient visual information processing (Draguhn et al., 2004; Hutcheon & Yarom, 2000; E.M. Izhikevich, 2003). Thus, I suggest that the amplitude spectrum is an average mapping between the amplitude and frequency of a dynamical system if measured in conditions ideal for the question at hand, and should be used as an individualized mapping for probing each subjects' dynamical system (Figure 0.3B).

Chapter 1: *Alpha and theta band behavioral rhythms characterize low and high fidelity visual information processing*

Is visual perception discrete or continuous? Although our visual experience feels continuous, the existence of contrary evidence has led to the dogged pursuit of this question since the start of vision science. Indeed, both the detection of visual stimuli and the perception of TMS-induced phosphenes have been found to depend on the phase of endogenous alpha oscillation (Busch et al., 2009; Dugue et al., 2011; Mathewson et al., 2011, 2009). Consistent

with these results, recent results have shown that attention-dependent visual detection fluctuates in the theta and alpha range (Fiebelkorn, Saalmann, & Kastner, 2013; Landau & Fries, 2012).

However, as these previous reports of behavioral rhythmicity rely on binary detection reports, they are limited by sparse behavioral measures. Additionally, they have not examined the continuum of visually-dependent behaviors from perception and attentional selection to working memory. Thus, I aimed to confirm the existence of behavioral rhythmicity in visual perception, and to determine if this rhythmicity is present in downstream visually-dependent processes using a rich behavioral paradigm allowing us to probe capacity limits at both cued and uncued locations in visual perception and memory.

Idesigned an experiment that expanded on the classic partial-report iconic memory paradigms(Sperling, 1960). Iconic and short-term memory corresponding to delays <400 ms or between 400ms and several seconds respectively. Iconic memory is a high capacity but fragile perceptual buffer system from which prioritized information is selected to be more enduringly encoded in short-term memory. I designed a visual task utilizing partial report designs, a continuum of delays from iconic to short-term memory, and a full-field flash to induce phase resetting of oscillatory neural activity to investigate a) whether alpha oscillations impact the fidelity of visual working memory representations and b) if this impact varies along the memory delay continuum.

Indeed, subjects recalled more cued letters and uncued-for letters just neighboring the explicitly cued letters, supporting the idea of iconic memory as a high capacity but imprecise perceptual buffer. Interestingly, these cued and neighboring responses under iconic delays are rhythmically structured in distinct ways. Cued recall was linked to with higher phase locking at theta frequencies, while neighbor recall was associated with both higher phase locking and power at alpha frequencies (Figure 1.5). Thus, I show theta vs alpha behavioral rhythmicity in high vs low fidelity visual perception and attentional selection, extending previous results finding

that theta and alpha rhythmicity depend on the spatial spread of attention (Fiebelkorn et al., 2013; Landau & Fries, 2012). Specifically, I find alpha rhythmicity is associated with spatially imprecise attentional allocation that has a cascading effect on subjects' ability to distinguish uncued locations from cued ones.

Importantly, this effect in the alpha band is associated with both increased behavioral phase locking and power. I hypothesize that these metrics are yoked measurements of the operation of a common dynamical system(Nelli et al., 2017) in which the phase and power of alpha oscillations are simultaneously indexing inhibitory processes in visual perception and attention(Mathewson et al., 2011). I further explore this possibility for a joint impact on behavior in yoked alpha metrics in Chapter 2.

Chapter 2: *Fluctuations in instantaneous frequency predict alpha amplitude during visual perception*:

Much of the empirical work concerning alpha oscillations has been carried out in the domain of visual perception, and this historic focus has led to the formation of the tonic and phasic inhibition accounts, which I outline above (Figure 0.2). However, in complex systems they can be tightly coupled, and indeed the alpha oscillation has been shown to be well-modeled by a harmonic oscillator, although detailed biophysical models exist(Aronson, Ermentrout, & Kopell, 1990; Boccaletti, Kurths, Osipov, Valladares, & Zhou, 2002; Eugene M Izhikevich, 2001). First, let the uncoupled driving and target regions oscillate at characteristic frequencies. When considered as a coupled system, alpha amplitude in the target region (A_T) will be a function of both the amplitude of the oscillatory drive (A_D) and the difference between the frequency of the driving (ω_D) and target oscillator (ω_T), which themselves depend on connectivity and local E/I activity (Hutcheon & Yarom, 2000; Wang, 2010) (Figure 0.4). This dependence complicates the traditional interpretation of alpha amplitude and instead suggests

that shifts in amplitude reflect changes in the frequency of the underlying dynamical system, which could arise given changes in oscillatory drive (ω_D), local dampening (ω_{eT}), or local characteristic frequency (ω_T; See Chapter 2).

The amplitude spectrum of typical EEG signals recorded over visual cortex shows a pronounced and focal bump centered on the dominant alpha frequency (Figure 0.3B). This focal alpha bump is thought to be the result of resonant responses between interacting neural oscillators (Draguhn et al., 2004; Hutcheon & Yarom, 2000; E.M. Izhikevich, 2003) (note the similarity to Figure 2.2a). Thus, I hypothesized that the frequency-amplitude relationship outlined above is reflected in each subject's alpha bump. I expect that changes in the instantaneous frequency will lead to changes in amplitude, and that the precise nature of these changes will be captured by the shape of each subject's spectrum (Figure 2.1a-c).

I used data from two separate experiments to empirically test this potential interdependence between frequency and amplitude. Our results show that shifts in alpha amplitude can be predicted by passing frequency through each subject's alpha spectrum, suggesting that these metrics do not index independent neural mechanisms of information processing as assumed. I argue instead for viewing these metrics as indexing a common dynamical system underlying modulations in both amplitude and frequency that is reflected in each subject's alpha bump. To this end, I found that how similar similarity of Predicted Amplitudes were to measured Amplitudes depended on the precise shape of each subject's idiosyncratic alpha bump. For example, Subject 5 in our experiment had an alpha bump highly correlated with Subject 2 (r=0.88, blue star in Figure 0.4 right panel) but poorly correlated with Subject 14 (r=-0.07, red star in Figure 0.4 right panel). I found that passing Subject 5's frequency data through Subject 2's amplitude spectra still yielded good amplitude predictions (PaA in figure), as opposed to Subject 14's (Figure 0.4). This drives home the fact that each individual subject's alpha bump is reflecting particular characteristics of the dynamic and resonant alpha band interactions that

impacts visual information processing

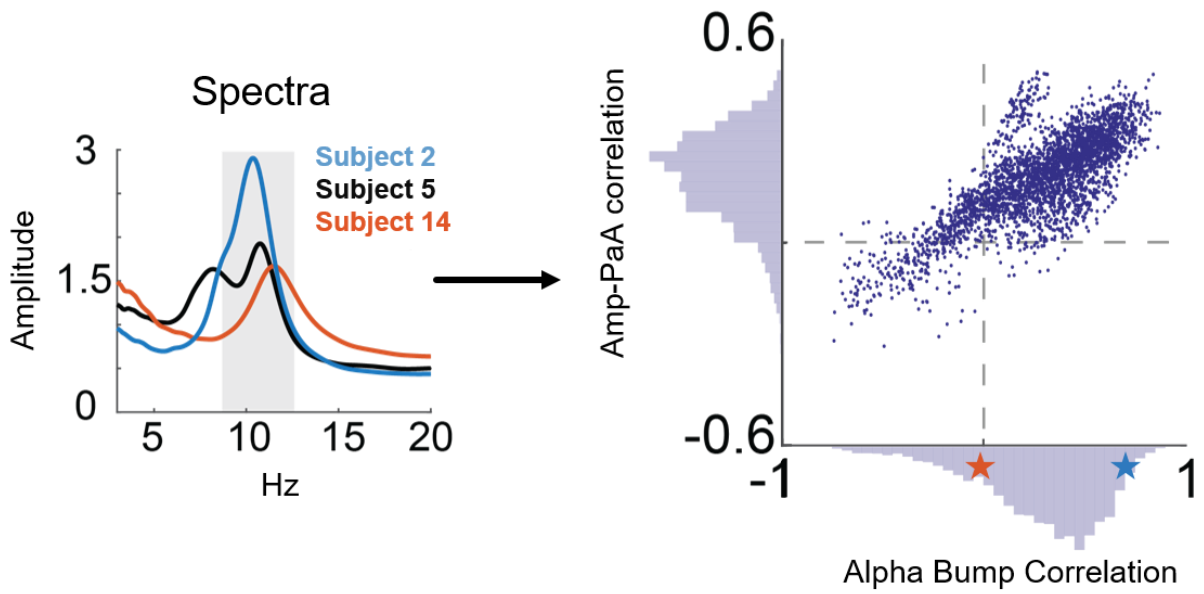

Figure 0.4: Each subject's idiosyncratic alpha bump matters. Three subject's alpha spectra are plotted as examples. When I shuffled the amplitude spectra between subjects, the Amp-PaA correlation is 0.28 on average, lower than the empirical results but still greater than zero. However, this is because there's a stereotyped shape of the general "alpha bump" -and on average subjects bumps are correlated at a rho of 0.2. This linear relationship is visualized on the right plot, where the degree of Amp-PaA correlation clearly depends on the correlation between subject's alpha bumps. Histograms on axes show counts collapsed on that axis. Red star indicates the correlation between the alpha bumps of Subjects 5 and 14, while Blue star indicates correlation between Subjects 5 and 2.

Additionally, I note that shifts both above and below peak alpha could be one mechanism through which amplitude decreases, supporting the hypothesis that desynchronization occurs through a selective shift in the frequency of a task-engaged neural circuit (Figure 2.1). However, enhanced behavior seems to be preferentially associated with faster frequencies, an observation that is consistent with previous observations but not with a more general desynchronization role for alpha frequency. This may be due to the precise relationship between the dominant frequency in the local population representing the stimulus and that of the more global, phenotypic alpha oscillation, leading us to the experiment described in Chapter 3.

Chapter 3: *The efficiency of visual processing depends on deviations of alpha rhythms from their endogenous peak frequency*

Up to this point, I show that alpha phase/frequency and amplitude appear to be indexing the same resonant, dynamic system that impacts behavior. Specifically, in Chapter 1 I show similar effects on alpha band behavioral rhythmicity as measured with both phase locking and power, and link alpha frequency with amplitude in Chapter two. However, complex interactions between driving and target neural regions determine the dynamics of this resonant alpha system that in turn impacts visual perception (Nelli et al., 2017). A link between this alpha drive and visual perception has not been established in humans. Thus, I sought to use SSVEP and source separation techniques to drive early visual alpha rhythms and determine their impact on the endogenous alpha oscillations and behavior.

Specifically, I entrained posterior alpha rhythms at a variety of frequencies in the alpha band using SSVEP while subjects performed a simple contrast change detection task (Figure 3.1B). Using task-independent estimates of peak alpha frequency, I then examined a) how perceptual performance depends on entrainment frequency relative to endogenous alpha frequency and b) the neural correlates of this dependence.

Two dissociable patterns of behavior emerged as a function of alpha drive relative to each subject's endogenous peak alpha frequency. In one group of subjects, entrainment at or above a subject's peak alpha frequency impaired perceptual performance, consistent with the inhibition account. In contrast, entrainment at or above peak alpha enhanced performance in the second group, consistent with the perceptual sampling account. Importantly, subjects in group one had higher endogenous peak alpha frequencies compared to group two, indicating peak alpha as a stable trait for each subjects dynamical system that determines how clamped oscillations in early visual regions interact with the endogenous system to differentially impact behavior.

Furthermore, I performed a state space analysis to determine how exactly these entrained rhythms are differentially impacting subjects with high vs low alpha frequencies. Indeed, endogenous alpha oscillations in subjects with higher frequencies traversed the alpha state space less efficiently when entrained at higher frequencies, and vice versa. Thus, I found that whether activity at a subject's peak alpha frequency impairs or enhances perceptual performance depends on each subject's intrinsic peak alpha frequency. This observation suggests an optimal dynamical range for the alpha oscillation, possibilities for which I discuss further in Chapter 3.

Concluding remarks

Here I reviewed a broad literature showing the impact of alpha oscillations on visual perception and cognition. I additionally outlined the three chapters of my thesis, which further elucidate the role of alpha oscillations on visual perception.

Future efforts in experimental design, analytical methods development, and computational modeling should explicitly probe the circuits that generate the alpha rhythm, and which of these circuits contribute to the alpha oscillation measured at the scalp. Additionally, rhythmic stimulation experiments (electric, magnetic, optogenetic, SSVEP, etc.) which can continuously vary the stimulating waveform and assess behavioral or physiological differences should be done in order to assess the causal impact of oscillations. Additionally, simultaneous recordings of field potentials and neuronal spiking will help us quantify relationships between alpha power, phase and frequency (See chapter 2).

This introduction, in part, is an adaptation of the material that appears in:

Nelli, S., Itthipuripat, S., Srinivasan, R., & Serences, J. T. (2017). Fluctuations in instantaneous frequency predict alpha amplitude during visual perception. *Nature communications*, *8*(1), 2071

Nelli S, Chen R, Serences J. (2019) Behavioral rhythmicity in alpha and theta bands differentially characterize precision of spatial attention. *In Prep*.

Nelli S, Serences J. (2019) The efficiency of visual processing depends on deviations of alpha rhythms from their endogenous peak frequency. *In Prep*.

The dissertation author was the primary investigator and author of these papers

REFERENCES

Adey, W. R. (1988). Do EEG-like Processes Influence Brain Function at a Physiological Level? BT - Dynamics of Sensory and Cognitive Processing by the Brain. In E. Başar (Ed.), (pp. 362–367). Berlin, Heidelberg: Springer Berlin Heidelberg.

Akam, T., & Kullmann, D. M. (2014). Oscillatory multiplexing of population codes for selective communication in the mammalian brain. *Nature Reviews. Neuroscience*, *15*(2), 111–22. http://doi.org/10.1038/nrn3668

Aronson, D. G., Ermentrout, G. B., & Kopell, N. (1990). Amplitude response of coupled oscillators. *Physica D: Nonlinear Phenomena*, *41*(3), 403–449. http://doi.org/10.1016/0167-2789(90)90007-C

Atallah, B. V., & Scanziani, M. (2009). Instantaneous Modulation of Gamma Oscillation Frequency by Balancing Excitation with Inhibition. *Neuron*, *62*(4), 566–577. http://doi.org/10.1016/j.neuron.2009.04.027

Başar, E. (2012). A review of alpha activity in integrative brain function: Fundamental physiology, sensory coding, cognition and pathology. *International Journal of Psychophysiology*, *86*(1), 1–24. http://doi.org/10.1016/j.ijpsycho.2012.07.002

Bastos, A. M. A. M., Vezoli, J., Bosman, C. A., Schoffelen, J. M., Oostenveld, R., Dowdall, J. R., … Fries, P. (2015). Visual areas exert feedforward and feedback influences through distinct frequency channels. *Neuron*, *85*(2), 390–401. http://doi.org/10.1016/j.neuron.2014.12.018

Blatow, M., Rozov, A., Katona, I., Hormuzdi, S. G., Meyer, A. H., Whittington, M. A., … Monyer, H. (2003). A novel network of multipolar bursting interneurons generates theta frequency oscillations in neocortex. *Neuron*, *38*(5), 805–817. http://doi.org/10.1016/S0896-6273(03)00300-3

Boccaletti, S., Kurths, J., Osipov, G., Valladares, D. L., & Zhou, C. S. (2002). The synchronization of chaotic systems, *366*, 1–101.

Bollimunta, A., Chen, Y., Schroeder, C. E., & Ding, M. (2008). Neuronal Mechanisms of Cortical Alpha Oscillations in Awake-Behaving Macaques. *Journal of Neuroscience*, *28*(40), 9976–9988. http://doi.org/10.1523/JNEUROSCI.2699-08.2008

Bosman, C. A., Schoffelen, J. M., Brunet, N., Oostenveld, R., Bastos, A. M., Womelsdorf, T., … Fries, P. (2012). Attentional Stimulus Selection through Selective Synchronization between Monkey Visual Areas. *Neuron*, *75*(5), 875–888. http://doi.org/10.1016/j.neuron.2012.06.037

Busch, N., Dubois, J., & VanRullen, R. (2009). The phase of ongoing EEG oscillations predicts visual perception. *The Journal of Neuroscience : The Official Journal of the Society for Neuroscience*, *29*(24), 7869–7876. http://doi.org/10.1523/JNEUROSCI.0113-09.2009

Buzsáki, G. C. N. (2006). *Rhythms of the brain*. *Rhythms of the Brain*. http://doi.org/10.1093/acprof:oso/9780195301069.001.0001

Draguhn, A., Buzsáki, G., Andreas, D., & Draguhn, A. (2004). Neuronal Oscillations in Cortical Networks. *Science*, *304*(June), 1926. http://doi.org/10.1126/science.1099745

Dugue, L., Marque, P., & VanRullen, R. (2011). The Phase of Ongoing Oscillations Mediates the Causal Relation between Brain Excitation and Visual Perception. *Journal of Neuroscience*, *31*(33), 11889–11893. http://doi.org/10.1523/JNEUROSCI.1161-11.2011

Fiebelkorn, I. C., Pinsk, M. A., & Kastner, S. (2018). A Dynamic Interplay within the Frontoparietal Network Underlies Rhythmic Spatial Attention. *Neuron*, *99*(4), 842–853.e8. http://doi.org/10.1016/j.neuron.2018.07.038

Fiebelkorn, I. C., Saalmann, Y. B., & Kastner, S. (2013). Rhythmic sampling within and between objects despite sustained attention at a cued location. *Current Biology : CB*, *23*(24), 2553–2558. http://doi.org/10.1016/j.cub.2013.10.063

Foxe, J. J., Simpson, G. V, & Ahlfors, S. P. (1998). Parieto-occipital approximately 10 Hz activity reflects anticipatory state of visual attention mechanisms. *Neuroreport*, *9*(17), 3929–3933. http://doi.org/10.1097/00001756-199812010-00030

Fries, P. (2005). A mechanism for cognitive dynamics: Neuronal communication through neuronal coherence. *Trends in Cognitive Sciences*, *9*(10), 474–480. http://doi.org/10.1016/j.tics.2005.08.011

Fries, P. (2015). Rhythms for Cognition: Communication through Coherence. *Neuron*, *88*(1), 220–235. http://doi.org/10.1016/j.neuron.2015.09.034

Fries, P., Reynolds, J. H., Rorie, a E., & Desimone, R. (2001). Modulation of oscillatory neuronal synchronization by selective visual attention. *Science (New York, N.Y.)*, *291*(FEBRUARY), 1560–1563. http://doi.org/10.1126/science.1055465

Fries, P., Womelsdorf, T., Oostenveld, R., & Desimone, R. (2008). The effects of visual

stimulation and selective visual attention on rhythmic neuronal synchronization in macaque area V4. *The Journal of Neuroscience : The Official Journal of the Society for Neuroscience*, *28*(18), 4823–4835. http://doi.org/10.1523/JNEUROSCI.4499-07.2008

Gasser, T., Bächer, P., & Steinberg, H. (1985). Test-retest reliability of spectral parameters of the EEG. *Electroencephalography and Clinical Neurophysiology*, *60*(4), 312–319. http://doi.org/https://doi.org/10.1016/0013-4694(85)90005-7

Grandy, T. H., Werkle-Bergner, M., Chicherio, C., Schmiedek, F., Lövdén, M., & Lindenberger, U. (n.d.). Peak individual alpha frequency qualifies as a stable neurophysiological trait marker in healthy younger and older adults. http://doi.org/10.1111/psyp.12043

Haas, L. F. (2003). Hans Berger (1873-1941), Richard Caton (1842-1926), and electroencephalography. *Journal of Neurology, Neurosurgery, and Psychiatry*, *74*(1), 9. http://doi.org/10.1136/jnnp.74.1.9

Haegens, S., Nácher, V., Luna, R., Romo, R., & Jensen, O. (2011). α-Oscillations in the monkey sensorimotor network influence discrimination performance by rhythmical inhibition of neuronal spiking. *Proceedings of the National Academy of Sciences of the United States of America*, *108*(48), 19377–82. http://doi.org/10.1073/pnas.1117190108

Händel, B. F., Haarmeier, T., & Jensen, O. (2011). Alpha oscillations correlate with the successful inhibition of unattended stimuli. *Journal of Cognitive Neuroscience*, *23*(9), 2494–2502. http://doi.org/10.1162/jocn.2010.21557

Hasenstaub, A., Shu, Y., Haider, B., Kraushaar, U., Duque, A., & McCormick, D. A. (2005). Inhibitory postsynaptic potentials carry synchronized frequency information in active cortical networks. *Neuron*, *47*(3), 423–435. http://doi.org/10.1016/j.neuron.2005.06.016

Hutcheon, B., & Yarom, Y. (2000). Resonance, oscillation and the intrinsic frequency preferences of neurons. *Trends in Neuroscience*, *23*(5), 216–222. http://doi.org/10.1016/S0166-2236(00)01547-2

Isaacson, J. S., & Scanziani, M. (2011). How inhibition shapes cortical activity. *Neuron*, *72*(2), 231–243. http://doi.org/10.1016/j.neuron.2011.09.027

Izhikevich, E. M. (2001). Resonate-and-fire neurons. *Neural Networks*, *14*(Special Issue), 883–894.

Izhikevich, E. M. (2003). Simple model of spiking neurons. *IEEE Transactions on Neural Networks*, *14*(6), 1569–1572. http://doi.org/10.1109/TNN.2003.820440

Kayser, C., Montemurro, M. A., Logothetis, N. K., & Panzeri, S. (2009). Spike-Phase Coding Boosts and Stabilizes Information Carried by Spatial and Temporal Spike Patterns. *Neuron*, *61*(4), 597–608. http://doi.org/10.1016/j.neuron.2009.01.008

Kelly, S. P., Gomez-Ramirez, M., & Foxe, J. J. (2009). The strength of anticipatory spatial biasing predicts target discrimination at attended locations: A high-density EEG study. *European Journal of Neuroscience*, *30*(May), 2224–2234. http://doi.org/10.1111/j.1460-9568.2009.06980.x

Klimesch, W. (1996). Memory processes, brain oscillations and EEG synchronization. *International Journal of Psychophysiology*, *24*(1–2), 61–100. http://doi.org/10.1016/S0167-8760(96)00057-8

Klimesch, W., Sauseng, P., & Hanslmayr, S. (2007). EEG alpha oscillations: the inhibition-timing hypothesis. *Brain Research Reviews*, *53*(1), 63–88. http://doi.org/10.1016/j.brainresrev.2006.06.003

Kuramoto, Y. (2003). *Chemical oscillations, waves, and turbulence*. Courier Corporation.

Lakatos, P., O'Connell, M. N., Barczak, A., Mills, A., Javitt, D. C., & Schroeder, C. E. (2009). The Leading Sense: Supramodal Control of Neurophysiological Context by Attention. *Neuron*, *64*(3), 419–430. http://doi.org/10.1016/j.neuron.2009.10.014

Landau, A. N., & Fries, P. (2012). Attention samples stimuli rhythmically. *Current Biology*, *22*(11), 1000–1004. http://doi.org/10.1016/j.cub.2012.03.054

Lopes da Silva, F. (1991). Neural mechanisms underlying brain waves: from neural membranes to networks. *Electroencephalography and Clinical Neurophysiology*, *79*(2), 81–93. http://doi.org/10.1016/0013-4694(91)90044-5

Lopes da Silva, F. H., Vos, J. E., Mooibroek, J., & van Rotterdam, A. (1980). Relative contributions of intracortical and thalamo-cortical processes in the generation of alpha rhythms, revealed by partial coherence analysis. *Electroencephalography and Clinical Neurophysiology*, *50*(5–6), 449–456. http://doi.org/10.1016/0013-4694(80)90011-5

Lorincz, M. L., Kékesi, K. A., Juhász, G., Crunelli, V., & Hughes, S. W. (2009). Temporal Framing of Thalamic Relay-Mode Firing by Phasic Inhibition during the Alpha Rhythm. *Neuron*, *63*(5), 683–696. http://doi.org/10.1016/j.neuron.2009.08.012

Mann, E. O., & Mody, I. (2010). Control of hippocampal gamma oscillation frequency by tonic inhibition and excitation of interneurons. *Nature Neuroscience*, *13*(2), 205–12. http://doi.org/10.1038/nn.2464

Mathewson, K. E., Gratton, G., Fabiani, M., Beck, D. M., & Ro, T. (2009). To see or not to see: prestimulus alpha phase predicts visual awareness. *The Journal of Neuroscience : The Official Journal of the Society for Neuroscience*, *29*(9), 2725–2732. http://doi.org/10.1523/JNEUROSCI.3963-08.2009

Mathewson, K. E., Lleras, A., Beck, D. M., Fabiani, M., Ro, T., & Gratton, G. (2011). Pulsed out of awareness: EEG alpha oscillations represent a pulsed-inhibition of ongoing cortical

processing. *Frontiers in Psychology*, *2*(MAY), 1–15. http://doi.org/10.3389/fpsyg.2011.00099

Meeuwissen, E. B., Takashima, A., Fernández, G., & Jensen, O. (2011). Increase in posterior alpha activity during rehearsal predicts successful long-term memory formation of word sequences. *Human Brain Mapping*, *32*(12), 2045–2053. http://doi.org/10.1002/hbm.21167

Mierau, A., Klimesch, W., & Lefebvre, J. (2017). State-dependent alpha peak frequency shifts: Experimental evidence, potential mechanisms and functional implications. *Neuroscience*, *360*, 146–154. http://doi.org/10.1016/j.neuroscience.2017.07.037

Nelli, S., Itthipuripat, S., Srinivasan, R., & Serences, J. T. (2017). Fluctuations in instantaneous frequency predict alpha amplitude during visual perception. *Nature Communications*, *8*(1). http://doi.org/10.1038/s41467-017-02176-x

Osaka, M. (1984). Peak Alpha Frequency of EEG during a Mental Task: Task Difficulty and Hemispheric Differences. *Psychophysiology*, *21*(1), 101–105. http://doi.org/10.1111/j.1469-8986.1984.tb02325.x

Palva, S., & Palva, J. M. (2007). New vistas for alpha-frequency band oscillations. *Trends in Neurosciences*, *30*(4), 150–158. http://doi.org/10.1016/j.tins.2007.02.001

Pfurtscheller, G. (2001). Functional brain imaging based on ERD / ERS, *41*, 1257–1260.

Rihs, T. A., Michel, C. M., & Thut, G. (2007). Mechanisms of selective inhibition in visual spatial attention are indexed by ??-band EEG synchronization. *European Journal of Neuroscience*, *25*(2), 603–610. http://doi.org/10.1111/j.1460-9568.2007.05278.x

Saalmann, Y. B., Pinsk, M. A., Wang, L., Li, X., & Kastner, S. (2012). The pulvinar regulates information transmission between cortical areas based on attention demands. *Science (New York, N.Y.)*, *337*(August), 753–6. http://doi.org/10.1126/science.1223082

Salinas, E., & Sejnowski, T. J. (2001). Correlated neuronal activity and the flow of neural information. *Nature Neuroscience*, *14*(7), 811–819. http://doi.org/10.1038/nn.2842

Samaha, J., & Postle, B. R. (2015). The speed of alpha-band oscillations predicts the temporal resolution of visual perception Jason Samaha and Bradley R. Postle. *Current Biology*, *25*, 2985–2990. http://doi.org/10.1016/j.cub.2015.10.007

Sauseng, P., Klimesch, W., Stadler, W., Schabus, M., Doppelmayr, M., Hanslmayr, S., … Birbaumer, N. (2005). A shift of visual spatial attention is selectively associated with human EEG alpha activity. *Eur J Neurosci*, *22*(11), 2917–2926. http://doi.org/EJN4482 [pii]\r10.1111/j.1460-9568.2005.04482.x

Shao, Z., & Burkhalter, A. (1996). Different balance of excitation and inhibition in forward and feedback circuits of rat visual cortex. *The Journal of Neuroscience : The Official Journal of*

the Society for Neuroscience, *16*(22), 7353–7365.

Silva, F. H. L. D. A., & Leeuwen, W. S. V. A. N. (1977). the Cortical Source of the Alpha Rhythm. *Neuroscience Letters*, *6*, 237–241.

Sperling, G. (1960). The information available in brief visual presentations. *Psychological Monographs*.

Strogatz, S. H. (2001). Exploring complex networks Steven. *Nature*, *410*(March). http://doi.org/10.1038/35065725

von Stein, A., Chiang, C., & König, P. (2000). Top-down processing mediated by interareal synchronization. *Proceedings of the National Academy of Sciences of the United States of America*, *97*(26), 14748–14753. http://doi.org/10.1073/pnas.97.26.14748

Voytek, B., Kayser, A. S., Badre, D., Fegen, D., Chang, E. F., Crone, N. E., … D'Esposito, M. (2015). Oscillatory dynamics coordinating human frontal networks in support of goal maintenance. *Nature Neuroscience*, (July), 1–10. http://doi.org/10.1038/nn.4071

Wang, X. J. (2010). Neurophysiological and computational principles of cortical rhythms in cognition. *Physiological Reviews*, 1195–1268. http://doi.org/10.1152/physrev.00035.2008.

Wehr, M. S., & Zador, A. M. (2003). Balanced inhibition underlies tuning and sharpens spike timing in auditory cortex. *Nature*, *426*(6965), 442–6. http://doi.org/10.1038/nature02116

Womelsdorf, T., Schoffelen, J.-M., Oostenveld, R., Singer, W., Desimone, R., Engel, A. K., & Fries, P. (2007). Modulation of neuronal interactions through neuronal synchronization. *Science (New York, N.Y.)*, *316*(5831), 1609–1612. http://doi.org/10.1126/science.1139597

Chapter 1: Behavioral rhythmicity in alpha and theta bands differentially characterize precision of spatial attention

Abstract

Rhythmic fluctuations in neural activity contribute to variability in the perception and recall of visual information. Specifically, theta (~4-7 Hz) and alpha (~8-12 Hz) band neural oscillations have been found to increase and impair, respectively, the ability to detect visual stimuli, deploy selective attention, and hold in mind information about stimuli over short periods of time (short-term memory). Interestingly, rhythmic fluctuations in visual detection have also been identified at similar frequencies. However, as these previous studies utilize sparse behavioral measures, little is known about whether theta vs alpha rhythmic behavioral fluctuations are selective to differential precision in and stages of visual information processing. To examine rhythmicity in behavior along the continuum from attentional selection to short-term memory, we designed a variant of a classic iconic memory paradigm. Subjects were briefly presented with an array of letters at an unpredictable time, and were post-cued to report a subset of these letters after either 100ms (iconic delay), 400ms (intermediate delay) or 1000ms (short-term memory delay). We found increased behavioral rhythmicity at theta frequencies for iconic delays when subjects correctly recalled cued letters. Additionally, we found that increased behavioral rhythmicity at alpha frequencies at iconic delays that was selective to when subjects incorrectly reported letters presented in locations immediately adjacent to the cued locations. These results demonstrate theta rhythmicity in high fidelity visual information processing, whereas alpha rhythmicity is selectively seen in the imprecise attentional selection of items from an iconic sensory representation.

Introduction

Repeated presentations of identical stimuli do not always result in identical behavioral responses. Historically, such fluctuations in perception, memory and behavior were thought to result from unstructured noise in neural processing, and thus this variability was typically treated as a nuisance factor and discarded (for review see (Faisal, Selen, & Wolpert, 2008)). However, recent work analyzing neural signals recorded from both single units and populations of neurons (LFPs and scalp electroencephalography, or EEG) has found stereotyped neural oscillations that give rise to systematic, as opposed to random, fluctuations in behavioral performance (Herweg et al., 2016; Klimesch, 1999; Lisman & Jensen, 2013; Lopes da Silva, 2013; Nelli, Itthipuripat, Srinivasan, & Serences, 2017; van Kerkoerle et al., 2014). Indeed, both spontaneous fluctuations in neural activity as well as fluctuations related to cognitive factors such as the deployment of visual attention contribute to variability in behavior (M. R. Cohen & Maunsell, 2011; Marlene R Cohen & Maunsell, 2009).

For example, theta oscillations have been associated with increased neural activity, memory processes, and high fidelity spatial encoding of stimuli or locations (Buzsáki & Moser, 2013; Hasselmo, Hay, Ilyn, & Gorchetchnikov, 2002; Lisman & Jensen, 2013; Voytek et al., 2015). In humans, scalp EEG theta (~4-7 Hz) power increases are associated with higher cognitive and memory loads as well as enhanced performance on memory and decision making tasks(Jacobs, Hwang, Curran, & Kahana, 2006; Jensen & Tesche, 2002). Thus, theta oscillations are thought to index an “on-line” state in which hippocampal and cortical systems are ready to encode and process incoming signals with high fidelity (Buzsáki, 2002; Lisman & Jensen, 2013; Scheeringa et al., 2008).

Additionally, scalp EEG oscillations in the alpha band (~8-12Hz) play a role in visual perception and attention. Stimulus detection is impaired during certain phases of the alpha cycle, suggesting the fidelity of visual perception is modulated by alpha phase (Busch, Dubois, & VanRullen, 2009; Dugue, Marque, & VanRullen, 2011; Mathewson, Gratton, Fabiani, Beck, &

Ro, 2009). Additionally, shifts of visual attention increase alpha power over regions of cortex dedicated to processing spatial locations that are now unattended (Foster & Awh, 2018; Kelly, Gomez-Ramirez, & Foxe, 2009; Nelli et al., 2017; Rihs, Michel, & Thut, 2007; P Sauseng et al., 2005; Worden, Foxe, Wang, & Simpson, 2000), consistent with other work suggesting alpha oscillations are a spatially selective mechanism mediating inhibition inefficient visual information processing (Jensen, Bonnefond, & VanRullen, 2012; Jensen & Mazaheri, 2010; Klimesch, Sauseng, & Hanslmayr, 2007; Noonan et al., 2016).

Thus, phase and power of theta and alpha band neural oscillations at a given moment appear to govern the degree to which information processing is facilitated or inhibited, respectively (Busch et al., 2009; Lisman & Jensen, 2013; Milton & Pleydell-Pearce, 2016; Raghavachari et al., 2001; von Stein, Chiang, & König, 2000; Voytek et al., 2010, 2015). Interestingly, prior reports have also demonstrated structured rhythmicity in detection performance at theta and alpha frequencies (Fiebelkorn, Saalmann, & Kastner, 2013; Landau, Schreyer, van Pelt, & Fries, 2015; VanRullen, Carlson, & Cavanagh, 2007). For example, Landau and Fries (2012) presented a brief target stimulus that could occur from 750ms before to 1000ms after a 33ms flash event designed to reset ongoing oscillations and orient attention to one of two hemifields (Landau & Fries, 2012). The authors found theta rhythmicity in target detection that emerged only after the flash event, and that the frequency of this rhythmic target detection increased when the target was presented in the opposite hemifield as the attention flash event. In another report, Fiebelkorn et al. (2013) had subjects report targets that could appear in different objects, and found theta vs alpha band rhythmic visual detection at differentially attended objects (Fiebelkorn et al., 2013). These reports show that visual detection waxes and wanes at the same theta and alpha frequencies observed in neural oscillations during similar tasks (Fiebelkorn, Pinsk, & Kastner, 2018).

However, these previous reports of behavioral rhythmicity are limited by their employment of binary detection reports, and also do not extend along the continuum of

behaviors from attentional selection of information within early visual representations to encoding and storage in short-term memory. The use of binary response metrics is a key point, as there is debate about whether unattended stimuli are excluded entirely from perceptual processing or if they are still processed but with lower fidelity (Broadbent, 1958; Treisman, 1964, 1969). In addition, while neural oscillations in the theta and alpha bands have been appear to enhance and impair behavior respectively, binary behavioral reports have only shown that rhythmicity frequency that is modulated by spatial attention.

Thus, we aim here to probe if the frequency of behavioral rhythmicity is modulated by the fidelity and precision of neural representations underlying a continuum of behaviors. To do this, we used a behavioral paradigm that allowed us to probe capacity limits at both cued and uncued locations in order to establish the selectivity of theta vs alpha behavioral rhythms on the precision of behavioral reports along the continuum from visual perception and attentional selection to short-term memory.

Results

Behavioral Task

To address how behavioral rhythmicity is modulated along the continuum from visual perception and attentional selection to short-term memory, we designed an experiment based on a classic partial-report paradigm that found remarkably faithful visual representations that remain perceptually available for a fraction of a second after a stimulus has vanished, termed iconic memory (Figure 1.1) (DI LOLLO, 1977; G Sperling, 1960). As these visual iconic representations are fragile, subject to rapid decay and being overwritten, they are thought of as a "perceptual buffer" from which information is selected for more durable but lower capacity storage in short-term memory (Cowan, 1988; Luck & Vogel, 1997; Shiffrin & Atkinson, 1969). Note, that only nonselective letter encoding occurs until the post-cue, at which time subjects allocate spatial attention within their visual representation to selectively report the cued letters

(Figure 1.1) (George Sperling & Gegenfurtner, 1993). Therefore, our design allowed us to probe rhythmicity in attentional selection during early stages of visual processing, as well as at longer delays for which recall increasingly depends on the sustained storage of information. In addition, the partial report design yields richer behavioral data compared with binary detection tasks, as we could probe the precision of attentional selection and fidelity of memory recall by quantifying how often subjects reported both cued and uncued elements of the target array.

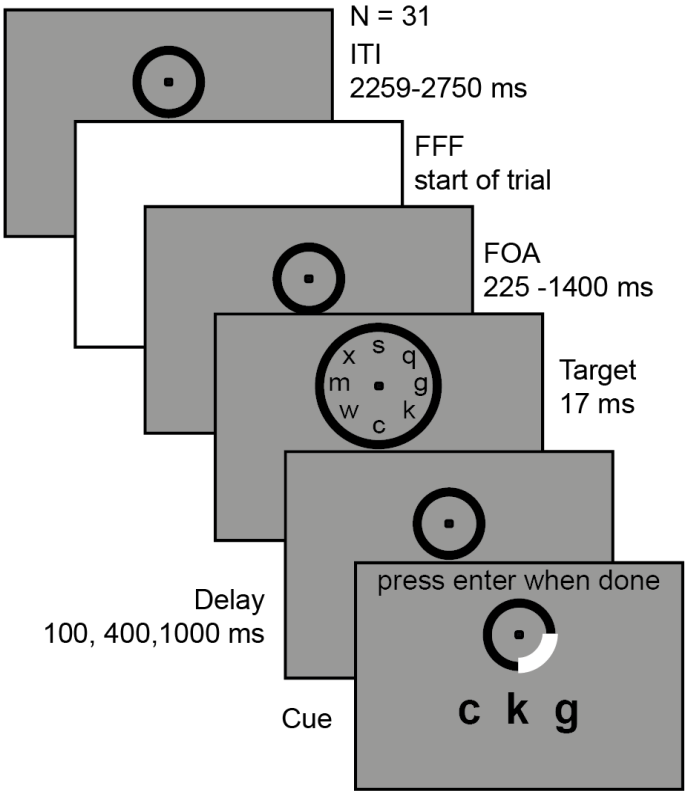

Figure 1.1: Task design. **A:** 31 subjects participated in the experiment. Trials started with a full-field flash (FFF), followed by variable Flash-Onset Asynchrony (FOA) after which an array of 8 letters appeared for 17ms (note the circular array is slightly enlarged here for visualization purposes, but was the same size as previous frames in the experiment). Either 100ms, 400ms, or 1000ms after the letters appeared (delay), subjects were cued to report 3 of the letters indicated by the location of a post-cue (white arc). Inter-trial intervals (ITIs) were chosen pseudo-randomly from a uniform distribution over 2259ms-2750ms.

In our task, each trial began with a full field flash (FFF) to trigger a phase reset of ongoing cortical oscillations (Lakatos et al., 2009; Makeig et al., 2002; Rizzuto et al., 2003), followed by a variable flash-onset-asynchrony (FOA) ranging from 225 ms to 1400 ms (in 25 ms

steps) after which subjects were presented with a brief (~17 ms) circular array of 8 letters. The presumed phase reset of ongoing oscillations by the FFF and brief letter array presentation allowed us to systematically probe behavioral rhythmicity resulting, theoretically, from phase aligned neural oscillations. Following the presentation of the letter array, subjects were instructed to respond with the 3 target letters indicated by the spatial position of the post-cue. This cue was presented either 100 ms (iconic delay), 400ms (intermediate delay), or 1000ms (short-term memory delay) after the offset of the target array. Varying the cue delay allowed us to assess the interaction between behavioral rhythmicity in attentional allocation and recall as visual representations transition from the iconic sensory buffer to storage in short-term memory.

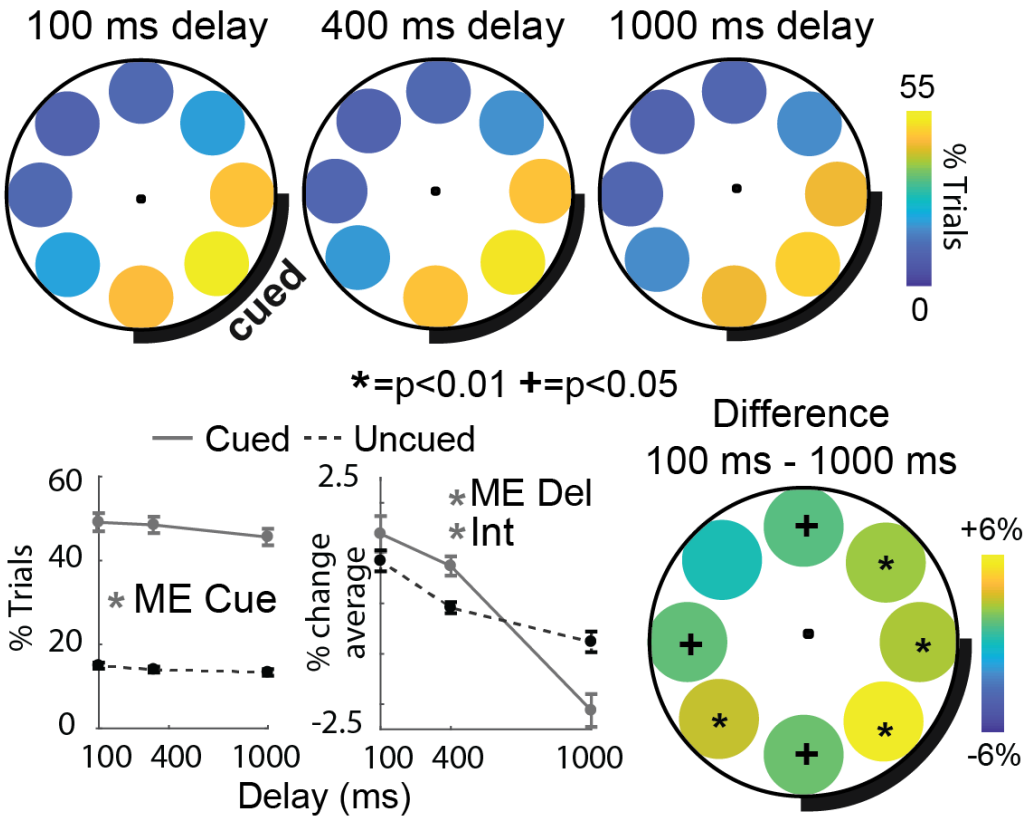

Figure 1.2: Spatial distribution of behavioral responses. Top row: Heat maps indicating the percent of trials on which subjects reported the letter presented at each location. For presentation purposes, we rotated response data so that the 3 cued locations were always in the lower-right quadrant indicated by the black bar (all 8 possible arrangements were equally likely to be cued in the actual experiment). Stars indicate significance at p=0.01, + indicates significance at p=0.05, determined through comparison with null distributions computed by randomizing condition label. Bottom Row, left panel: % trials reported decreases at uncued locations and with longer post-cue delays; error bars indicate ±1SEM. Middle panel: Delay x Cue interaction highlighted by subtracting mean recall within each cue condition. Error bars indicate ±1SEM. Gray stars in bottom left plots indicate significance assessed with a repeated-measures two-way ANOVA with Delay and Cue as factors. Bottom right heat map shows percentage of items recalled for each location at the longest cue delay subtracted from the shortest delay; significance determined by comparing paired t -statistics with those obtained by randomizing delay label 5000 times.

Post-cue delay affects recall independent of flash-onset-asynchrony (FOA)

We first analyzed the data without regard to the FOA to establish that our partial report paradigm produced the classic iconic memory recall effects (G Sperling, 1960) by subjecting the mean number of letters reported to a two-way repeated measures ANOVA with post-cue delay (100ms, 400ms, and 1000ms) and cue validity (cued, uncued) as factors. We found that recall of any of the 8 on-screen letters was higher at iconic delays compared to short-term memory

delays (Figure 1.1 Bottom left panel: Main effect of delay, $F(2,60) = 59.5$, $p<10^{-14}$; to generate p-values for this and subsequent ANOVAs F-values were compared to a null distribution of F-values generated from randomizing condition labels 5,000 times; mean recalled letters ±1SEM: 100ms delay = 2.22 ± 0.08, 1000ms delay = 2.04 ± 0.08 letters, $t(30) = 8.64$, $p<10^{-8}$; see Methods). Additionally, subjects were able to selectively report the cued subset of letters, indicating they understood the task (Figure 1.1; main effect of cue validity, $F(1,30) = 328.5$, $p<10^{-15}$). Finally, subjects were more likely to report cued letters at shorter compared to longer delays (Figure 1.1; interaction between delay and cue: $F(2,60) = 5.7$, $p=0.006$). Post-hoc t-tests revealed a more nuanced pattern such that the increased likelihood of a letter being reported at the iconic compared to the short-term memory delay decreased with distance from the cue. In particular, the two locations just *neighboring* the cue were much more likely to be reported at iconic delays (Figure 1.1 Bottom right panel; t(30)s = 2.5, 6.6, 3.0, 4.2, 2.4, 0.3, 2.8, 4.1, with p's = 0.02, $<10^{-15}$, = 0.004, < 0.001, = 0.02, = 0.75, =0.01, $<10^{-15}$ from the most clockwise cued location to its clockwise neighbor, respectively; to generate p-values for this and all subsequent t-statistics were compared to a null distribution obtained from 5000 randomizations of condition labels).

Letter recall decreases with increasing cue delay and distance from cued positions

Because subjects over-reported neighboring (i.e. adjacent to cue) letters at iconic delays, we next divide responses into cued, neighboring and opposite (i.e. opposite from the cue; Figure 1.3A; see Methods). Cued, neighbor and opposite recall all decreased with increasing cue delays, confirming that iconic sensory representations are high capacity (Reeves & Sperling, 1986; G Sperling, 1960) but relatively fragile (Becker, Pashler, & Anstis, 2000) (main effect of delay $F(2,60) = 26.43$, 18.05, 3.69 with p's < 10^{-8}, $<10^{-6}$, = 0.031 for cued, neighbor and opposite reports respectively; Significance determined by comparing F-values from one-way repeated-measures ANOVA with delay interval as a factor to ANOVAs with randomized delay

labels; see Methods). As observed in the previous section, post-cue delay had less of an effect on behavioral reports with increasing distance from the cued location, confirmed by assessing slopes from linear fits to individual subjects' recall metrics (Figure 1.3A; ME Delay: $F(2,60) = 5.98$, $p=0.004$, Delay x Distance interaction: $F(4,60) = 11.39$, $p < 10^{-7}$, 2-way repeated measures ANOVA with delay and distance as factors; on average subjects reported -4.0%, -2.75% and -0.98% fewer letters per second of delay for cued, neighbor and opposite responses, respectively; t-tests of slopes against zero: t(30)'s = -5.84, -4.46 and -2.22, p's $<10^{-15}$, $<10^{-15}$, and =0.027 for cued, neighbor and opposite recall, determined through 5000 randomizations of delay). Finally, post hoc t-tests revealed that iconic representations are particularly characterized by the imprecise recall of neighboring letters, as only neighbor recall significantly dropped from the iconic to intermediate delay conditions (Figure 1.3A; paired t-tests: t(30)'s = 1.39, =4.72, = 1.3, p's = 0.18, $<10^{-15}$, = 0.21 for cued, neighbor and opposite responses respectively, significance determined from 5000 randomizations of delay condition). Finally, guesses (i.e. reports of letters not presented in the target array) actually increased with increasing cue delays (Figure 1.3B; Main effect of repeated one way ANOVA $F(2,60) = 30.46$, $p< 10^{-9}$; average Beta value was 0.12 more letters per second, $t(30) = 6.06$, $p<10^{-5}$). This fact that guessing increases at longer delays is important because it confirms we subjects are imprecise within the iconic representation and not simply more likely to randomly respond. Finally, as opposite responses only showed marginally significant slopes over all delays and did not show a reduction from iconic to intermediate delays, we choose to exclude opposite responses from the rhythmicity results in the main text for ease of reading. Instead we mention opposite letter rhythmicity results as a control for the specificity and spatial spread of any observed behavioral rhythms where appropriate (Figure 1.7).

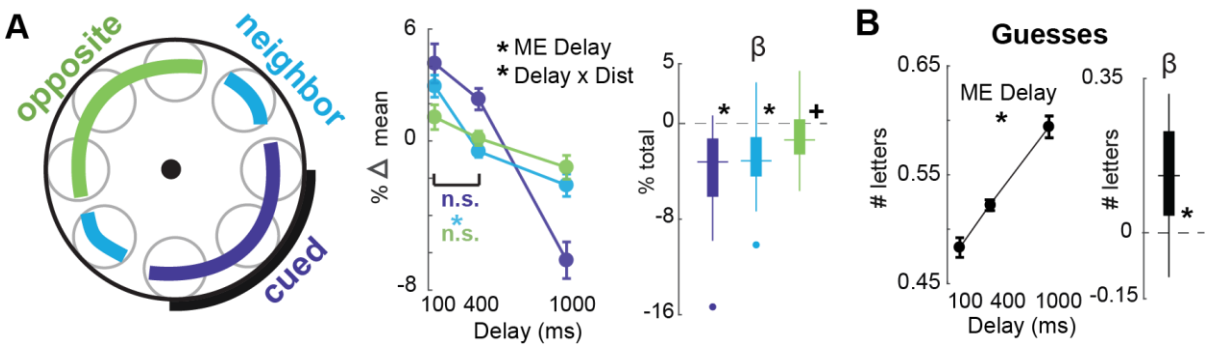

Figure 1.3: The impact of delay on cued, neighbor and opposite letter responses. **A:** Left Panel: We quantify three different types of behavioral responses by averaging over letters reported from the cued, neighboring or opposite regions of the letter array. For all plots, * indicates $p<0.01$, + = $p<0.05$ as determined through randomizing condition labels 5000 times. Middle Panel: Percent change from mean is plotted to display the interaction in which the effect of delay falls off with distance from cue; determined with repeated measures two-way ANOVA on each of the behavioral measures. Right Panel: Single subject slopes are plotted for each behavioral metric, significance determined by comparing t-statistics against zero to distribution of t-statistics from slopes determined through randomization of condition label. **B:** We also quantified guesses, or letters that were reported but not presented. These responses showed an increase with delay, determined through repeated measures one-way ANOVA and single subject beta values significantly above zero using a t-test. For both statistical tests, significance was determined through comparison to a null distribution obtained by randomizing condition labels 5000 times.

Variability of recall within FOA and approach to analyzing rhythmicity in behavior

In the previous section, we established that iconic delays are characterized by high capacity but imprecise, fragile recall, consistent with previous reports (Becker et al., 2000; G Sperling, 1960). The fact that subjects do not know which locations will be cued means only nonselective letter encoding occurs until the post-cue, at which time subjects allocate spatial attention to selectively report cued letters (George Sperling & Gegenfurtner, 1993). Thus, we next investigated how the reset of ongoing rhythms impacts the interaction between this initial nonselective encoding and the continuum from perception to more durable memory representations by quantifying behavioral rhythmicity.

To do this, we take a slightly different analysis approach compared to previous results that have found rhythmic visual detection as these results average over all trials of a certain FOA, thus obscuring within-FOA variability. Averaging over all instances of a particular FOA

assumes that there is consistent within-FOA behavior across trials, which has not been confirmed. The existence of high within-FOA variability would, in our view, necessitate subsampling trials before subjecting them to Fourier-based analysis in order to preserve this variability. Therefore, we first compared within-FOA and between-FOA variability using a repeated measures one-way ANOVA (i.e. FOA-related Mean-squared error and “error”, or non-FOA, Mean-squared error). While on average there was more between vs within FOA variance for both cued and neighbor responses, this effect was weak (Figure 1.4A; average single subject F ratios = 1.14, 1.02; 7/31 and 4/31 subjects had F ratios with parametric p’s<0.05 for cued and neighbor responses respectively). Across subjects, only cued responses showed consistently greater between vs within FOA variance across subjects (t-tests against 1 on F ratios: t(30)s = 3.37, 0.50 p’s = 0.002, 0.53 for cued and neighbor responses respectively; significance computed by randomizing mean squared errors 5000 times; See Methods).

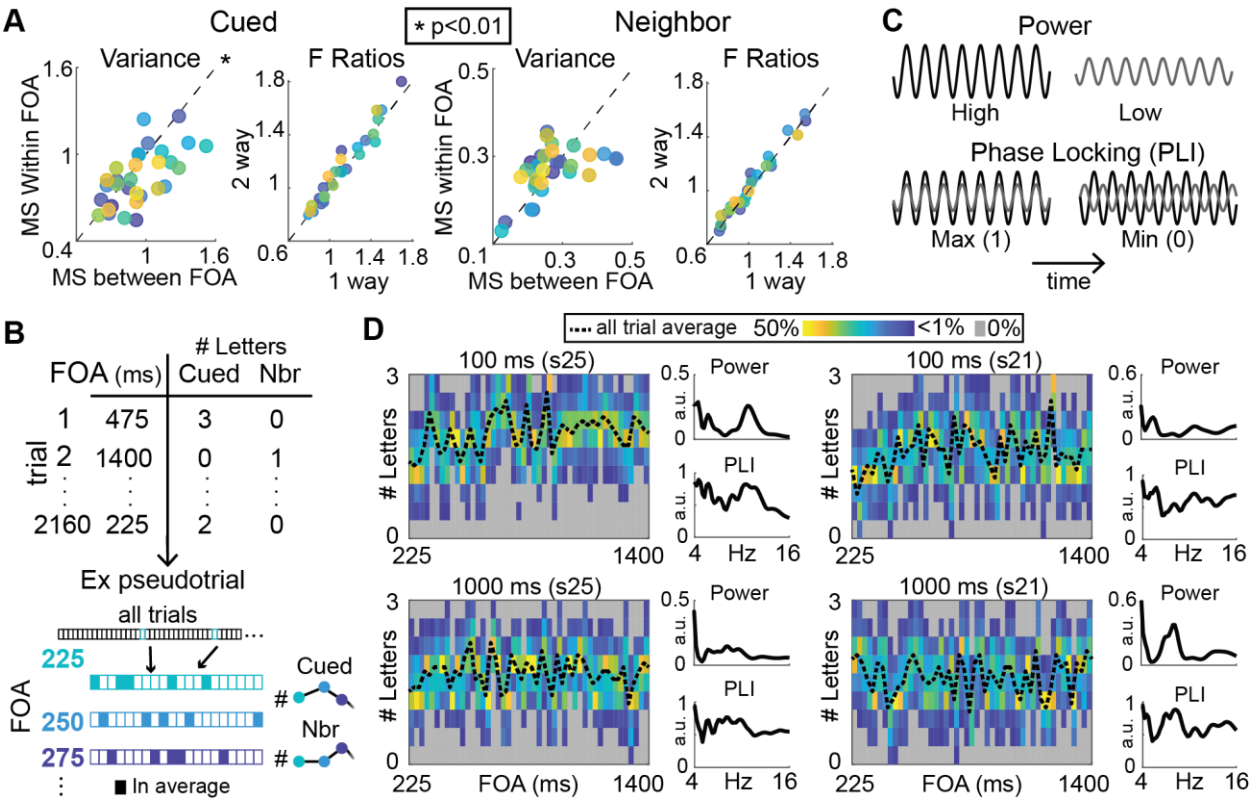

Figure 1.4: FOA Variance, pseudotrial construction and spectral metrics. **A:** Variance within and between FOA is compared by plotting the mean squared errors assessed using a one way ANOVA (left panels). Corresponding F-values of main effect of FOA was also compared between repeated measures one- (x-axis) and two- (y-axis) way ANOVAs. Dotted black lines plotted at unity, each subject is plotted in a different color, * indicates that greater between than within FOA variance. **B**: Top: An example matrix of response data at cued and neighbor locations. We subsampled this data to create pseudotrials (bottom). The process for one hypothetical pseudotrial is used as an example. For each FOA, a behavioral response was averaged over an independent, randomly chosen subset of 5 trials. This process was repeated to create 150 pseudotrials for both cued and neighbor (nbr) responses. **C:** Sinusoidal cartoon depictions of high vs low phase locking and power are plotted, the x-dimension represents time. These metrics will be used to assess behavioral rhythmicity. **D:** Heat maps of cued response pseudotrials are shown for the shortest and longest delays for example subjects 25 and 21 (s25 and s21). Yellow to blue colored areas indicate a high to low pseudotrials count for a specific number of letters and FOA, while gray areas indicate that no pseudotrials fell in that bin. Dotted line indicates the timecourse obtained by averaging over all trials within FOA. Finally, corresponding power and phase locking (PLI) plots are shown to the right of the example pseudotrial timecourses.

Thus, while there is *on average* more between vs within FOA variance, this analysis highlights considerable within-FOA variance across subjects. Thus instead of averaging over all trials of a particular FOA we created pseudotrials by averaging cued and neighbor recall over 5

randomly chosen trials for each FOA, essentially bootstrapping behavioral data to retain this within FOA variability so it is controlled for when assessing behavioral rhythmicity (Figure 1.4B; data averaged simultaneously over all FOAs traditional way available in Supplementary Results; see Methods). Additionally, this resampling allows us to assess both power and phase locking, along with their variability, at each frequency for each behavioral metric (Figure 1.4C; See methods). High power at a particular frequency measures the average *amount* of rhythmicity, agnostic to phase. High phase locking, on the other hand, indicates behavior is *consistently* phase locked with respect to the FFF (Figure 1.4C). We show pseudotrial counts and the trace obtained by averaging over all trials for two example subjects at the shortest and longest delays, along with corresponding power and phase locking estimates (Figure 1.4D).

Theta rhythmicity in cued recall

We next investigated the central hypothesis of this manuscript – whether the frequency of behavioral rhythmicity in letter recall is modulated by response precision and delay. For cued responses, we found that phase locking in the theta range increased with decreasing delays (Figure 1.5A; at 5.25 Hz, phase locking decreased from 0.62 ± 0.15 SD to 0.53 ± 0.12 SD from 100 ms to 1000 ms delays respectively; one-way repeated measures ANOVA with post-cue delay as factor: $F(2,60) = 5.04$, $p=0$; red dots indicate frequencies with $p< 0.05$, black stars indicate values that survive FDR correction at 0.05). A similar trend that did not survive FDR correction was seen at flanking frequencies (5 Hz and 5.5 Hz: $F(2,60)$'s = 2.7, 3.7, p's = 0.038, 0.006). Together, this indicates that cued iconic memory recall displays enhanced phase locking in the theta range.

While no main effects of post-cue delay survived FDR correction in the power analyses, there was a trend for increased theta power at the *longest* delay (Figure 1.5A, 6, 6.25 and 6.5 Hz; $F(2,60)$'s = 4.9, 5.5, 4.4, p's = 0.011, 0.011, 0.026 respectively). This is interesting because it mirrors an increase in theta power selective for longer, short-term memory delays that was

significant when power as computed the all-trial average (Figure 1.6A and Supplementary Results).

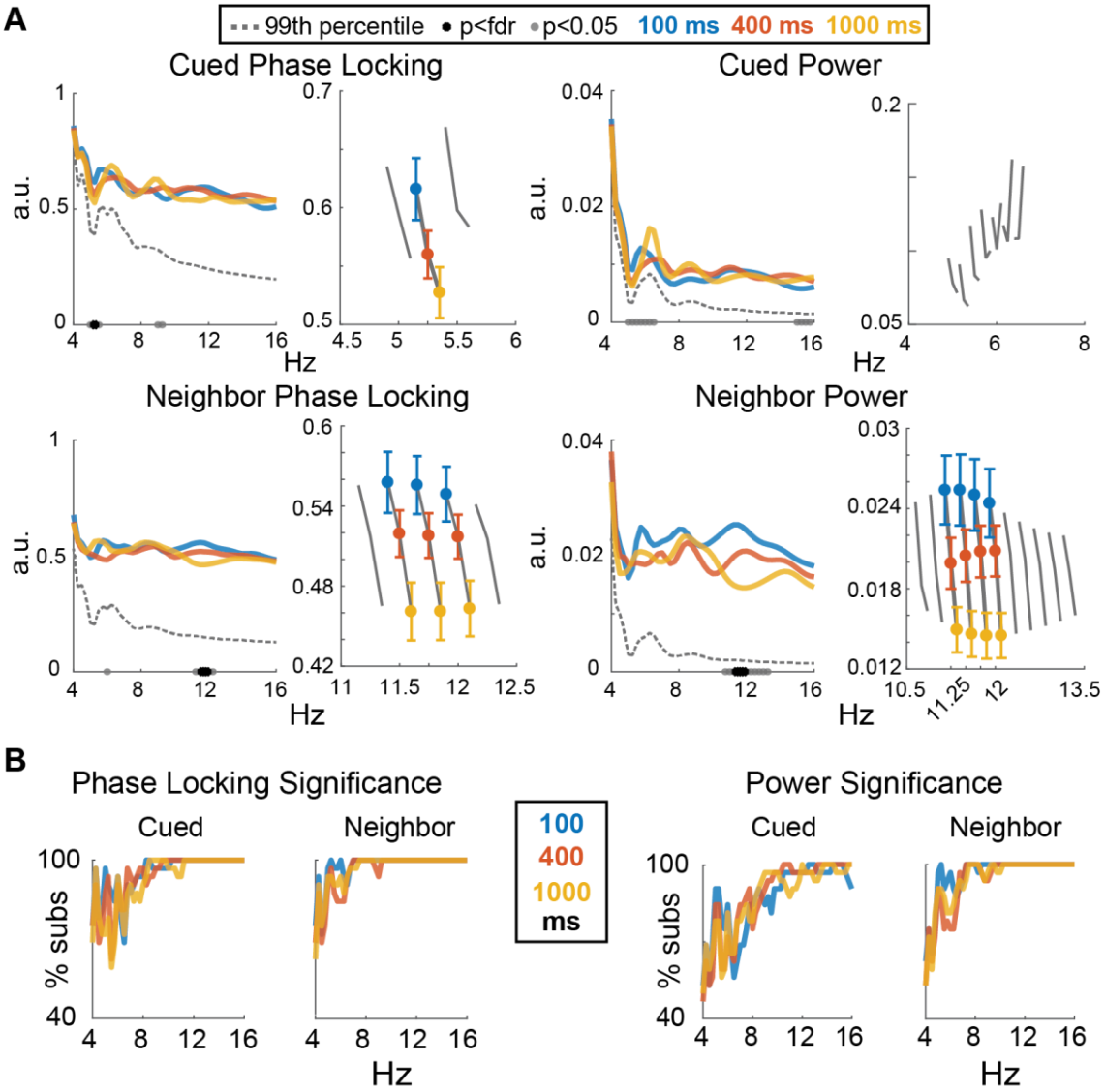

Figure 1.5: Rhythmic fluctuations in behavior. **A:** Left panels: Phase locking and power averaged over subjects, plotted for cued and neighbor responses. Dotted lines indicate the average 99th percentile of metrics randomized over subjects (see Methods). Frequencies with significant effect of post-cue delay indicated on the x axis (One-way repeated measures ANOVA; black stars mark frequencies that survive FDR correction at 0.05, gray dots do not survive FDR correction). Right Panels: Effects at significant frequencies are plotted. Colored points are plotted for frequencies that survive FDR correction, error bars indicate ±1SEM (significance determined by comparing to F values to those obtained from randomizing FOA over all delays). Gray lines are plotted for frequencies that do not survive FDR correction. **B:** Percent of subjects that show significantly greater than chance phase locking or power are plotted for each of the three delays ($p< 0.05$, significance determined by comparing power or phase locking at each frequency to those computed from 5000 timecourses obtained by randomizing FOA).

Alpha rhythmicity in neighbor recall during iconic delays

Interestingly, rhythmicity in neighbor responses was modulated by post-cue delay, but at alpha frequencies (Figure 1.5A; one-way repeated measures ANOVA, red dots indicate frequencies with $p< 0.05$, black stars indicate values that survive FDR correction at 0.05). Specifically, phase locking decreased with increasing delays at 11.5, 11.75 and 12 Hz ($F(2,60) = 5.6, 5.4, 4.4$, p's = 0.003, 0, 0.002 respectively). A similar trend that did not survive FDR correction was seen at flanking frequencies (11.25 and 12.25 Hz: $F(2,60)$'s = 4.9, 3.3, p's = 0.012, 0.013). Additionally, neighbor recall showed a monotonic decrease in power with increasing delays at similar alpha frequencies ($F(2,60)$s = 8.1, 8, 7.3, 6.4; at 11.5 Hz this effect was a decrease from 0.025 ± 0.015 SD to 0.021 ± 0.01 SD to 0.15 ± 0.01 SD at 100, 400 and 1000ms respectively). We also confirmed these effects from timecourses computing by averaging over all instances of an FOA simultaneously (Supplementary Results). Importantly, this effect was specific to the nearby, neighboring letters in the array, as no main effects of delay survived FDR correction in identical analyses concerning opposite responses (Figure 1.7B).

Together, these data provide evidence that iconic representations subject to an alpha rhythmic process governs imprecise spatial attentional allocation within iconic representations.

Broadband behavioral rhythmicity

Finally, subjects showed significantly greater than chance phase locking and power across the much of the power spectrum for both cued and neighbor responses (dotted black lines in Figure 1.5A and Figure 1.5B). This effect became especially pronounced at higher frequencies, where all subjects showed above-chance rhythmic behavior (individual subject significance evaluated at $p < 0.05$ determined by comparison to 5000 randomized timecourses). This indicates a substantial amount variability in the encoding of the letter array.

Conclusion

Partial report experiments utilizing short post-cue delays have identified the existence of iconic memory, a buffer stage between the perception of a stimulus and its consolidation into short-term memory previously characterized by high capacity but fragile representations (Reeves & Sperling, 1986; G Sperling, 1960; George Sperling & Gegenfurtner, 1993). Indeed, we found that recall of both cued and uncued letters decreased along the continuum from iconic representations to short-term memory encoding. Iconic delays were particularly characterized by subjects responding with letters just neighboring the cued letters, but also by fewer guesses. In sum, our data show that iconic representations are high capacity but subject to imprecise encoding and attentional allocation.

Interestingly, cued and neighboring letter responses appear to be rhythmically structured in distinct ways at iconic delays. Specifically, the recall of cued items was specifically associated with increased phase locking at theta frequencies, consistent with previous findings that theta oscillations positively impact cognitive and decision making performance (Landau, Marianne, Pelt, & Fries, 2015; Paul Sauseng, Klimesch, Schabus, & Doppelmayr, 2005; vanVugt, Simen, Nystrom, Holmes, & Cohen, 2012). This suggests the involvement of theta phase in the spatially precise attentional selection of perceived items. Interestingly, theta power was increased with increasing delays, in line with findings that theta rhythms underlie short-term memory processes (Jensen & Tesche, 2002; Klimesch, 1999; Paul Sauseng, Griesmayr, Freunberger, & Klimesch, 2010). Thus, while the precise allocation of attention within the iconic, perceptual representation fluctuated phasically in the theta band, theta rhythmicity in memory is not phase aligned. Thus, it is possible that short-term memory encoding occurs with an ongoing theta rhythm distinct from a phase-locked, evoked theta rhythm that is involved in perception. Further experiments with simultaneous neural recordings are necessary to confirm this possibility.

In addition, alpha rhythmic neighbor recall was associated with both increasing phase locking and power with decreasing delays. As both the power and phase of neural alpha oscillations have been previously found to underlie cortical inhibition and attentional allocation (Busch et al., 2009; Jensen et al., 2012; Jensen & Mazaheri, 2010; Kelly et al., 2009; Klimesch et al., 2007), we hypothesize that alpha rhythmic behavioral mechanisms underlie spatial imprecision in attentional selection, which has a cascading effect on subjects ability to distinguish uncued from cued letters in the iconic representation. Interestingly, how the phase and power of alpha oscillations in the brain simultaneously represent inhibitory processes is underexplored(Mathewson et al., 2011), although these results are consistent with previous findings that these metrics may be yoked measurements of a common underlying dynamical system(Nelli et al., 2017).

Together, our data show differential theta-rhythmic precise and alpha-rhythmic imprecise attentional selection using a paradigm with continuous response metrics. Note that alpha rhythmic detection is seen at passively monitored, cued objects in one previous report. We reconcile this with our results by observing the fact that letters are first passively encoded, after which subjects actually incorrectly confuse cued with neighbor letters. In that same report, theta rhythmicity was observed at uncued but actively monitored objects in that experiment, and we suggest our finding of theta rhythmicity in at cued locations is a result of a similar *active* engagement of attention in the iconic representation. Thus, our findings extend previous results showing that theta and alpha rhythmicity depend on the spatial spread of attention (Fiebelkorn et al., 2013; Landau & Fries, 2012).

Additionally, our results find elevations in both imprecise alpha and high-fidelity theta behaviors during iconic memory delays, providing a potential explanation for the representations maintained over short, iconic delays can be simultaneously high capacity but fragile. Further experiments exploring whether the dynamics of these behaviors are nested and whether they correspond to neural oscillations will be fruitful in understanding iconic representations.

Finally both phase locking and power analyses indicate that behavior shows fluctuations above chance at a wide range of frequencies and from iconic to short-term memory delays. This could indicate the presence of unstructured noise on top of structured, behavioral rhythms, or could be associated with specific cognitive operations employed in our task, possibilities that necessitates further explicit investigation.

Methods

Apparatus and Stimuli

The experiment was implemented using Psychtoolbox in the MATLAB programming environment running on a Windows PC with the XP operating system. Subjects were positioned 60 cm from the display and stimuli were presented on a 15-inch CRT monitor with 1024 x 768 resolution and 120 Hz refresh rate. The luminance output of the monitor was measured using a Minolta LS110 and linearized in the stimulus presentation software.

Memory Task

Here we use a partial report technique first reported in George Sperling 1960. Participants were instructed to recall 3 out of the 8 letters from a segment of the circle. Since the cue was randomized, participants had no prior knowledge about which letters to report and had to pay attention to as many letters as possible. Subjects were instructed to report all three letters corresponding with the spatial cue, and to guess when they were uncertain. The cue was centered on each of the 8 letter locations with equal probability, and with a uniform distribution over all trials and blocks. Subjects could freely report any number of letters with unrestricted time. However, if a subject's mean or median response time was greater than 4500 ms, they received feedback that they should respond more quickly. As subjects entered letters, these letters appeared on the screen above the empty circle. Subjects were instructed to press enter

when they were done. Finally, subjects were rewarded for reporting the 3 cued letters and penalized for reporting any other letters, with a mean reward of $2.45.

Each trial was separated by a variable ITI between 2250 and 2750 ms. At the beginning of each trial, the entire screen flashed white. A black circle with fixation point in the center was kept on the screen at all times except for when the entire screen flashed. At 1 of 48 possible variable intervals after this flash (pseudo-randomly chosen but uniform over all experimental blocks) an array of 8 letters was presented. The 8 presented letters could change on each trial but were sampled only from 16 possible letters. Out of 26 letters in the English Alphabet, the 6 vowels (‘a’, ‘e’, ‘I’, ‘o’, ‘u’, ‘y’) were excluded to prevent subjects from forming words to aid in memory recall. To get rid of further potential mnemonic devices or unintended sources of visual confusability, 4 additional consonants were excluded if they were rotated or constrained versions of other consonants (‘b’, ‘m’, ‘p’, ‘w’). Thus, on each trial 8 of the 16 possible letters were chosen to be presented around the circle.

On each trial, subjects were asked to report three of the eight presented letters at one of three different delays after the presentation of the array: 100 ms (iconic), 400 ms (border between iconic and short-term memory), and 1000 ms (short-term memory). Manipulating cue delay allowed us to replicate the results of Sperling’s experiment and further explore the relationship between behavioral rhythmicity and the continuum from perception to memory.

Each subject completed 2 to 4 sessions of 15 blocks each, where each block comprised of 48 trials. This lead to a minimum of 1440 trials, or 10 per FOA x Memory condition, and a maximum of 2880 trials, or 20 per FOA x Memory condition. Most subjects completed 3 sessions, leading to 15 trials per FOA x Memory condition (25/31 subjects, 2160 total trials).

Response metrics

For each trial, 3 different types of behavioral metrics were quantified. First, subjects could have accurate response counts from 0 – 3, depending on how many of the cued letters

were reported. Neighbor counts ranged from 0-2, depending on if one or both of the letters directly next to the cued location were reported. Opposite counts ranged from 0-3, and a response was considered a opposite response if it was one of the three letters not cued and not neighboring the cue (i.e. the letters farthest from the cued location). Responses of any of these three types contributed to the on-screen counts, which ranged from 0-3 and considered whether a typed letter was on the screen at all. Finally, error counts ranged from 0 to the number of responses made on each trial, and only consisted of reported letters that were not on the screen (note that skipped responses did not contribute to the error response count). Randomized values for each response metric were also created by shuffling the FOA and delay labels for response data 5000 times.

Subsampled behavioral data analysis

While previous studies have taken the mean over all instances of each FOA, this ignores much of the information that may be conveyed in the variability of responses over trials. We note that the ratios of between to within FOA variance were slightly but not significantly larger in a model controlling for delay ($t(30)$'s = 1.32, 0.77, 0.72, p's = 0.20, 0.45, 0.48 for cued, neighbor and opposite metrics respectively; paired t-tests on main effect of FOA subtracting one way repeated measures ANOVA from two way repeated measures ANOVA with FOA and delay as factors).

Due to this substantial within FOA variation, we chose to subsample FOA x Delay conditions in our behavioral estimates that were submitted to time frequency analyses. Fully averaged timecourses are still reported, but we also developed a subsampling method. During this method, we subsample 4, 5, or 6 trials within each FOA and contrast condition, and construct 150 subsampled trials from these timecourses. We determined these subsamples by computing the number of potential trial average combinations within FOA x Delay condition. Specifically, for subsamples from 1-10 we found 10, 45, 120, 210, 252, 210, 120, 45, 10 and 1

potential combinations of trial averages within FOA x Delay condition, respectively. Thus, we chose to analyze 4, 5, and 6 trial subsamples in order to maximize the within FOA variance we observed while still obtaining smooth behavioral estimates to submit to time frequency analysis. Note that this is somewhat conservative since the potential number of combinations is actually much higher than this since trials are selected independently for each FOA within a given pseudotrial. Using this method we are able to assess a more direct hypothesis of how this oscillatory modulation of visual memory should happen – namely phase locking. Phase locking over these subsampled trials should be high if responses are in fact consistent.

Supplementary Results

All trial effects

We found similar delay effects for all trials. Theta rhythmicity in cued responses increased with delay (effects that survive FDR correction at p=0.05: $F(2,60)$'s = 4.42, 5.65, 4.76, p's = 0.0002, 0.0002, 0.003 at 6, 6,25 and 6.5 Hz respectively; way repeated measures ANOVA red dots indicate frequencies with $p < 0.05$, black stars indicate values that survive FDR correction at 0.05).

Alpha rhythmicity in neighbor responses similarly decreased with delay (1 way repeated measures ANOVA). Specifically, at 10.75-12.25 Hz, alpha power decreased with increasing delays ($5.11 \leq F(2,60)\text{'s} \leq 7.78$, $0 \leq p\text{'s} \leq 0.005$). Finally, opposite responses did show rhythmicity at 9.5 Hz that decreased with delay ($F(2,60) = 3.12$, $p = 0.001$).

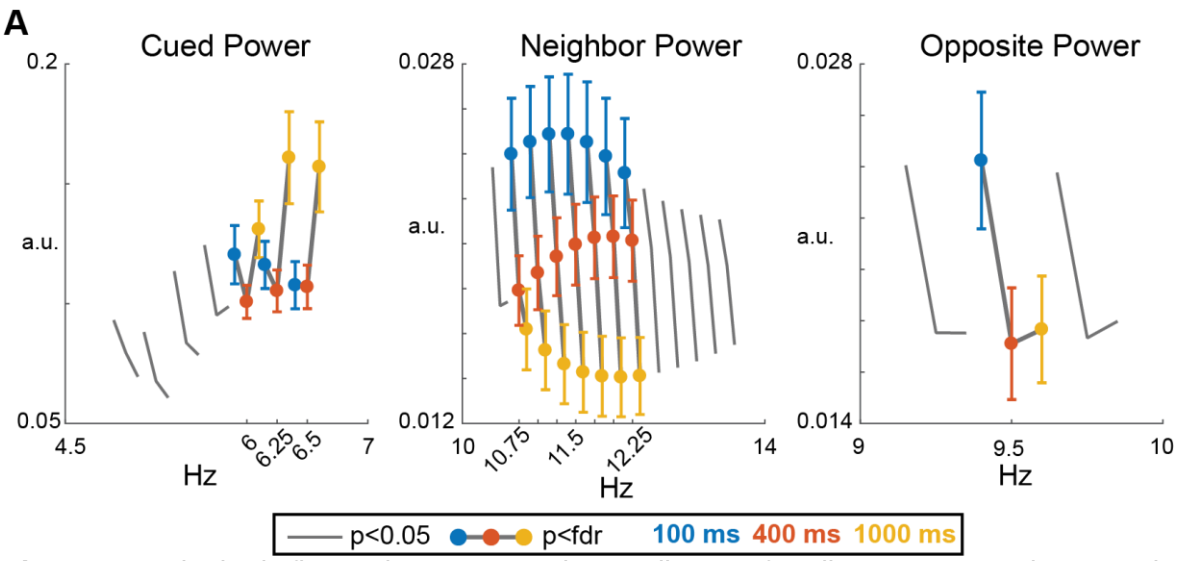

Figure 1.6: Rhythmic fluctuations averaged over all FOAs for all response metrics **A:** Only cued, neighbor, and opposite power are assessed, as phase locking requires more than one trial of data. Frequencies that show significant effects of delay after FDR correction are indicated by colored dots and numbered on the x axis, gray lines without colored dots indicate effects that do not survive FDR correction. The average phase locking or power are plotted for each of the 3 memory conditions, error bars indicate ±1 SEM.

Opposite responses

While on average there was more between vs within FOA variance for opposite responses, this effect was weak (Figure 1.7; average single subject F ratios = 1.02 and only 1 out of 31 subjects had F statistics with parametric p's<0.05 for opposite responses). Across subjects, opposite responses did not show consistently greater between vs within FOA variance (t-tests against 1 on F ratios: t(30) = 0.49, p = 0.5, significance computed by randomizing mean squared errors 5000 times; See Methods).

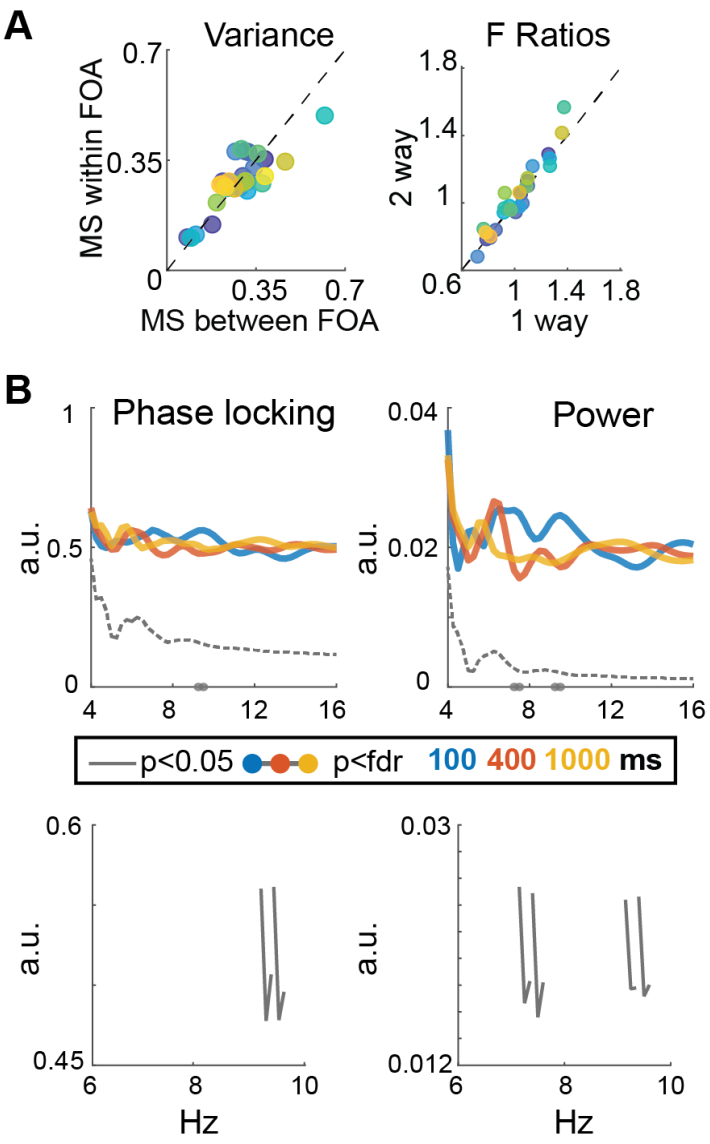

Figure 1.7: Opposite response results. **A:** Variance within and between FOA is compared by plotting the mean squares and corresponding F-values from main effects assessed using repeated measures 1 (x-axis) and 2 (y-axis) way ANOVAs. Dotted black lines plotted at unity, each subject is plotted in a different color, * indicates that there was more between than within FOA variance. **B:** Top Panels: Phase locking and power averaged over subjects are plotted for opposite responses. Dotted lines indicate the 99th percentile of randomized phase locking or power averaged over subjects. Frequencies that show significant effects of delay are indicated on the x axis (One way repeated measures ANOVA; black stars mark frequencies that survive FDR correction at 0.05, gray dots do not survive FDR correction). Bottom Panels: Frequencies with a significant effect of delay are plotted. The average phase locking or power are plotted for each of the delay conditions, colored points are plotted for frequencies that survive FDR correction on which error bars indicate SEM (significance determined by comparing to F values from ANOVAs on PLI and power computed from 3 timecourses chosen from 5000 in which we randomized FOA). Gray lines are plotted for frequencies at which the effect does not survive FDR correction.

Chapter 1, in full, is a reprint of the material as it appears in: Nelli, S., Chen, R., & Serences, J. T. (2019). *In prep*. The dissertation author was the primary investigator and author of this paper.

REFERENCES

Becker, M. W., Pashler, H., & Anstis, S. M. (2000). The role of iconic memory in change-detection tasks. *Perception*, *29*(3), 273–286. http://doi.org/10.1068/p3035

Broadbent, D. (1958). *Perception and communication*. *Perception and communication*. London: Pergamom Press. http://doi.org/10.1108/eb015727

Busch, N., Dubois, J., & VanRullen, R. (2009). The phase of ongoing EEG oscillations predicts visual perception. *The Journal of Neuroscience : The Official Journal of the Society for Neuroscience*, *29*(24), 7869–7876. http://doi.org/10.1523/JNEUROSCI.0113-09.2009

Buzsáki, G. (2002). Theta Oscillations in the Hippocampus. *Neuron*, *33*(3), 325–340. http://doi.org/10.1016/S0896-6273(02)00586-X

Buzsáki, G., & Moser, E. I. (2013). Memory, navigation and theta rhythm in the hippocampal-entorhinal system. *Nature Neuroscience*, *16*(2), 130–138. http://doi.org/10.1038/nn.3304

Cohen, M. R., & Maunsell, J. H. R. (2009). Attention improves performance primarily by reducing interneuronal correlations. *Nature Neuroscience*, *12*(12), 1594–1600. http://doi.org/10.1038/nn.2439

Cohen, M. R., & Maunsell, J. H. R. (2011). When Attention Wanders: How Uncontrolled Fluctuations in Attention Affect Performance. *Journal of Neuroscience*, *31*(44), 15802–15806. http://doi.org/10.1523/JNEUROSCI.3063-11.2011

Cowan, N. (1988). Evolving conceptions of memory storage, selective attention, and their mutual constraints within the human information-processing system. *Psychological Bulletin*. US: American Psychological Association. http://doi.org/10.1037/0033-2909.104.2.163

DI LOLLO, V. (1977). Temporal characteristics of iconic memory. *Nature*, *267*, 241. Retrieved from https://doi.org/10.1038/267241a0

Dugue, L., Marque, P., & VanRullen, R. (2011). The Phase of Ongoing Oscillations Mediates the Causal Relation between Brain Excitation and Visual Perception. *Journal of Neuroscience*, *31*(33), 11889–11893. http://doi.org/10.1523/JNEUROSCI.1161-11.2011

Faisal, a A., Selen, L. P. J., & Wolpert, D. M. (2008). Noise in the nervous system. *Nature Reviews Neuroscience*, *9*(4), 292–303. http://doi.org/10.1038/nrn2258.Noise

Fiebelkorn, I. C., Pinsk, M. A., & Kastner, S. (2018). A Dynamic Interplay within the

Frontoparietal Network Underlies Rhythmic Spatial Attention. *Neuron*, *99*(4), 842–853.e8. http://doi.org/10.1016/j.neuron.2018.07.038

Fiebelkorn, I. C., Saalmann, Y. B., & Kastner, S. (2013). Rhythmic sampling within and between objects despite sustained attention at a cued location. *Current Biology : CB*, *23*(24), 2553–2558. http://doi.org/10.1016/j.cub.2013.10.063

Foster, A. J. J., & Awh, E. (2018). The role of alpha oscillations in spatial attention: Limited evidence for a suppression account. *Current Opinion in Psychology*. http://doi.org/10.1016/j.copsyc.2018.11.001

Hasselmo, M. E., Hay, J., Ilyn, M., & Gorchetchnikov, A. (2002). Neuromodulation, theta rhythm and rat spatial navigation. *Neural Networks*, *12*(5), 689–707. http://doi.org/10.1016/S0893-6080(02)00057-6

Herweg, N. A., Apitz, T., Leicht, G., Mulert, C., Fuentemilla, L., & Bunzeck, N. (2016). Theta-Alpha Oscillations Bind the Hippocampus, Prefrontal Cortex, and Striatum during Recollection: Evidence from Simultaneous EEG-fMRI. *Journal of Neuroscience*, *36*(12), 3579–3587. http://doi.org/10.1523/JNEUROSCI.3629-15.2016

Jacobs, J., Hwang, G., Curran, T., & Kahana, M. J. (2006). EEG oscillations and recognition memory: Theta correlates of memory retrieval and decision making. *NeuroImage*, *32*(2), 978–987. http://doi.org/10.1016/J.NEUROIMAGE.2006.02.018

Jensen, O., Bonnefond, M., & VanRullen, R. (2012). An oscillatory mechanism for prioritizing salient unattended stimuli. *Trends in Cognitive Sciences*, *16*(4), 200–205. http://doi.org/10.1016/j.tics.2012.03.002

Jensen, O., & Mazaheri, A. (2010). Shaping functional architecture by oscillatory alpha activity: gating by inhibition. *Frontiers in Human Neuroscience*, *4*(November), 186. http://doi.org/10.3389/fnhum.2010.00186

Jensen, O., & Tesche, C. D. (2002). Frontal theta activity in humans increases with memory load in a working memory task. *European Journal of Neuroscience*, *15*, 1395–1399. http://doi.org/10.1046/j.1460-9568.2002.01975.x

Kelly, S. P., Gomez-Ramirez, M., & Foxe, J. J. (2009). The strength of anticipatory spatial biasing predicts target discrimination at attended locations: A high-density EEG study. *European Journal of Neuroscience*, *30*(May), 2224–2234. http://doi.org/10.1111/j.1460-9568.2009.06980.x

Klimesch, W. (1999). EEG alpha and theta oscillations reflect cognitive and memory performance: A review and analysis. *Brain Research Reviews*, *29*(2–3), 169–195. http://doi.org/10.1016/S0165-0173(98)00056-3

Klimesch, W., Sauseng, P., & Hanslmayr, S. (2007). EEG alpha oscillations: the inhibition-timing hypothesis. *Brain Research Reviews*, *53*(1), 63–88. http://doi.org/10.1016/j.brainresrev.2006.06.003

Lakatos, P., O'Connell, M. N., Barczak, A., Mills, A., Javitt, D. C., & Schroeder, C. E. (2009). The Leading Sense: Supramodal Control of Neurophysiological Context by Attention.

Neuron, *64*(3), 419–430. http://doi.org/10.1016/j.neuron.2009.10.014

Landau, A. N., & Fries, P. (2012). Attention samples stimuli rhythmically. *Current Biology*, *22*(11), 1000–1004. http://doi.org/10.1016/j.cub.2012.03.054

Landau, A. N., Marianne, H., Pelt, S. Van, & Fries, P. (2015). Distributed Attention Is Implemented through Theta-Rhythmic Gamma Modulation. *Current Biology*, *25*(17), 2332–2337. http://doi.org/10.1016/j.cub.2015.07.048

Landau, A. N., Schreyer, H. M., van Pelt, S., & Fries, P. (2015). Distributed Attention Is Implemented through Theta-Rhythmic Gamma Modulation. *Current Biology*, 1–6. http://doi.org/10.1016/j.cub.2015.07.048

Lisman, J. E., & Jensen, O. (2013). The Theta-Gamma Neural Code. *Neuron*, *77*(6), 1002–1016. http://doi.org/10.1016/j.neuron.2013.03.007

Lopes da Silva, F. (2013). EEG and MEG: Relevance to neuroscience. *Neuron*, *80*(5), 1112–1128. http://doi.org/10.1016/j.neuron.2013.10.017

Luck, S. J., & Vogel, E. K. (1997). The capacity of visual working memory for features and conjunctions. *Nature*, *390*, 279. Retrieved from https://doi.org/10.1038/36846

Makeig, S., Westerfield, M., Jung, T.-P., Enghoff, S., Townsend, J., Courchesne, E., & Sejnowski, T. J. (2002). Dynamic Brain Sources of Visual Evoked Responses. *Science*, *295*(5555), 690 LP-694. http://doi.org/10.1126/science.1066168

Mathewson, K. E., Gratton, G., Fabiani, M., Beck, D. M., & Ro, T. (2009). To see or not to see: prestimulus alpha phase predicts visual awareness. *The Journal of Neuroscience : The Official Journal of the Society for Neuroscience*, *29*(9), 2725–2732. http://doi.org/10.1523/JNEUROSCI.3963-08.2009

Mathewson, K. E., Lleras, A., Beck, D. M., Fabiani, M., Ro, T., & Gratton, G. (2011). Pulsed out of awareness: EEG alpha oscillations represent a pulsed-inhibition of ongoing cortical processing. *Frontiers in Psychology*, *2*(MAY), 1–15. http://doi.org/10.3389/fpsyg.2011.00099

Milton, A., & Pleydell-Pearce, C. W. (2016). The phase of pre-stimulus alpha oscillations influences the visual perception of stimulus timing. *NeuroImage*. http://doi.org/10.1016/j.neuroimage.2016.02.065

Nelli, S., Itthipuripat, S., Srinivasan, R., & Serences, J. T. (2017). Fluctuations in instantaneous frequency predict alpha amplitude during visual perception. *Nature Communications*, *8*(1). http://doi.org/10.1038/s41467-017-02176-x

Noonan, M. P., Adamian, N., Pike, X. A., Printzlau, F., Crittenden, B. M., & Stokes, M. G. (2016). Distinct Mechanisms for Distractor Suppression and Target Facilitation. *Journal of Neuroscience*, *36*(6), 1797–1807. http://doi.org/10.1523/JNEUROSCI.2133-15.2016

Raghavachari, S., Kahana, M. J., Rizzuto, D. S., Caplan, J. B., Kirschen, M. P., Bourgeois, B., … Lisman, J. E. (2001). Gating of human theta oscillations by a working memory task. *The Journal of Neuroscience : The Official Journal of the Society for Neuroscience*, *21*(9),

3175–3183. http://doi.org/21/9/3175 [pii]

Reeves, a, & Sperling, G. (1986). Attention gating in short-term visual memory. *Psychological Review*, *93*(2), 180–206. http://doi.org/10.1037/0033-295X.93.2.180

Rihs, T. A., Michel, C. M., & Thut, G. (2007). Mechanisms of selective inhibition in visual spatial attention are indexed by ??-band EEG synchronization. *European Journal of Neuroscience*, *25*(2), 603–610. http://doi.org/10.1111/j.1460-9568.2007.05278.x

Rizzuto, D. S., Madsen, J. R., Bromfield, E. B., Schulze-bonhage, A., Seelig, D., Aschenbrenner-scheibe, R., & Kahana, M. J. (2003). Reset of human neocortical oscillations during a working memory task. *Proceedings of the National Academy of Sciences*, (21). http://doi.org/10.1073/pnas.0732061100

Sauseng, P., Griesmayr, B., Freunberger, R., & Klimesch, W. (2010). Control mechanisms in working memory: A possible function of EEG theta oscillations. *Neuroscience and Biobehavioral Reviews*, *34*(7), 1015–1022. http://doi.org/10.1016/j.neubiorev.2009.12.006

Sauseng, P., Klimesch, W., Schabus, M., & Doppelmayr, M. (2005). Fronto-parietal EEG coherence in theta and upper alpha reflect central executive functions of working memory. *International Journal of Psychophysiology*, *57*, 97–103. http://doi.org/10.1016/j.ijpsycho.2005.03.018

Sauseng, P., Klimesch, W., Stadler, W., Schabus, M., Doppelmayr, M., Hanslmayr, S., … Birbaumer, N. (2005). A shift of visual spatial attention is selectively associated with human EEG alpha activity. *Eur J Neurosci*, *22*(11), 2917–2926. http://doi.org/EJN4482 [pii]\r10.1111/j.1460-9568.2005.04482.x

Scheeringa, R., Bastiaansen, M. C. M., Petersson, K. M., Oostenveld, R., Norris, D. G., & Hagoort, P. (2008). Frontal theta EEG activity correlates negatively with the default mode network in resting state. *International Journal of Psychophysiology*, *67*(3), 242–251. http://doi.org/10.1016/J.IJPSYCHO.2007.05.017

Shiffrin, R. M., & Atkinson, R. C. (1969). Storage and retrieval processes in long-term memory. *Psychological Review*, *76*(2), 179–193. http://doi.org/10.1037/h0027277

Sperling, G. (1960). The information available in brief visual presentations. *Psychological Monographs*.

Sperling, G., & Gegenfurtner, K. (1993). Information Transfer in Iconic Memory Experiments. *Journal of Experimental Psychology: Human Perception and Performance*.

Treisman, A. M. (1964). Selective attention in man. *British Medical Bulletin*, *20*(1), 12–16.

Treisman, A. M. (1969). Strategies and models of selective attention. *Psychological Review*. US: American Psychological Association. http://doi.org/10.1037/h0027242

van Kerkoerle, T., Self, M. W., Dagnino, B., Gariel-Mathis, M.-A., Poort, J., van der Togt, C., & Roelfsema, P. R. (2014). Alpha and gamma oscillations characterize feedback and feedforward processing in monkey visual cortex. *Proceedings of the National Academy of Sciences*, *111*(40), 14332 LP-14341. Retrieved from

http://www.pnas.org/content/111/40/14332.abstract

VanRullen, R., Carlson, T., & Cavanagh, P. (2007). The blinking spotlight of attention. *Proceedings of the National Academy of Sciences*, *104*(49), 19204–19209. http://doi.org/10.1073/pnas.0707316104

vanVugt, M. K., Simen, P., Nystrom, L. E., Holmes, P., & Cohen, J. D. (2012). EEG oscillations reveal neural correlates of evidence accumulation. *Frontiers in Neuroscience*, *6*(JULY), 1–13. http://doi.org/10.3389/fnins.2012.00106

von Stein, a, Chiang, C., & König, P. (2000). Top-down processing mediated by interareal synchronization. *Proceedings of the National Academy of Sciences of the United States of America*, *97*(26), 14748–14753. http://doi.org/10.1073/pnas.97.26.14748

Voytek, B., Canolty, R. T., Shestyuk, A., Crone, N. E., Parvizi, J., & Knight, R. T. (2010). Shifts in gamma phase-amplitude coupling frequency from theta to alpha over posterior cortex during visual tasks. *Front Hum Neurosci*, *4*(October), 191. http://doi.org/10.3389/fnhum.2010.00191

Voytek, B., Kayser, A. S., Badre, D., Fegen, D., Chang, E. F., Crone, N. E., … D'Esposito, M. (2015). Oscillatory dynamics coordinating human frontal networks in support of goal maintenance. *Nature Neuroscience*, (July), 1–10. http://doi.org/10.1038/nn.4071

Worden, M. S., Foxe, J. J., Wang, N., & Simpson, G. V. (2000). Anticipatory biasing of visuospatial attention indexed by retinotopically specific alpha-band electroencephalography increases over occipital cortex. *The Journal of Neuroscience*, *20*(6), RC63. http://doi.org/Rc63

Chapter 2: Fluctuations in instantaneous frequency predict alpha amplitude during visual perception

Abstract

Rhythmic neural activity in the alpha band (8-13 Hz) is thought to play an important role in the selective processing of visual information. Typically, modulations in alpha amplitude and instantaneous frequency are thought to reflect independent mechanisms impacting dissociable aspects of visual information processing. However, in complex systems with interacting oscillators such as the brain, amplitude and frequency are mathematically dependent. Here we record electroencephalography (EEG) in human subjects and show that both alpha amplitude and instantaneous frequency predict behavioral performance in the same visual discrimination task. Consistent with a model of coupled oscillators, we then show that fluctuations in instantaneous frequency predict alpha amplitude on a single trial basis, empirically demonstrating that these metrics are not independent. This interdependence suggests that changes in amplitude and instantaneous frequency reflect a common change in the excitatory and inhibitory neural activity that regulates alpha oscillations and visual information processing.

Introduction

Encoding and transferring sensory information between neural ensembles relies on a balance of excitatory and inhibitory neural activity (E/I balance) that is reflected in ongoing oscillatory activity (Akam & Kullmann, 2014; Anderson, Carandini, Ferster, & Sherman, 2000; Atallah & Scanziani, 2009; Azouz & Gray, 2000; Brunel & Wang, 2003; Carandini & Heeger, 2012; Draguhn, Buzsáki, Andreas, & Draguhn, 2004; Pascal Fries, 2005, 2015; Heeger, 1992; Isaacson & Scanziani, 2011; F. Lopes da Silva, 2013; Mazzoni, Panzeri, Logothetis, & Brunel, 2008; Saalmann, Yuri B., Pigarev, Ivan N., Vidyasagar, 2007; Salinas & Sejnowski, 2001; van Vreeswijk & Sompolinsky, 1996). Many studies of information processing in visual cortex have

focused on the role of oscillatory activity in the alpha band – a particularly prominent set of oscillations ranging from approximately 8-13Hz. One theory, referred to here as the desynchronization account, holds that default alpha amplitude is relatively large in visual cortex, reflecting strong population-level synchronization and suppression of visual information processing. In contrast, when processing visual input, the E/I balance in relevant local circuits shifts, leading to a local desynchronization from the default rhythm and a subsequent reduction in alpha amplitude (P Fries, Reynolds, Rorie, & Desimone, 2001; Pascal Fries, Womelsdorf, Oostenveld, & Desimone, 2008; Wolfgang Klimesch, 1996; Wolfgang Klimesch, Sauseng, & Hanslmayr, 2007; Pfurtscheller, 2001; Salinas & Sejnowski, 2001; Shao & Burkhalter, 1996; von Stein, Chiang, & König, 2000). Consistent with this framework, high alpha amplitude is associated with reduced perceptual sensitivity, presumably due to a failure of relevant local circuits to desynchronize from the default rhythm(Busch, Dubois, & VanRullen, 2009; Dugue, Marque, & VanRullen, 2011; Mathewson, Gratton, Fabiani, Beck, & Ro, 2009). Furthermore, alpha amplitude modulations track the relevance of stimuli in a topographically selective manner: spatial attention decreases amplitude in areas of visual cortex encoding attended regions of the visual field and increases amplitude in areas encoding task-irrelevant regions (Bosman et al., 2012; Foxe, Simpson, & Ahlfors, 1998; P Fries et al., 2001; Händel, Haarmeier, & Jensen, 2011; Kelly, Gomez-Ramirez, & Foxe, 2009; Meeuwissen, Takashima, Fernández, & Jensen, 2011; Rihs, Michel, & Thut, 2007; Sauseng et al., 2005; Yamagishi, Callan, Anderson, & Kawato, 2008). Finally, the relatively slow time-scale of these amplitude modulations (>100ms) suggests correspondingly slow alterations between periods of efficient and inefficient visual information processing (For review see (Wolfgang Klimesch et al., 2007)).

While the desynchronization hypothesis focuses on relatively slow changes in alpha amplitude, rapid, cycle-by-cycle fluctuations in alpha oscillations are also thought to reflect alterations in the E/I balance and hence the efficacy of visual information processing (Atallah & Scanziani, 2009; Busch et al., 2009; Dugue et al., 2011; Hasenstaub et al., 2005; Lakatos et al.,

2009; Lakatos, Karmos, Mehta, Ulbert, & Schroeder, 2008; Mathewson et al., 2009; Samaha & Postle, 2015; Womelsdorf et al., 2007). This account, referred to here as the instantaneous frequency account, posits that epochs of neural excitability and efficient visual information processing are associated with a particular phase of ongoing alpha oscillations. These shorter and more rapidly occurring alternations in the E/I balance are thought to enhance perception both by sharpening feature tuning to stimuli and by temporally concentrating neural activity, thereby increasing the probability of propagation of activity to downstream areas (Draguhn et al., 2004; P Fries et al., 2001; Isaacson & Scanziani, 2011; E.M. Izhikevich, 2003; Kayser, Montemurro, Logothetis, & Panzeri, 2009; Lowet, Roberts, Peter, Gips, & Weerd, 2016; Wehr & Zador, 2003). Consistent with this account, a recent report suggests that instantaneous alpha frequency reflects the temporal density of periods of maximal perceptual sensitivity and the rate at which visual information is sampled and processed (Samaha & Postle, 2015). Thus, similar to the desynchronization account, the instantaneous frequency account also holds that alpha oscillations index changes in the E/I balance and the efficiency of information processing. However, the transitions between information processing states indexed by instantaneous frequency are theoretically linked to changes in the sampling rate of the visual system and occur on a finer temporal scale than the more sustained transitions associated with alpha amplitude modulations.

As outlined above, alpha amplitude (A) and instantaneous frequency (ω) are typically assumed to reflect independent processes, meaning that a sinusoidal voltage measurement (V) at time *t* can be written simply as $\mathbf{V}(t) = A\sin(\omega t)$. However, work in mathematics and dynamical theory suggests that these assumptions may be an over simplification, especially in complex systems like the brain (for review see (Boccaletti, Kurths, Osipov, Valladares, & Zhou, 2002)). Instead, interactions between the oscillations in driving and target neural regions could give rise to interdependencies between amplitude and frequency. As a simple analogy, imagine jumping on a trampoline with a partner jumping at very dissimilar rate, or frequency. In this case,

the height, or amplitude, of your jumps will be relatively low. As your partner changes the frequency (and phase) of their jumps to match yours, the amplitude of your jumps will increase (a situation referred to as resonance). However, even with maximal resonance you cannot jump infinitely high because of other factors such as air resistance and the finite stretchiness of the trampoline, forces that act as damping mechanisms. Although not a perfect analogy, this conceptual framework can serve as a starting point to understand interactions between the amplitude and instantaneous frequency of cortical responses in the alpha band. Here we sought to first articulate the formal relationship between frequency and amplitude, and then to empirically test the proposed relationship using EEG. Our results suggest that amplitude and frequency are linked and thus both metrics likely reflect the operation of a common dynamical system that supports efficient visual information processing.

Results

Linking Amplitude and Frequency

Amplitude and frequency are often discussed as independent metrics, although in complex systems they can be tightly coupled. Consider two interacting neural ensembles that naturally oscillate at different characteristic frequencies, such as might be observed in the thalamo-cortical or cortico-cortical circuits that give rise to alpha oscillations (Başar, Schurmann, Başar-Eroglu, & Karaka, 1997; F. H. Lopes da Silva, Vos, Mooibroek, & van Rotterdam, 1980). Here we focus on coupled harmonic oscillators for simplicity, although detailed biophysical models exist(Aronson, Ermentrout, & Kopell, 1990; Boccaletti et al., 2002; Eugene M Izhikevich, 2001). First, let the uncoupled driving and target regions oscillate at characteristic frequencies ω_D and ω_T, which themselves depend on connectivity and local E/I activity (Hutcheon & Yarom, 2000; Wang, 2010). When considered as a coupled system, alpha amplitude in the target region (A_T) will be a function (f) of both the amplitude of the oscillatory drive (A_D) and the difference

between the frequency of the driving and target oscillator, or $A_T = A_D * f(\omega_T - \omega_D)$ (See Methods for model and derivation). Additionally, the neural oscillations evoked by stimuli are transient (i.e. damped), making neurons sensitive to fine temporal structure in sensory inputs or inputs from other neuronal populations(Eugene M Izhikevich, 2001). Interestingly, the damping mechanisms that regulate the oscillatory response to these inputs (for example: leak conductance, capacitance, and voltage-gated currents(Draguhn et al., 2004)) will also modulate the *effective* characteristic frequency in the target region (ω_{eT})(Draguhn et al., 2004; Hutcheon & Yarom, 2000). This means that the maximum possible characteristic frequency in the target region is bounded by the theoretical characteristic frequency ($\omega_T \geq \omega_{eT}$). Substituting into the above statement, we now have $A_T = A_D * f(\omega_{eT} - \omega_D)$ (Methods). This potential dependence complicates the traditional interpretation of alpha amplitude and instead suggests that shifts in amplitude reflect changes in the instantaneous frequency of the underlying dynamical system, which could arise given changes in oscillatory drive (ω_D), local dampening (ω_{eT}), or local characteristic frequency (ω_T; Methods).

The amplitude spectrum of typical EEG signals recorded over visual cortex shows a pronounced and focal bump centered on the dominant alpha frequency (Figure 2.1b). This focal alpha bump is thought to be the result of resonant responses between interacting neural oscillators (Draguhn et al., 2004; Hutcheon & Yarom, 2000; E.M. Izhikevich, 2003) (note the similarity to Figure 2.2.1a). Thus, we hypothesized that the frequency-amplitude relationship outlined above is reflected in each subject's alpha bump. We expect that changes in the instantaneous frequency will lead to changes in amplitude, and that the precise nature of these changes will be captured by the shape of each subject's spectrum (Figure 2.1a-c).

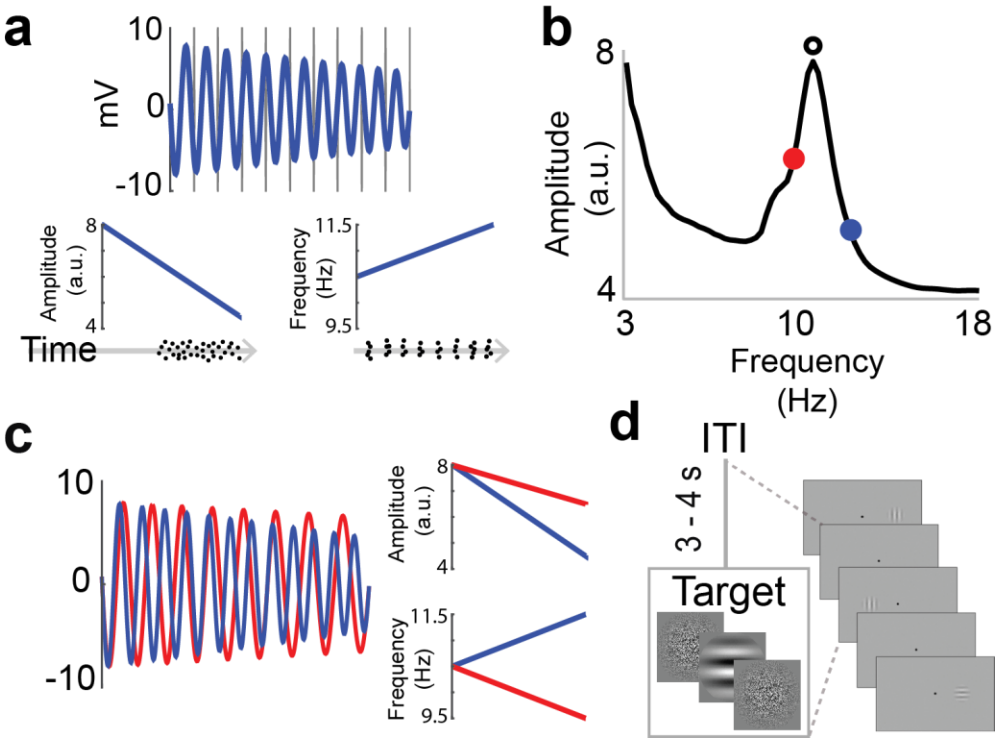

Figure 2.1: Hypothesis and task design **a)** A simulated example of an alpha oscillation that is both increasing in frequency and decreasing in amplitude over time, as exemplified in the left and right plots underneath, respectively. Vertical lines indicate evenly spaced time bins matching 1 cycle of the initial oscillatory frequency. Plotted below the amplitude and frequency traces are hypothetical raster plots corresponding with periods of efficient visual information processing according to the desynchronization and instantaneous frequency hypotheses, respectively. **b)** Amplitude spectrum from a representative subject. Note the general 1/f distribution of amplitude over frequency, and the pronounced bump in the alpha range. The circular outline indicates peak alpha frequency, while gray dots indicate hypothetical shifts away from the peak alpha frequency over the course of the trials outlined in c**. c)** Along with the same example trial in b), now termed a correct trial, we have plotted a hypothetical incorrect trial that decreases in frequency and amplitude with magnitudes corresponding with the spectrum in c). Note that on the left side of the panel, the two traces are in phase, but become out of phase over the course of the trial, meaning frequency shifts could lead to offsets in phase through a relative speeding or slowing of the underlying signals. In addition to phase offsets, shifts in frequency away from peak alpha could also impact alpha amplitude as shown in the bottom right panel. **d)** Task Design. The target was a Gaussian - windowed Gabor (mean contrast = 5%) presented for 8.3 ms. The target was immediately preceded and followed by one frame (~8.3 ms each) of Gaussian - windowed white noise. Between target presentations, subjects passively fixated at the center of a grey screen for 3000-4000 ms (uniform distribution of ITIs). Target location (centered 8.5º left or right from fixation) was randomly selected with the only constraint that an equal number of trials were presented on both sides of fixation.

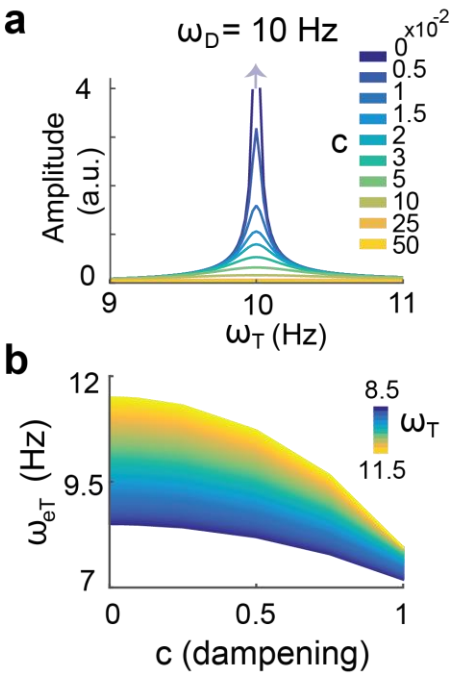

Figure 2.2: Oscillatory drive and dampening link amplitude and frequency **a)** When being driven at 10 Hz, amplitude in the target region is determined by the local frequency for a range of damping values (indicated by the colored lines and legend). With zero dampening (purple line), and frequency in the target region = 10 Hz, runaway resonance occurs (i.e. amplitude approaches infinity), as indicated by the purple arrow. **b)** This dampening that prevents infinite amplitude also effects the effective frequency in the target region, further determining where the target region falls on the x-axis of panel A. With more damping, the effective frequency in the target region falls.

Experiment 1

Visual Discrimination

To test the potential interdependence between instantaneous frequency and amplitude, we designed a task in which subjects reported whether a low contrast Gabor presented for ~8.3 ms was horizontal or vertical (two alternative-forced-choice orientation discrimination task, Figure 2.1d). A target Gabor could be presented on either the left or right side of the screen with a variable interval of 3000-4000 ms separating presentations. Performance during EEG recording was carefully titrated to 65% (± 2.8% SD) to obtain enough incorrect trials. Mean reaction time was 1106 ms, with faster RTs for correct (1073 ms) as compared to incorrect (1170 ms) trials (paired t-test $t(15) = -6.33$, $p < 0.0001$). Finally, subjects performed equally well

on trials with vertical and horizontal targets and displayed no bias toward targets presented on one side of the screen (paired t-test, both t(15)'s < 0.87, p's>0.4).

Characterizing ERPs Alpha Amplitude and Alpha Frequency

Before directly assessing the potential link between alpha amplitude and instantaneous frequency, we first make contact with similar experimental paradigms by replicating event related potential (ERP), alpha amplitude, and instantaneous frequency results from electrode groups contralateral and ipsilateral to the target location (Figure 2.3a, Methods). We characterized task-related modulations of two ERP components evident in the grand average waveforms: an early negative deflection thought to index sensory processing and attentional selection (Heinze, Luck, Mangun, & Hillyard, 1990; Hickey, Van Zoest, & Theeuwes, 2010; Itthipuripat, Cha, Rangsipat, & Serences, 2015; G. R. Mangun & Hillyard, 1988; G R Mangun & Hillyard, 1987; George R. Mangun & Buck, 1998; Voorhis & Hillyard, 1977), and a central-parietal late positive deflection thought to index post-sensory decision-related processing (e.g., decision difficulty, speed, and confidence) (Elton et al., 1997; Itthipuripat, Ester, Deering, & Serences, 2014; George R. Mangun & Buck, 1998; Squires, Donchin, & Squires, 1977; Yordanova, Kolev, & Polich, 2001). The early negative deflection (210-260 ms post-stimulus, see Methods) was significantly larger in electrodes contralateral compared to ipsilateral to the target ($t(15) = -3.4$, $p = 0.0001$), and showed a significant interaction between electrode location and behavioral performance ($t(15) = -3.1$, $p = 0.01$, Figure 2.3b,c; Table 2.1). The late positive deflection (460-510 ms post stimulus, see Methods) was larger on correct compared to incorrect trials ($t(15) = 6.5$, $p=0.0$), and higher amplitude in contralateral compared to ipsilateral electrodes ($t(15) = 2.1$, $p=0.0499$, Figure 2.3b,c; Table 2.1). Note that the slightly delayed peaks of our ERP components are consistent with the low contrast of our stimulus and difficulty of our task(Busch et al., 2009; Cravo, Rohenkohl, Wyart, & Nobre, 2013; George R. Mangun & Buck,

1998). Together, these results suggest that sensory representations were topographically selective and that decision processes were impaired on incorrect trials.

Table 2.1: Analysis of the early negative and the late positive event-related potentials. First, data were analyzed as a function of the location of electrodes with respect to the target (i.e. the amplitude of ERP responses in electrodes that were contralateral or ipsilateral to the target). Next, comparisons were made between correct and incorrect trials, separately for contralateral and ipsilateral electrodes. Finally, the interaction between electrode position (contralateral/ipsilateral) and behavioral accuracy was assessed. Note that all statistical tests are reported as t-tests on difference scores instead of F-values that would be obtained in an analysis of variance (ANOVA). This was done to maintain consistency across comparisons, and produces identical outcomes (t is the square root of F in this situation). All tests report t-tests on the average amplitude values within pre-defined 50 ms windows from 210-260 and 460-510 ms post stimulus for the END and LPD respectively. T values were compared against distributions obtained empirically by randomizing condition labels 10,000 times and then repeating the same statistical test (see Methods). * indicates a significant effect at p = 0.05.

	Early Negative Deflection	**Late Positive Deflection**
Contralateral vs Ipsilateral	*t(15) =-3.435, p= 0.0001	*t(15) = 2.129, p=0.0499
Accuracy, contralateral electrodes	t =-1.745, p=0.0984	*t(15) = 6.548, p=0.0
Accuracy, ipsilateral electrodes	t=1.258, p=0.2281	*t(15) = 7.028, p=0.0
Location x Accuracy Interaction	*t(15) = -3.053, p = 0.01	t(15) =-1.244, p=0.2301

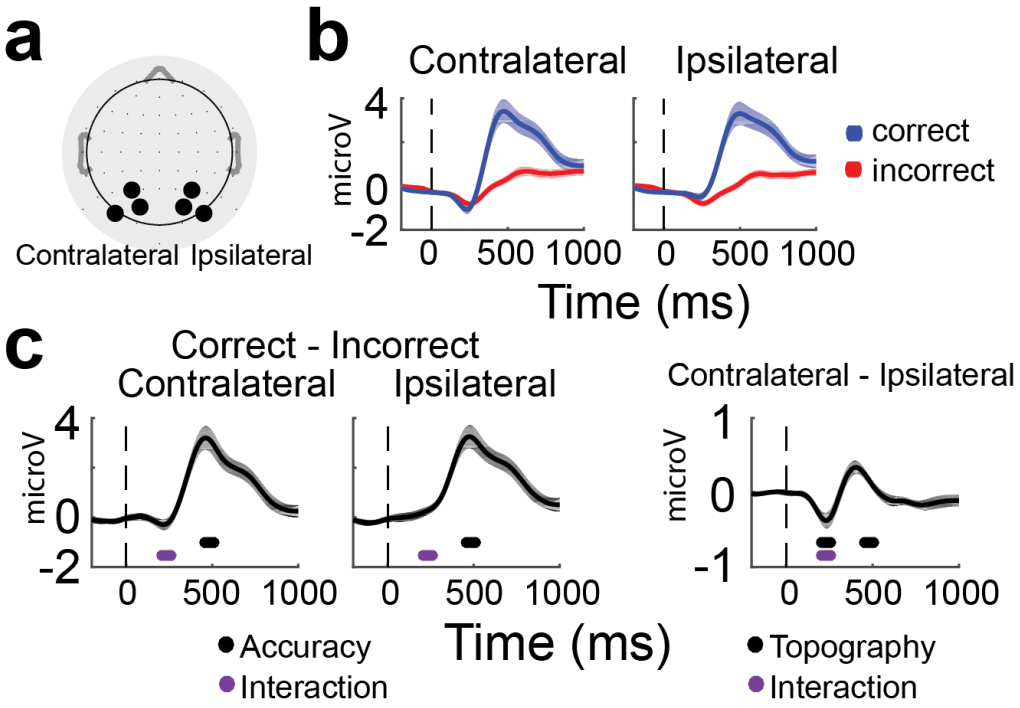

Figure 2.3 Event-related potentials confirm involvement of perceptual processes. **a** ERPs on correct (blue) and incorrect (red) trials in the contralateral and ipsilateral electrodes indicated in the topography plot to the right in panel b (note that electrode labels are flipped accordingly so that, by convention, electrodes contralateral to the target are shown on the left, see Methods). Dashed vertical line indicates target onset. **b** Topography for contralateral and ipsilateral electrodes used for all analyses are outlined on the 64 electrode Biosemi electrode scheme used in these experiments. **c** Difference waves between correct and incorrect trials. The END is more negative in contralateral than ipsilateral electrodes, resulting in a significant interaction between behavioral performance (correct vs. incorrect) and electrode location (contralateral vs. ipsilateral). Most significantly, there is a sustained increase in LPD amplitude on correct as compared with incorrect trials in both contralateral and ipsilateral electrodes. Dots below waveforms indicate a significance difference from zero as obtained from resampled t-tests performed on average amplitudes within the 50 ms time windows indicated by the dot width (210–260 and 460–510 ms post stimulus for the END and LPD, respectively). Significant main effects are indicated in black while purple indicates a significant interaction, all at P = 0.05

Next, we examined whether modulations in alpha amplitude predicted behavioral performance. Note that many previous studies utilized attentional cues and analyzed anticipatory, pre-stimulus decreases in alpha amplitude (Mathewson et al., 2009; Rohenkohl & Nobre, 2011; Yamagishi et al., 2008). However, since there was no advanced information concerning target location or timing in our paradigm, we expected to find amplitude decreases only for review [64]). Consistent with previous reports, the average magnitude of post-stimulus alpha amplitude decreases depended on both behavioral accuracy and electrode location such

that there were larger decreases on correct trials, in contralateral electrodes compared to ipsilateral electrodes (leading to an interaction between behavioral performance and electrode location; Figure 2.4a;[17,26,33,64,6517,26,33,64,65]). These amplitude decreases are consistent with the desynchronization account that decreases in alpha amplitude reflect a desynchronization of local alpha rhythms from a state that impairs visual information processing.

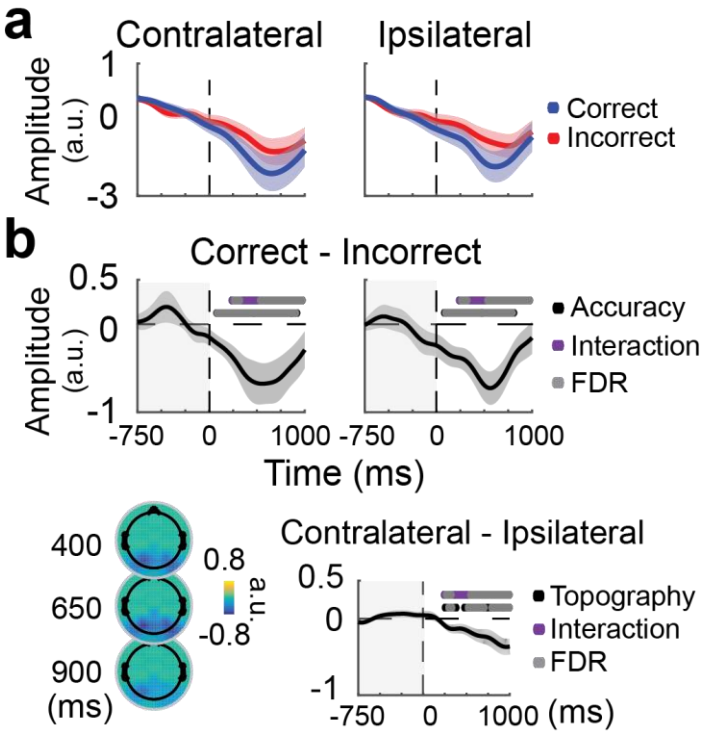

Figure 2.4: Topographically selective decreases in posts-timulus amplitude predict accuracy **a)** The timecourse of alpha amplitude on correct (blue) and incorrect (red) trials in the contralateral and ipsilateral electrodes indicated in Figure 2.1. Amplitude timecourses are baselined to -1000 to -750 ms pre stimulus, and shaded areas indicate ±1 SEM within subject. **b)** Alpha amplitude decreases more on correct compared to incorrect trials in both contralateral and ipsilateral electrodes. Furthermore, the decrease in alpha amplitude is topographically selective, displaying larger decreases contralateral to the target. Topographic plots indicate the difference between correct and incorrect trials averaged over 100 ms bins centered on 0.4, 0.65 and 0.9 seconds after stimulus onset. All dots indicate significance from zero, evaluated by comparing the obtained t-value with a null distribution of t-values computed by shuffling the condition labels 10,000 times. This analysis was done on a timepoint-by-timepoint basis from stimulus onset to +1 second, as indicated by the non-shaded areas (see Methods). Main effects with P<0.05 are indicated in black, and gray dots indicate significance after FDR correction at P=0.05.

We then assessed whether higher instantaneous alpha frequency results in enhanced sensitivity to incoming visual information, as recently reported by Samaha & Postle 2015 (Samaha & Postle, 2015) (for instantaneous frequency derivation see Methods and (Cohen, 2014)). On average, we found significantly faster pre-stimulus instantaneous alpha frequency on correct trials, but only in contralateral electrodes ($t(15) = 3.4$, $p=0.0008$, Figure 2.5a,b; Table 2.2). These pre-stimulus shifts in instantaneous frequency may reflect a voluntary process of preparing for target processing. However, we cannot rule out the possibility that these shifts in frequency reflect spontaneous fluctuations because we did not use a pre-cue and we post-hoc sorted the trials based on behavioral performance. In either case, this pattern of results is consistent with the hypothesis that increases in instantaneous alpha frequency in regions processing relevant information correspond to more efficient sampling and processing of visual information. Indeed, instantaneous frequency shifts of similar magnitudes have been reported to impact the effective resolution of visual perception(Samaha & Postle, 2015) and spike timing in biophysical models (Cohen, 2014).

Table 2.2: Amplitude, Frequency and PaA are modulated by experimental conditions. The empirically observed amplitude, instantaneous frequency and predicted alpha amplitude (PaA) as a function of electrode location and behavioral performance. All tests report the maximum or minimum timepoint-by-timepoint t-values over a temporal window extending from target onset to 1000ms after target onset for the amplitude and PaA metrics, and from -500ms to target onset for the frequency analysis. T-values were compared against distributions obtained empirically by randomizing condition labels 10,000 times and then repeating the same statistical test (see Methods). Reported t-values are from the timepoint with smallest p-value. * indicates that p-values were significant after FDR correction at alpha = 0.05 from stimulus onset to +1,000ms (amplitude and PaA) or -500ms to target onset (instantaneous frequency).

	Amplitude	**Instantaneous Frequency**	**PaA**
Contralateral vs Ipsilateral	*t(15) = -3.576, p=0.0	t(15)= - 1.823, p=0.0827	t(15) = - 3.167, p =0.0009
Accuracy (contralateral electrodes)	*t(15) =-2.9994, p=0.0006	*t(15) = 3.399, p=0.0015	t(15) = -2.279, p = 0.0141
Accuracy (ipsilateral electrodes)	*t(15) = -3.878, p=0.0	t(15) = 1.583, p= 0.135	*t(15) = -3.597, p=0.0001
Location x Accuracy Interaction	*t(15) = -3.197, p= 0.0002	t(15) = 2.549, p=0.0248	t(15) = 2.134, p=0.0399

Predicting alpha amplitude (PaA)

As shown in Figure 2.5c, instantaneous alpha frequency is highly dynamic and fluctuates by 5.93 ± 0.64 Hz over the course of single trials (mean ± SD, Figure 2.5c). To test the hypothesis that task-related instantaneous frequency shifts result in concurrent modulations in alpha amplitude, we used instantaneous frequency to index into amplitude spectra for each subject and electrode. This analysis effectively treats the spectra as look-up-tables to generate predicted alpha amplitudes (PaA) on each timepoint and trial (Figure 2.1b, Figure 2.9c, see Methods).

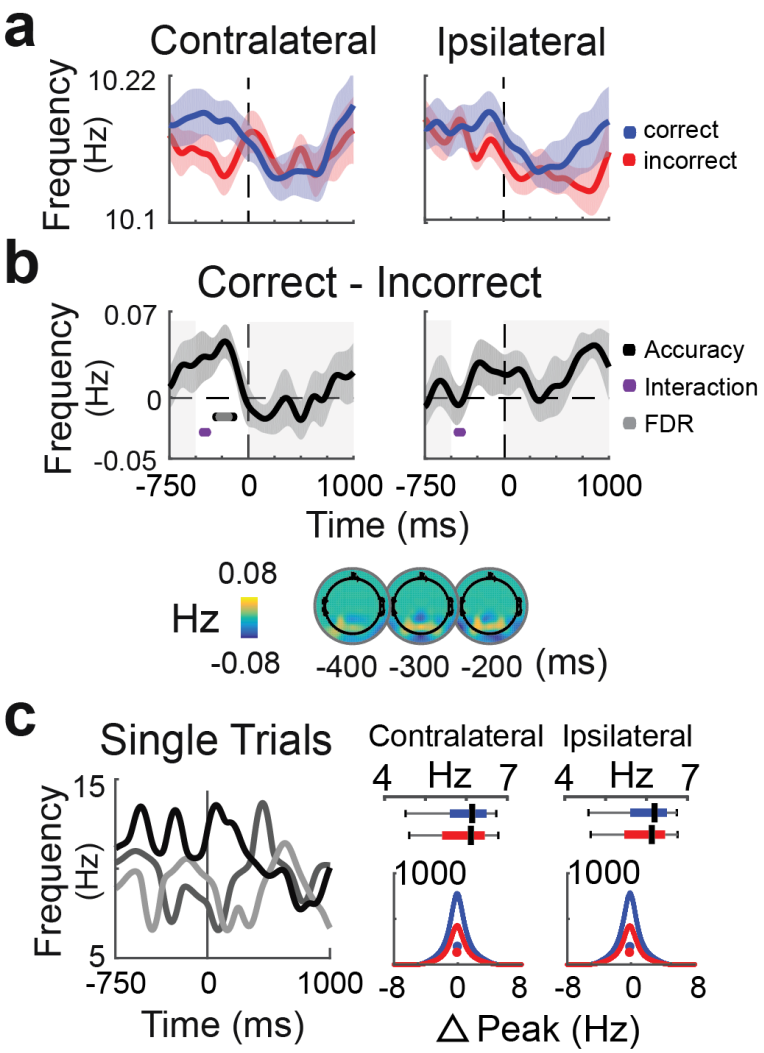

Figure 2.5: Topographically selective increases in pre-stimulus frequency predict accuracy. **a** Contralateral and Ipsilateral electrodes show distinct target- locked patterns in instantaneous frequency. Blue indicates correct trials, red indicates incorrect trials, shaded areas indicate ± 1 SEM within subject. **b** A pre-stimulus elevation in frequency on correct as compared to incorrect trials is localized to Contralateral electrodes. All dots indicate significance from zero, evaluated by comparing the obtained t-value with a null distribution of t-values computed by shuffling the condition labels 10,000 times. This analysis was done on a timepoint-by-timepoint basis from −500ms to stimulus onset, as indicated by the non-shaded areas (see Methods). Significant main effects are indicated in black, whereas gray dots indicate significance after FDR correction at P = 0.05. For illustration, Correct— Incorrect topographies reveal elevated pre-stimulus alpha frequency in 100ms bins centered around −400, −300 and −200ms before the stimulus. **c** Three example trials of instantaneous frequency highlight single trial dynamics. Boxplots on the upper right indicate the average single trial dynamic range (max—min) of instantaneous frequency on correct (blue) and incorrect (red) trials. Histograms in the lower right show distributions of instantaneous frequency as a function of the distance from peak alpha over all subjects, timepoints, and electrodes in each of the four conditions. Dots in histograms indicate the median shift for that condition

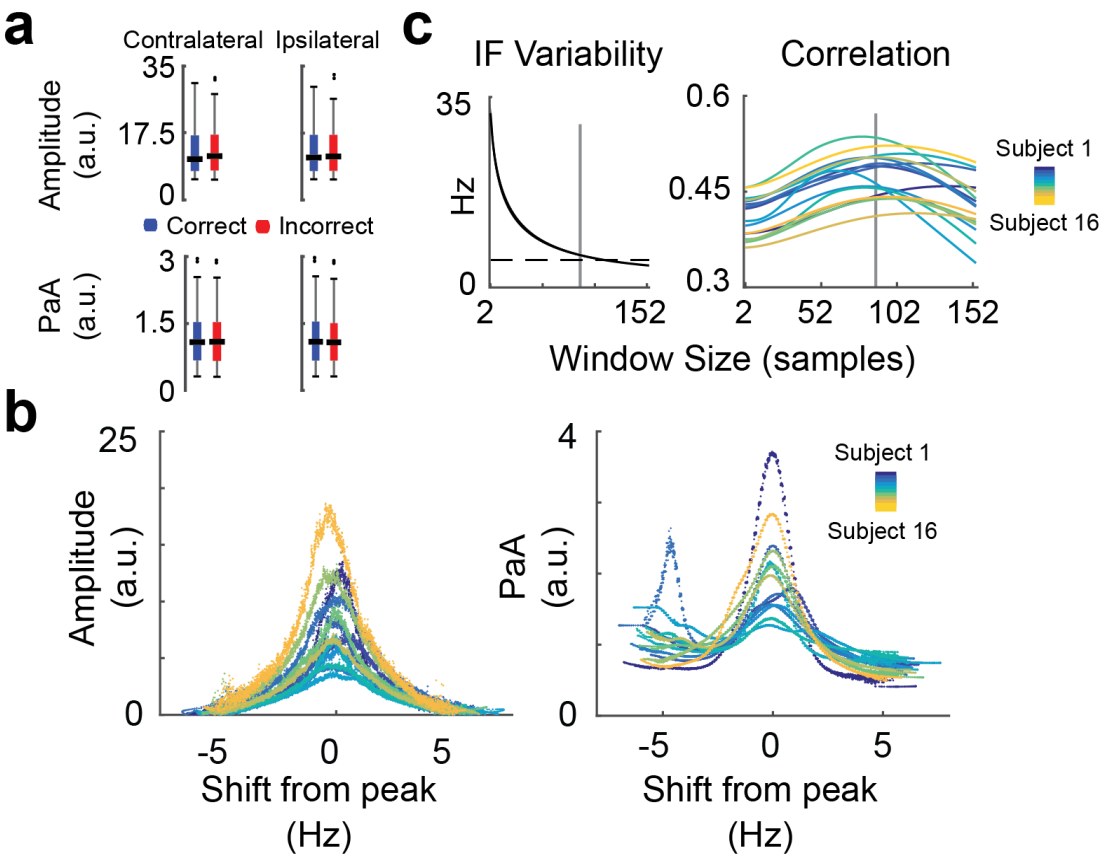

Figure 2.6: Characterization of Instantaneous Frequency and PaA. **a)** The mean dynamic range of PaA and alpha amplitude on single trials. The max – min of PaA and Amplitude was taken on each trial, and the median over trials was stored for each subject and electrode. Data for all 3 contralateral electrodes were concatenated and displayed here. **b)** Mean amplitude and PaA vary with distance from peak alpha frequency. Each color is a single subject, all data are averaged over the 3 contralateral electrodes. Note that the shape of PaA reflects the amplitude spectra of each subject. **c)** PaA-Amplitude correlations and single trial instantaneous frequency dynamic range are plotted as a function of the window size used to estimate instantaneous frequency. The gray vertical line indicates the window size reported in previous analyses, chosen as the earliest point that variability nears the +/- 5 Hz bandpass range.

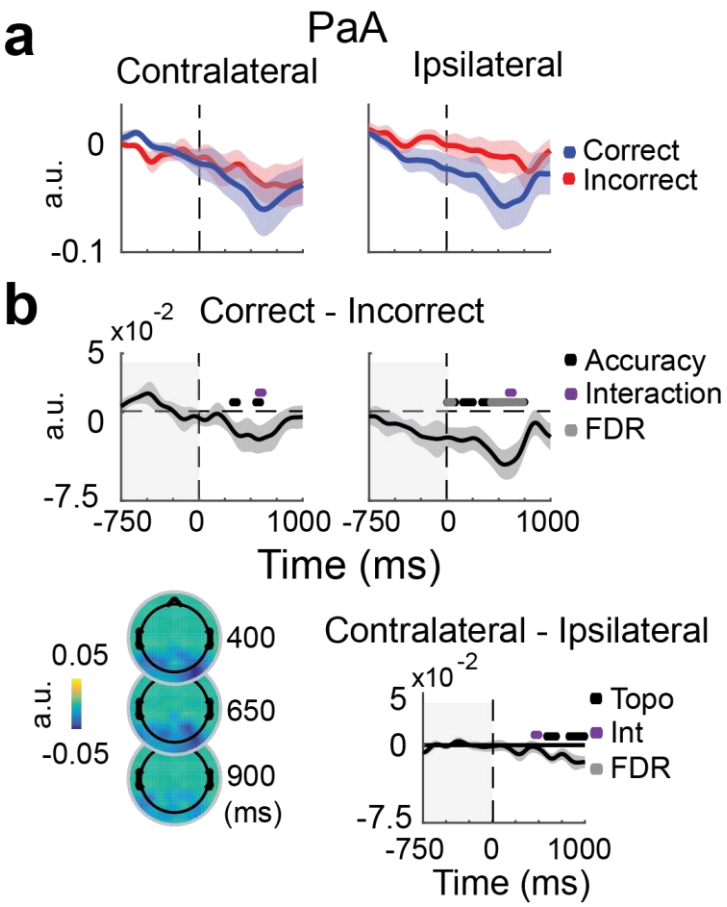

Figure 2.7: Shifts in instantaneous frequency predict alpha amplitude. **A)** On a trial-by-trial and timepoint-by-timepoint basis, instantaneous frequency was used to generate predicted alpha amplitudes (PaA). PaA was baselined to the same interval used for alpha amplitude (−1000:−750 pre-target). Shaded areas indicate ± 1 SEM within subjects for correct (blue) and incorrect (red) trials. Reported results are averaged over the same groups of contralateral and Ipsilateral electrodes previously reported. **B)** Correct— Incorrect differences are plotted for Contralateral and Ipsilateral electrodes. For illustration, topoplots indicate Correct—Incorrect topographies averaged over 100 ms bins centered on 400, 650, and 900 s after stimulus onset. All dots indicate significance from zero, evaluated by comparing the obtained t-value with a null distribution of t-values computed by shuffling the condition labels 10,000 times. This analysis was done on a timepoint- by-timepoint basis from stimulus onset to + 1000 ms, as indicated by the non-shaded areas (see Methods). Main effects of accuracy indicated in blue and yellow in contralateral and ipsilateral electrodes, red indicates a main effect of topography. Gray dots indicate significance after FDR correction at $P < 0.05$

If the amplitude spectrum is a valid transformation between instantaneous frequency and amplitude, PaA modulations should track measured amplitude modulations. Indeed, average PaA on correct and incorrect trials resembled measured modulations in alpha amplitude (Figure 2.7a, Figure 2.4a). Post-stimulus decreases in PaA depended on accuracy and electrode

location in a manner similar, although not identical, to alpha amplitude (Figure 2.7b, Table 2.2). As we were interested with the relationship between instantaneous frequency and amplitude within single trials, we computed timepoint-by-timepoint correlations between PaA and amplitude across all trials and found a significant relationship (mean correlation = 0.4773 ± 0.0732 SD, p = 0, Table 2.3, Figure 2.7a; left panels, see Methods). These correlations were stable over time, and did not depend on behavioral performance or the position of the electrode with respect to the target (p-values do not survive FDR correction, Figure 2.6a; Table 2.4). Finally, modulations in PaA on single trials closely tracked those observed in amplitude (Figure 2.6b).

Table 2.3: Correlations are specific to the alpha bump. Control look-up table analyses were performed to generate PaA_{noise}, $PaA_{shuffled}$, and $PaA_{1/f}$, which were then correlated with amplitude (see Methods). Average correlation coefficients ± standard deviation are shown for all analyses. PaA_{noise} was generated with a series of white noise spectra as look-up-tables, producing small correlations with amplitude indistinguishable from 0. $PaA_{shuffled}$ was generated by repeatedly shuffling the frequency axis of a given look-up-table, but again $PaA_{shuffled}$ was uncorrelated amplitude. $PaA_{1/f}$ was generated with look-up-tableS captured the 1/f component but did not contain the characteristic alpha bump. $PaA_{1/f}$ was also uncorrelated to the empirically observed alpha amplitudes. *indicates significance of empirically obtained PaA values, computed by comparing T-tests against zero of these values to T-tests the shuffled PaA values, and then FDR correcting at P=0.05.

Correlation (Mean ± SD)	**PaA_{Noise}**	**$PaA_{Shuffled}$**	**$PaA_{1/f}$**	**$PaA_{Empirical}$**
Correct	$-3.35*10^{-20}$± $9.2*10^{-16}$	-0.0173 ± 0.1209	-0.0624 ± 0.0948	*0.4745 ± 0.0728, p=0
Incorrect	$4.08*10^{-20}$± $6.8*10^{-16}$	-0.0183 ± 0.1318	-0.0594 ± 0.1045	*0.4802 ± 0.0736, p=0

Table 2.4: Predicted alpha amplitude – amplitude correlations are stable. Predicted alpha amplitude shows a stable correlation with observed amplitude both over time and between experimental conditions. All tests report single time-point sliding t-tests performed on correlation values after values were compared against distributions obtained empirically by randomizing condition labels 10,000 times and then repeating the same statistical test (see Methods). Reported t-values are from the timepoint with smallest p-value. * indicates that p-values were significant after FDR correction at alpha = 0.05 from -500ms before stimulus onset to 1000ms after stimulus onset.

	Correlation
Contralateral vs Ipsilateral	t(15) = 3.006, p=0.0072
Contralateral Accuracy	t(15) = -2.893, p=0.0015
Ipsilateral Accuracy	t(15) = -2.203, p=0.0467
Location x Accuracy Interaction	t(15) = 2.0355, p=0.0514

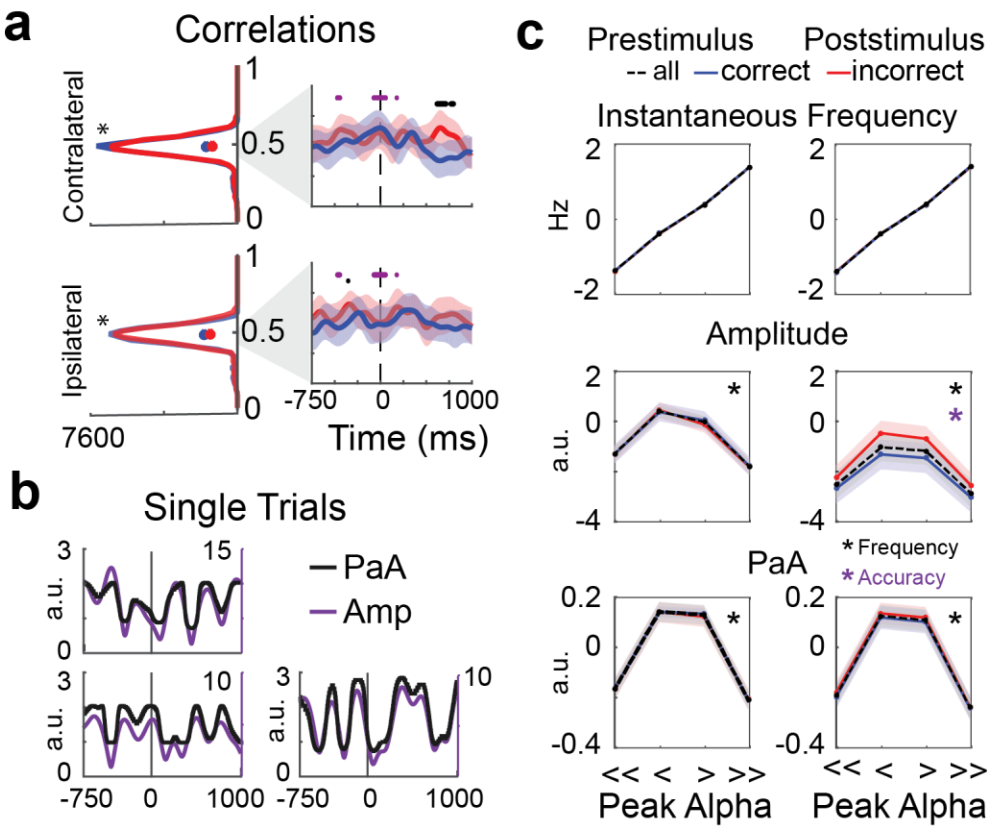

Figure 2.8: Predicted alpha amplitude correlates with observed amplitude. **a)** To assess how well PaA corresponds with alpha amplitude, we computed correlation values for each subject and electrode for each timepoint over the entire –750 to 1000 ms peri-stimulus interval. Histograms show correlation values concatenated over all subjects, timepoints and electrodes on correct (blue) and incorrect (red) trials in the contralateral and ipsilateral electrodes. Stars on each panel indicate that all correlation values shown in these histograms are significantly different from correlations obtained with shuffled LUTs (see Methods, Supp Fig. 4). Dots in histograms indicate the median correlations for that condition. Timecourses panels on the right show these correlations are relatively stable over time, where the y-axes of the plots run from 0.425 to 0.525, corresponding to the gray shaded area in the histogram. All dots indicate significant difference in the correlations between conditions, evaluated by comparing the obtained t-value with a null distribution of t- values computed by shuffling the condition labels 10,000 times. This analysis was done on a timepoint-by-timepoint basis from −500 to + 1000 ms, as indicated by the non-shaded areas. Main effects of are in black, whereas purple indicates an interaction. Gray dots indicate significance after FDR correction at 0.05. **b)** Three example trials from three different subjects show that PaA shifts on single trials mirror those in alpha amplitude. The y-axis and traces for PaA are indicated in black, while those for amplitude are purple. Note that the y-axis range is different in each subplot to maximize visibility of amplitude and PaA (see Methods). **c** Trials were sorted according to mean pre (−350:−50 ms) and post (350:650 ms) stimulus frequency. Average amplitude and PaA were then computed on these trials and timepoints. Trials were further split by accuracy, as indicated by blue and red lines. Significant differences were evaluated using a two-way repeated-measures ANOVA. Black stars indicate a significant effect of frequency, whereas a purple star indicates a significant effect of accuracy in the two-way ANOVA

To further investigate how frequency, amplitude and behavior are related via the non-monotonic shape of the amplitude spectra in the alpha band, we next sorted trials into four bins based on average instantaneous frequency in pre-stimulus and post-stimulus epochs that were significant in the analyses presented in Figures 2.4B and 2.5B (see Methods). We binned trials based on whether average frequency was much lower than peak alpha, lower than peak alpha, greater than peak alpha, or much greater than peak alpha (quartile split). We then averaged pre or post-stimulus alpha amplitude and PaA over the trials in each of these bins. We observed a clear inverted-U relationship between amplitude and instantaneous frequency in both pre-stimulus and post-stimulus epochs (Table 2.5, Figure 2.8c). This is consistent with the main analysis showing that each subject's alpha spectrum maps changes in instantaneous frequency onto changes in alpha amplitude (see Figure 2.1). Furthermore, only 25.1 ± 5% SD of trials in each pre-stimulus bin were still in that bin in the post-stimulus epoch, again emphasizing the dynamic changes in frequency that occur across single trials (25% is expected purely by chance).

Table 2.5: Frequency and accuracy similarly predict amplitude and PaA**.** Within frequency and accuracy condition, mean amplitude and PaA in pre and post stimulus epochs from -350:-50 ms or 350:650 ms relative to the stimulus were averaged (timepoints chosen according to the significant timepoints from Figures 2.4 and 2.5). Trials were binned by their average pre or post stimulus frequency, and then amplitude and PaA was computed for each of these bins. We then computed a two-way repeated measures ANOVA with frequency and accuracy as factors. F-values were compared against distributions obtained empirically by randomizing condition labels 10,000 times and then repeating the same statistical test (see Methods). * indicates that p-values were significant alpha = 0.05. All statistics are reported for contralateral channels, as plotted in Figure 2.7C.

	Amplitude		**PaA**	
	Prestimulus	**Poststimulus**	**Prestimulus**	**Poststimulus**
Frequency (bins 1-4)	*F(3, 15) = 16.921, p=0.0	*F(3, 15) =16.895, p=0.0	*F(3,15) = 28.73, p = 0.0	*F(3, 15) =28.57, p=0.0
Accuracy (correct vs incorrect)	F(1, 15) = 0.12, p=0.748	*F(1, 15) = 9.169, p=0.0028	F(1, 15) = 0.229, p=0.669	F(1, 15) = 2.49, p=0.1328
Frequency-Accuracy Interaction	F(3, 15) = 0.11, p=0.958	F(3, 15) = 1.218, p=0.323	F(3, 15) = 0.269, p=0.858.	F(3, 15) = 0.314, p=0.829

Together, these analyses show that amplitude modulations were accurately predicted by passing instantaneous frequency through amplitude look-up-tables, evidenced by similar average PaA and amplitude waveforms, significant timepoint-by-timepoint PaA - amplitude correlations, and similar modulations of PaA and amplitude over single trials.

As both instantaneous frequency and amplitude are computed from bandpass filtered EEG data, we next addressed the concern that PaA-amplitude correlations were an artifact of filtering by passing instantaneous frequency through 5000 randomly generated white noise look-up-tables to generate PaA_{Noise} (see Methods). This analysis yielded correlations between PaA_{Noise} and actual alpha amplitude that were close to 0 (mean correlation = $3.4*10^{-21} \pm 8.1*10^{-16}$ SD, Figure 2.9 Table 2.3). We next evaluated the empirical probability of observing the PaA – amplitude correlations reported in Figure 2.7 under the null hypothesis of no relationship between these factors. To do this, we shuffled the frequency axis of each look-up-table, and passed instantaneous frequency through these shuffled look-up-tables to generate PaA_{Shuff}, a

process we repeated 5000 times for each subject and electrode (see Methods). Average correlations between PaA_{Shuff} and amplitude were ~24x smaller than those empirically observed, and P-values computed by comparing observed correlations to the PaA_{Shuff} correlations were all = 0 (mean correlation = -0.0178 ± 0.1265 SD, Table 2.3, Figure 2.9). Finally, to evaluate whether our results are specific to the unique shape of the resonant alpha bump, we fit a two-term exponential model to each spectrum, generating a new set of look-up-tables that captured only the 1/f falloff and not the alpha-bump (see Methods). We then passed instantaneous frequency through these new look-up-tables to generate $PaA_{1/f}$. Again, $PaA_{1/f}$ was weakly correlated with amplitude (mean correlation = -0.0624 ± 0.0948 SD, Table 2.3). Together, these additional analyses indicate that the correlations obtained are not simply artifacts of our analysis pipeline, but instead reflect an intrinsic relationship between frequency and amplitude well described by the shape of each subject's alpha bump centered on their peak alpha frequency (Figure 2.9).

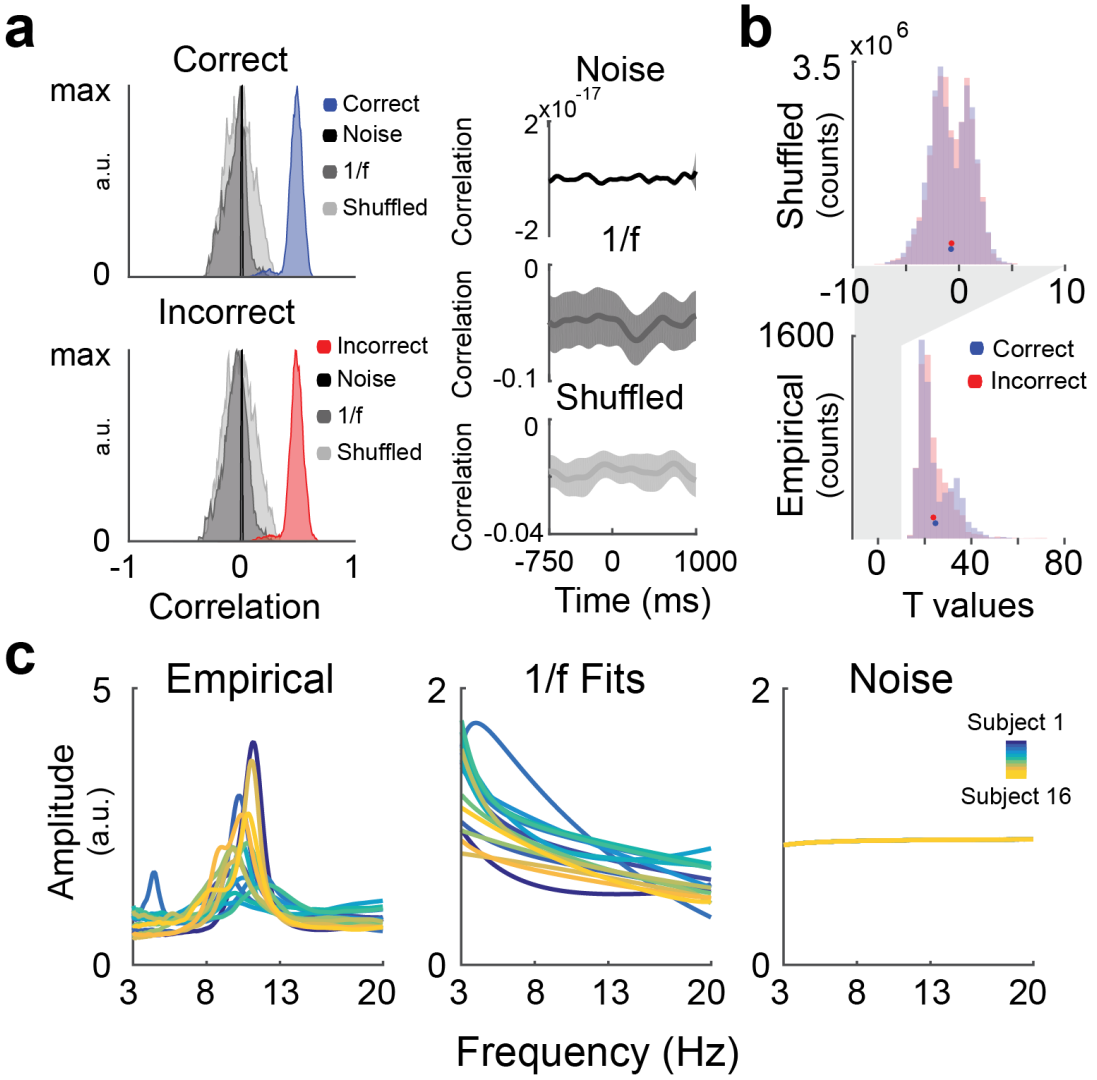

Figure 2.9: Empirically observed correlations reflect an intrinsic relationship between amplitude and frequency. **a)** Plotted are histograms comparing the correlations for correct and incorrect trials for PaA computed with Noise, 1/f, and Shuffled LUTs (from black to light gray) with those empirically observed (blue and red) in contralateral electrodes. Each of these histograms are normalized to their maximum in order to show them on the same plot. The right panel shows timecourses for these alternative LUTs averaged over the contralateral electrodes. **b)** T-values computed from the shuffled spectrum are displayed for correct (blue) and incorrect (red) trials. Note the x-axis of these histograms correspond with the gray shaded area on the empirically observed T-value histogram. **c)** Empirical, 1/f fits and Noise LUTs averaged over contralateral electrodes are shown for each subject in a different color. Note the different y-axis for the empirical spectra. The “hooked” 1/f fit for the subject in blue is due to that subject’s additional prominent peak in the high delta/low theta range.

Experiment 2

Generalizing the link between Amplitude and Frequency

To assess the generalizability of the predictive relationship between frequency and amplitude, we computed PaA for a previously published data set in which 14 subjects completed 4 sessions and 2 subjects completed 6 sessions of a two-interval contrast discrimination task (with 1,176 trials per session; for more details see reference (Itthipuripat et al., 2014)). Briefly, after an attentional cue, two oriented stimuli were presented for 300ms to the left and right of fixation, followed by a blank interval of 600-800 ms followed by a second presentation of two oriented stimuli for another 300ms. The oriented stimuli were rendered at a variable contrast level ranging from 0% to 81.13% and subjects had to indicate which of the two stimulus presentation intervals contained a slight contrast increment. We focused our analysis on data from the 'divided attention' cue condition in which either stimuli could be the target, because this condition most closely matched the spatial uncertainty of the stimuli in Experiment 1.

Consistent with the first experiment, we observed event-related shifts in average instantaneous frequency and amplitude in the same contralateral and ipsilateral groups of electrodes reported in the first experiment (Figure 2.10a). Importantly, these modulations in instantaneous frequency and amplitude are linked, as indicated by high single timepoint correlations between PaA and amplitude (0.458 ± 0.063 SD, Figure 2.10b), and the similarity in average PaA and amplitude waveforms (Figure 2.10a).

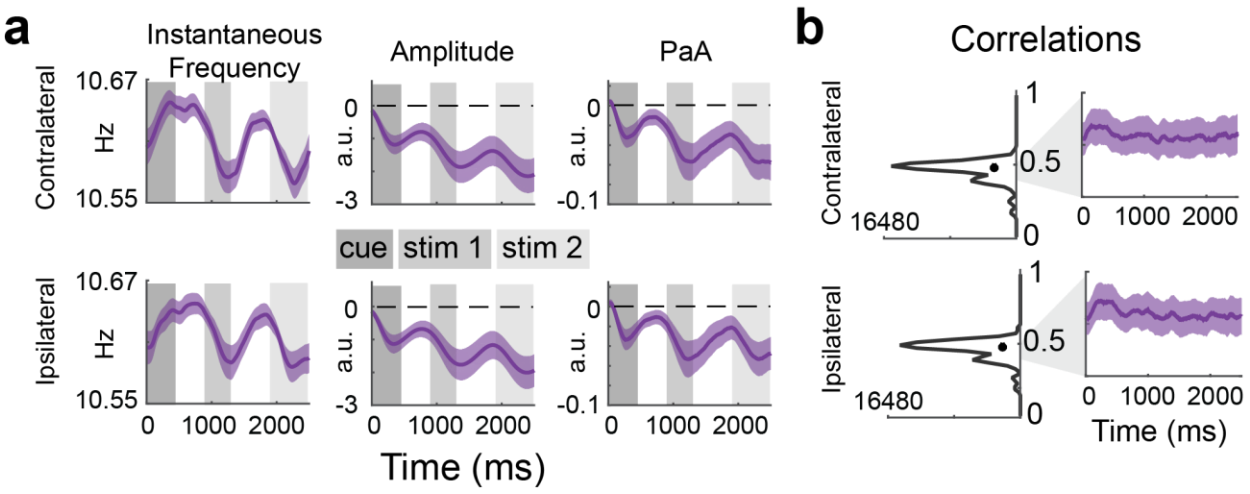

Figure 2.10: Frequency, amplitude and PaA in Experiment 2. **A)** Average instantaneous frequency, amplitude, and PaA in the same contralateral and ipsilateral electrodes examined previously, shaded areas indicate ± 1 SEM within subjects. All data are locked to the onset of the cue (indicated by dark shading). Alpha amplitude shows event-related decreases corresponding to the onset of the cue, stimulus array 1 and stimulus array 2. Similarly, the rightmost panel shows that average shifts in PaA mirror these changes in amplitude. **B)** Histogram of single trial correlations collapsed across subjects, timepoints, and electrodes. Traces to the right indicate timecourses of these correlations. Timecourses show these correlations are relatively stable over time, where the y- axes of the plots run from 0.4 to 0.5, corresponding to the gray shaded area in the histogram

In the more complex paradigm used in Experiment 2, stimuli were presented for 300ms and were mostly suprathreshold. Thus, unlike Experiment 1, the design of Experiment 2 was not ideal to investigate the impact of alpha modulations on behavioral performance. However, for completeness, we examined the link between alpha amplitude, alpha frequency and behavioral performance using the data from Experiment 2. Like the modulations reported in Experiment 1, we observed lower post-stimulus alpha amplitude in contralateral posterior channels on correct compared to incorrect trials, reflected in an interaction between topography and accuracy ($F(1,14) > 4.44$, Figure 2.11; Table 2.6). In addition, contralateral instantaneous alpha frequency increased before the onset of the first stimulus on correct compared to incorrect trials, but only when stimulus contrast was low (reflected in an interaction between accuracy and contrast with $F(1,14) > 3.31$; Figure 2.11; Table 2.7). The observation of a significant effect only with low contrast stimuli is consistent with the findings from Experiment 1 in which there was a high

degree of sensory uncertainty because stimulus location was unpredictable and the stimuli were low-contrast and masked (see Methods).

Table 2.6: Amplitude during the divided attention condition as a function of electrode location and behavioral performance. All tests report the maximum and minimum timepoint-by-timepoint F-values over poststimulus timepoints. F-values were compared against distributions obtained empirically by randomizing condition labels 5,000 times and then repeating the same statistical test (see Methods). * indicates that p-values were significant after FDR correction at alpha = 0.05 from stimulus onset to +750ms. The minimum uncorrected p-value is also reported for each interval (note all intervals have a maximum uncorrected p-value of 0.05 since they were chosen on this basis).

	Post Stimulus 1 Amplitude	**Post Stimulus 2 Amplitude**
Topography (contralateral vs ipsilateral)	$4.39 < F(1,14) < 6.73$ $0.02 \leq p < 0.05$	n.s.
Accuracy (correct vs incorrect)	n.s.	$4.24 < F(1,14) < 5.60$ $0.026 \leq p < 0.05$
Contrast (levels 1-3)	$3.23 < F(1,14) < 4.87$ $0.013 \leq p < 0.05$	$3.19 < F(1,14) < 5.18$ $0.008 \leq p < 0.05$
Topography x Accuracy	$4.46 < F(1,14) < 10.71$ *****$0.005 \leq p < 0.05$	$4.44 < F(1,14) < 15.40$ *****$0 \leq p < 0.05$
Topography x Contrast	n.s.	n.s.
Accuracy x Contrast	n.s.	$3.50 < F(1,14) < 3.65$ $0.047 \leq p < 0.05$
Topography x Accuracy x Contrast	n.s.	n.s.

Table 2.7: Frequency during the divided attention condition as a function of electrode location and behavioral performance. All tests report the maximum and minimum timepoint-by-timepoint F-values over prestimulus timepoints. F-values were compared against distributions obtained empirically by randomizing condition labels 5,000 times and then repeating the same statistical test (see Methods). * indicates that p-values were significant after FDR correction at alpha = 0.05 from -500 to stimulus onset. The minimum uncorrected p-value is also reported for each interval (note all intervals have a maximum uncorrected p-value of 0.05 since they were chosen on this basis).

	Pre Stimulus 1 Frequency	**Pre Stimulus 2 Frequency**
Topography (contralateral vs ipsilateral)	$4.6 < F(1,14) < 8.44$ $0.009 \leq p < 0.05$	n.s.
Accuracy (correct vs incorrect)	$4.41 < F(1,14) < 4.42$ $0.048 \leq p < 0.05$	n.s.
Contrast (levels 1-3)	$3.31 < F(1,14) < 3.70$ $0.030 \leq p < 0.05$	n.s.
Topography x Accuracy	n.s.	n.s.
Topography x Contrast	$3.37 < F(1,14) < 4.01$ $0.031 \leq p < 0.05$	n.s.
Accuracy x Contrast	$3.31 < F(1,14) < 10.44$ $*0 \leq p < 0.05$	n.s.
Three Way Interaction	n.s.	n.s.

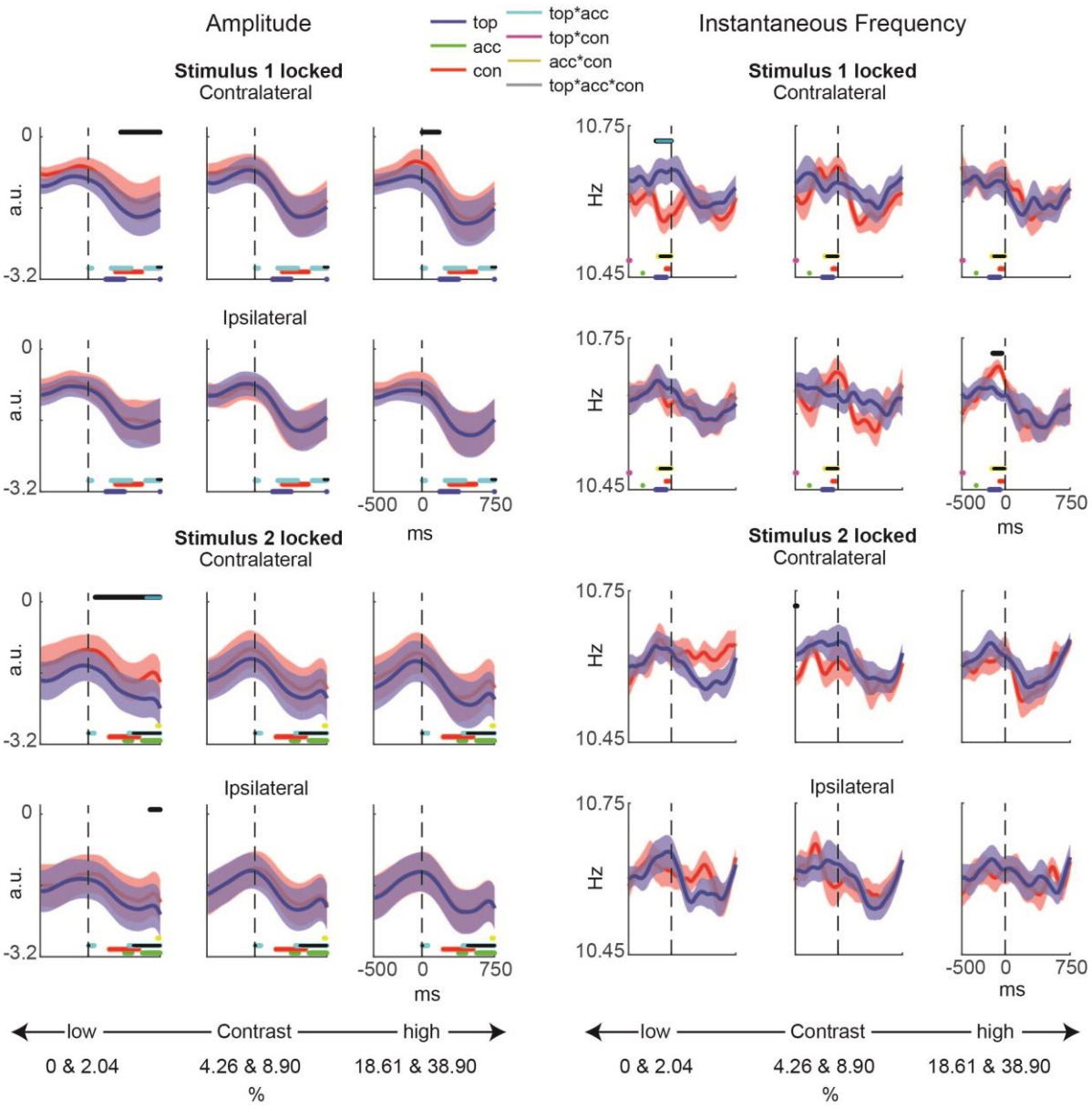

Figure 2.11: Data from Experiment 2. Amplitude (left panel) and frequency (right panel) locked to the onset of the first stimulus (top half) and the onset of the second stimulus (bottom half). All plots are during the divided attention condition, and are shown as a function of topography (contralateral and ipsilateral) and behavioral performance (correct in blue, incorrect in red). Results of a 3-way repeated-measures ANOVA analysis with topography, accuracy and contrast level are plotted at the bottom of each subplot indicating uncorrected p-values < 0.05 with colors corresponding to the legend. Effects that survive FDR correction are in black (full results of this analysis are described in Tables 2.6 and 2.7). Post-hoc t-tests were performed between correct and incorrect timecourses to further understand these effects. Timepoints with $p < 0.05$ from these t-tests are plotted at the top of each subplot in black, with timepoints that survive FDR correction in cyan (contralateral) or yellow (ipsilateral). In keeping with previous figures, all amplitude statistics were performed on post-onset timepoints, while frequency statistics were performed on pre-onset timepoints. Note that like other analyses of Experiment 1, all p-values reported here were determined by randomizing conditions 5,000 times and comparing observed values to these empirical distributions.

Taken together, we found that alpha amplitude can be predicted from instantaneous frequency in two different tasks with different stimuli and cognitive demands. This suggests that each subjects' amplitude spectrum is a general link between the modulations in frequency and amplitude that correlate with changes in visual perception.

Discussion

In the present study, we show that alpha amplitude and instantaneous frequency are linked by the spectral characteristics of each subject's alpha oscillation This result suggests that amplitude and frequency do not reflect unique properties of cortical oscillations., Instead, amplitude may depend on how close instantaneous frequency is to peak alpha, as predicted by a simple model based on coupled oscillators. Furthermore, modulations of alpha oscillations impact visual information processing. Our data is consistent with two lines of research that highlight the importance of either alpha amplitude or shifts in instantaneous alpha frequency. We found a contralateral decrease in alpha amplitude and an increase in instantaneous frequency when subjects correctly discriminated a brief target. Historically, these results have been discussed largely in the context of different theoretical frameworks, with amplitude primarily associated with desynchronization(Wolfgang Klimesch et al., 2007) and frequency associated with changes in the sampling rate of incoming visual information (Samaha & Postle, 2015). However, our results suggest a revision of these traditional accounts and highlight the need for a more unified framework.

Note that post-stimulus drops in alpha amplitude on correct trials correspond to shifts in instantaneous frequency both above and below peak alpha, as no mean post-stimulus differences in instantaneous frequency are observed between correct and incorrect trials. However, the fact that correlations between frequency and amplitude remain stable after the stimulus suggests that changes in instantaneous frequency are related to those in amplitude. To

understand this, it is important to remember that amplitude and frequency do not have a unique, one-to-one mapping. Instead, they are related by the non-monotonic bump shape of the amplitude spectra. This means that significant differences in one metric may average out in another metric. For example, amplitude could be equal at timepoints in which instantaneous frequency has moved from below to above peak alpha (or vice versa). Thus, it is possible that before the stimulus, an increase in instantaneous frequency enhances perception, but upon stimulus presentation a shift either above or below peak alpha is necessary for efficient visual information processing.

These observations suggest a possible mechanism for how the desynchronization of alpha oscillations results in efficient sensory processing. In the desynchronization account, fewer visual neurons are entrained at a common alpha frequency as activity in relevant circuits shifts to process sensory stimuli. The current data suggest that shifts in instantaneous alpha frequency predict changes in alpha amplitude, which could be interpreted as a mechanism for this “drop out”. For example, shifts in instantaneous alpha frequency away from the peak or resonant frequency – akin to a pianist drifting from a metronome – may be the mechanism by which desynchronization and drops in alpha amplitude occur. At a neural level, these frequency changes could occur when the E/I balance shifts to allow the formation of local circuits that process relevant sensory stimuli (Gray & Singer, 1989; Mazzoni et al., 2008; Okun & Lampl, 2008; Vogels, Sprekeler, Zenke, Clopath, & Gerstner, 2011). For example, changes in the activity of specific sub-sets of inhibitory interneurons likely modulate the instantaneous frequency of the local circuit (Atallah & Scanziani, 2009; Blatow et al., 2003; Buzsáki & Chrobak, 1995; Mann & Mody, 2010; Wang, 2010). Thus, increases and decreases in instantaneous frequency could be due to a variety of changes in the E/I balance during sensory processing and future research will be required to determine the contribution of factors such as dampening, changes in a region’s characteristic frequency, and changes in the driving region’s characteristic frequency.

Finally, in addition to alpha amplitude and frequency, several previous studies have found a correlation between behavioral performance and alpha phase (Busch et al., 2009; Dugue et al., 2011; Mathewson et al., 2009). While we did not find consistent dependence of performance on alpha phase, the non-stationarities that we observed in instantaneous frequency might impair our ability to detect performance-related phase offsets (Cohen, 2014; Lowet et al., 2016) (Figure 2.12, see Figure 2.1c). Further work is needed to understand how frequency shifts might contribute previously reports of phasic modulations in perceptual sensitivity.

In sum, our results show that fluctuations in the instantaneous frequency of alpha oscillations are associated with both behavioral performance and alpha amplitude. This suggests that changes in instantaneous frequency and amplitude do not reflect completely independent mechanisms for mediating visual information processing, and our results provide new insights into understanding how coupled changes in oscillatory frequency and amplitude jointly impact visual information processing.

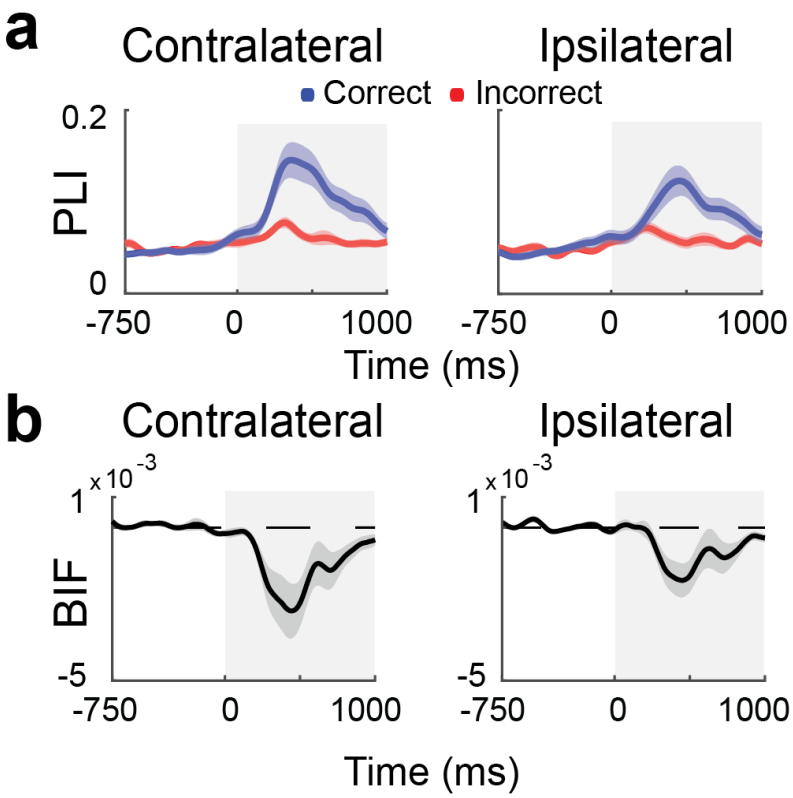

Figure 2.12: Phase Locking and Bifurcation are not associated with accuracy. **a)** Contralateral and Ipsilateral phase locking values are plotted for correct and incorrect trials. There are no significant differences in prestimulus (indicated by the unshaded regions) phase locking between conditions. **b)** Similarly, prestimulus phase bifurcation (BIF) in contralateral and ipsilateral electrodes does not show significant difference from zero, indicating no significant phase concentration on either incorrect or correct trials (see Methods). Phase bifurcation ranges from 1 (perfect phase locking in both conditions at opposite phases) to -1 (perfect phase locking in only one condition), while values around zero indicate random distributions for correct and incorrect trials. Note that post-stimulus phase locking is not easily interpreted due to phase resets and ERPs(Busch et al., 2009; Dugue et al., 2011; VanRullen, 2016).

METHODS

Subjects

In Experiment 1, 17 subjects (eight male) were recruited at the University of California San Diego and all data were collected at UCSD's Perception and Cognition Lab. The age range of the subjects was 19-30 years old (22.06 mean ± 3.98), and all subjects had normal or corrected to normal vision. All subjects provided written informed consent in accordance with the Institutional Review Board at UCSD. Subjects were compensated $10 / hour for behavioral training and $15 / hour for EEG. One subject was excluded due to a high number of

independent components showing blink related activity (i.e. 5 frontally localized components exceeding >30 mV).

Experiment 2 is described in detail in Itthipuripat et al 2014(Itthipuripat et al., 2014). In brief, 17 subjects (18-31 years old, 9 females) underwent a 2.5-hour behavioral training session and then 14 subjects completed 4 EEG sessions and 2 subjects completed 6 EEG sessions for a total of 4704 or 7056 trials, respectively. One subject withdrew after the second EEG session, yielding 16 subjects for the final analysis.

Apparatus and Stimuli

The experiment was implemented using Psychtoolbox in the MATLAB programming environment running on a Windows PC with the XP operating system. Subjects were positioned 60 cm from the display and stimuli were presented on a 15-inch CRT monitor with 1024 x 768 resolution and 120 Hz refresh rate. The luminance output of the monitor was measured using a Minolta LS110 and linearized in the stimulus presentation software.

In Experiment 1, all stimuli appeared 8.5° of visual angle to the left or to the right (with equal probability) of the central fixation point (with 0° offset from the horizontal meridian). At the start of each stimulus presentation sequence, a disk of Gaussian white noise (5.7° diameter) was presented for one video frame (8.33 ms) in one of the two possible locations. Next, either a vertically or horizontally oriented Gabor target stimulus was presented for one video frame in the same spatial position as the white noise stimulus (also 5.7° diameter). Following the offset of the Gabor, a second white noise stimulus was presented for one video frame. Subjects reported whether the orientation of the Gabor stimulus was vertical or horizontal by pressing one of two buttons on a small keypad. Subjects were instructed to respond as quickly as possible, and to do their best to avoid blinking until after a response was made. After subjects responded, there was an inter-target-interval (ITI) of 3000-4000 ms (pseudo randomly sampled from a uniform

distribution). Each experimental block (72 trials) lasted for approximately 7 minutes. Subjects completed 14 blocks of trials during the EEG recording session.

The main goal of Experiment 1 was to determine whether frequency shifts in the alpha band predicted behavioral performance. Before the EEG recording session, the contrast threshold yielding vertical/horizontal discrimination accuracy between 60 - 65% was determined in a separate thresholding session using the method of constant stimuli. In the EEG recording session, the mean accuracy across subjects after trial exclusion was 65% ± +/-2.8%, and mean contrast was 5.02% ±1.12% (mean ± SD). Aside from titrating contrast to estimate the threshold for each subject, the stimulus presentation sequence and timing of the trials in the behavioral and the EEG sessions were identical.

In Experiment 2, subjects performed a two-interval forced choice contrast discrimination task in which each trial began with a 500 ms cue instructing subjects to attend to locations in either the left, right or both hemifields (100% valid)(Itthipuripat et al., 2014). The cue was followed by a 400-600 ms inter-stimulus interval (ISI) in which only the fixation point was present. At a pseudo-randomly chosen time within this ISI window, a first stimulus pair was presented (two sinusoidal Gabor patches, one in each hemifield) for 300 ms, where each Gabor was presented at one of seven pedestal contrasts. After another 600-800 ms ISI in which only the fixation point was visible, a second pair of Gabors was presented for 300 ms. A small contrast increment was added to the pedestal contrast of the target Gabor patch during either the first or second presentation interval, and subjects were asked to report if the increment occurred during the first or second presentation. For the first 6 pedestal levels, the magnitude of the contrast increment was adjusted to maintain ~76% accuracy, while accuracy the highest pedestal contrast level could not be titrated because the contrast was too high and so was not included in the analysis in Figure 2.9 (consistent with exclusion of that condition in the published manuscript(Itthipuripat et al., 2014)). Additionally, several aspects of this design make it conceptually different from the relatively simple design employed in Experiment 1 to examine

frequency and amplitude modulations. These include the longer (300 ms) stimulus presentation, the reliance of the task on working memory during the delay interval, the presentation of bilateral stimuli, and the use of different pedestal contrasts in each hemifield on each trial (as contrast is known to modulate frequency(Cohen, 2014)).

EEG recording

All EEG recordings took place in a sound-attenuated and electromagnetically shielded room (ETS Lindgren, Cedar Park, TX). EEG and electrooculogram (EOG) were recorded with a Biosemi Active2 System (Amsterdam, The Netherlands) using a headcap with standard Biosemi 64 electrode layout. In addition to the 64 scalp electrodes, one reference electrode was placed on each mastoid, and 6 electrodes were placed around the eyes to identify and reject trials with blink and saccade artifacts. All EEG data were recorded at a sampling rate of 512 Hz. Event triggers were recorded in the EEG data file to mark the time of target presentation and the time of the subject's response.

EEG preprocessing

After data collection, data from the scalp electrodes were re-referenced to the algebraic mean of the two mastoid electrodes. Then, the raw time series from each electrode was bandpass filtered between 0.1 to 55 Hz using a third order Butterworth filter to attenuate slow drift and 60 Hz line noise. After filtering, data were epoched into 6 second intervals centered on the presentation of each target. Trials were excluded from further analysis if the EOG electrodes located above or below either eye reached ± 85 mV (blinks) or EOG electrodes located outside either outer canthi reached ± 45 mV (saccades) within ±1 second of target presentation (7.8% ± 8 % S.D. of trials were excluded). Additionally, entire blocks of trials were rejected when there was a failure to record the precise timing of any of the target onsets (i.e. a trigger that was sent to the EEG recording software was not recorded: 5 out of 256 total blocks across all subjects).

For each subject, electrodes showing voltage fluctuations exceeding the 95th percentile of data from all electrodes and timepoints were also excluded from further analysis (1.8 ± 1.8 S.D. electrodes excluded). Finally, trials with RTs > 2000 ms were excluded from further analysis (another 4.8% of trials). After applying these exclusion criteria, subjects had an average of 868 ± 89 S.D. trials, 35% of which were incorrect. Thus, a proportionate number of correct and incorrect trials were rejected due to artifacts. In addition, after artifact rejection, 50.25% (range 48.7% - 53.2% across subjects) of remaining target presentations were on the left side of the screen, indicating that artifacts were distributed equally between left and right targets. Performance was quite stable across the course of the EEG recording session (paired t-test comparing accuracy in the first and last block $t(15)<0.058$, $p> 0.95$).

Statistics

For all analyses we report results from contiguous groups of 3 electrodes of interest (EOIs) located over the left and right occipital cortex identified a priori based on previous studies – namely: P3, Po7 Po3 over left occipital cortex and P4, Po8 and Po4 over right occipital cortex(Itthipuripat et al., 2014; G. R. Mangun & Hillyard, 1988; G R Mangun & Hillyard, 1987; Sauseng et al., 2005). All data are arranged according to target location such that electrodes were subsequently referred to as contralateral and ipsilateral electrodes throughout the paper. Finally, all statistical comparisons were paired t-tests where p-values were computed using an empirical null distribution of t-values computed by randomizing condition labels 10,000 times (except for Figure 2.8c and Figure 2.9 where ANOVAs were used, see below). For example, to compare responses between contralateral and ipsilateral electrodes, we generated an empirical null distribution by pseudo-randomly swapping or maintaining the contralateral/ipsilateral labels on each trial for each subject and then repeating the entire statistical analysis pipeline as normal (and this procedure was repeated 10,000 times). Thus, note than any p-values reported as 0 indicate that the observed effect was larger than any of the 10,000 iterations of this

randomization procedure. For consistency across analyses, we also used t-tests on difference scores to evaluate interaction terms, in which case the t-values we report are equivalent to the square root of the F-values that are produced by an analysis of variance (ANOVA). For ERPs, statistical comparisons were performed on average amplitudes in 50 ms time windows centered on peak latencies in the grand average waveforms(Luck, 2012), or from 210-260 and 460-510 ms post stimulus for the END and LPD respectively(Busch et al., 2009; Hickey et al., 2010; Itthipuripat et al., 2015, 2014; George R. Mangun & Buck, 1998). Note that our slightly delayed ERP epochs (when compared to some previous studies) are consistent with the low contrast of our stimulus and difficulty of our task(Busch et al., 2009; Cravo et al., 2013; George R. Mangun & Buck, 1998). Otherwise, statistical comparisons were performed at each sample in either a 500 ms prestimulus epoch (for instantaneous frequency) or a 1000 ms poststimulus epoch (amplitude, PaA), based on previous studies (Busch et al., 2009; Dugue et al., 2011; Pascal Fries et al., 2008; Wolfgang Klimesch, 1996; Wolfgang Klimesch et al., 2007; Mathewson et al., 2009; Pfurtscheller, 2001; von Stein et al., 2000). Statistical comparisons of the correlations between real alpha amplitude and PaA were performed over the entire 1750 ms epoch to err on the side of being conservative since there is no precedent in the literature. All p-values were then FDR corrected at p<=0.05(Benjamini & Hochberg, 2016).

For the analysis in Figure 2.8c, trials were sorted based on their average frequency in either a pre (-350:-50 ms) or post (350:650 ms) stimulus epoch based on timepoints significant for Figures 2.4B and 2.5B. Specifically, the lowest (<<) bin consisted of trials in the lower half of a median split of trials with a mean frequency below peak alpha. Accordingly, the second lowest (<) bin were trials in the upper half of a median split of trials with frequency below peak alpha. The > and >> bins were computed similarly, but were composed of trials with means greater than peak alpha. Average amplitude and PaA were then computed for these trials and epochs. A two-way repeated-measures ANOVA with frequency bin and accuracy was used to assess how amplitude and PaA depended on frequency in these epochs, and p-values were computed

by comparing observed F values to a distribution obtained from 10,000 randomizations of condition labels. Finally, Figure 2.9 and Tables 2.6 and 2.7 were computed using a three-way repeated measures ANOVA with the pedestal contrast of the target (collapsed across consecutive pedestals to yield 3 instead of 6 levels), accuracy and topography as factors. The analyses in Figure 2.9 and Table 2.6 and 2 use only the divided attention trials to make the interpretation of these timecourses more comparable to those analyzed in Experiment 1 (in which the location of the target was not pre-cued). P-values were computed by comparing F-values to distributions obtained by shuffling condition labels 5,000 times.

ERPs

ERPs were obtained by averaging stimulus-locked time courses for each electrode of interest and then using a low-pass third order Butterworth filter with a cutoff frequency = 5 Hz). All time frequency analyses were performed using custom MATLAB scripts (see below for details). To avoid edge artifacts, all filtering was applied to 6 second epochs centered on stimulus presentation, after which peri-stimulus time epochs of interest were extracted (i.e. epochs +-1,000 ms around the presentation of each target). Note that all statistical analyses were performed on data before the 5Hz low-pass filter was applied. The low-passed data were presented in the figures for visualization purposes only. Also note that there was not a pronounced P1 component (assessed by using a cutoff frequency of 15 Hz), consistent with the use of a low contrast or briefly presented target stimulus(Busch et al., 2009; Itthipuripat et al., 2014).

Alpha amplitude

The time course of stimulus-locked alpha amplitude at each electrode's peak alpha frequency was extracted by bandpass filtering the data with a third order Butterworth filter spanning ± 2.5 Hz centered on the peak frequency to EEG data from each electrode and

subject and then applying a Hilbert transform to this filtered time series. As in the preprocessing of the EEG data for generating ERPs (see above), we applied the bandpass filter to a 6,000 ms epoch surrounding target onset to avoid contaminating the peri-stimulus window (±1,000 ms) with edge artifacts. Alpha amplitude on trial *k* at time *t* was estimated by Hilbert transforming the bandpassed time series to yield a complex representation of the form $Ce^{i\omega}$. Note that C describes the amplitude and ω the frequency of the signal. Thus, we take the absolute value of these complex coefficients to yield an amplitude estimate:

$$A_{k(t)} = \left| C_{k(t)} e^{i\omega_{k(t)}} \right|$$

All amplitude values were then baselined on a trial-by trial basis by subtracting the mean amplitude -1000 to -750 ms before the stimulus.

Instantaneous Frequency

Instantaneous frequency is defined as the first derivative in time of the phase of the EEG signal, or the change in phase per unit time as time approaches zero (see (Cohen, 2014) for review). For each subject and EOI, artifact free epochs were bandpass filtered at ±2.5 Hz around peak alpha using a 3rd order Butterworth filter (again, bandpass filtering done on 6000 ms epochs surrounding target onset to attenuate edge artifacts in the peri-stimulus window). We then applied a Hilbert transform to the filtered data from each epoch to obtain the amplitude and phase of the EEG response at each point in time on each trial. The phase angle was unwrapped to be cumulative so that there were no discontinuities at –pi and pi. We then calculated instantaneous frequency by approximating the derivative of these unwrapped phase angles. To yield an estimate of frequency in Hz at time *t* and trial *k*, we then normalized this approximate derivative by the sampling rate (*sr*). Because computing numerical derivatives of discretely sampled timeseries can produce sharp discontinuities, we attenuate the influence of these

outliers by low-pass filtering our estimates of the derivative of the phase angle. More formally, we estimated the instantaneous frequency on trial *k* and time *t* by fitting a line of the following form to the unwrapped phase data in temporal window of 88 data samples centered on time t:

$$p_{\mathrm{t,k}} = d\phi_{\mathrm{k(t)}}\mathbf{x} + I_{\mathrm{t,k}}$$

Where $p_{\mathrm{t,k}}$ corresponds to the estimated unwrapped phase, parameterized by scalar $d\phi_{\mathrm{k(t)}}$, or an estimated slope (change in phase angle ϕ), vector x, the time axis, and scalar $I_{\mathrm{t,k}}$, the y intercept. The window size of 172 ms for x, corresponding to 88 data samples at *sr* = 512 Hz, was selected because it was the smallest window that kept the average instantaneous frequency fluctuations on single trials within the 5 Hz wide bandpass range (Figure 2.2.1). Given this fit, we defined instantaneous frequency at time *t* and trial *k*:

$$\omega_{inst}(\mathrm{k,t}) = \frac{d\phi_{\mathrm{k(t)}}}{2\pi} * sr + I_{\mathrm{t,k}}$$

Where $\omega_{inst}(\mathrm{k,t})$ corresponds to an estimate of the instantaneous frequency at time *t* on trial *k*. The regression lines were estimated using a least squares fitting algorithm to the unwrapped phase data and the fits were generally quite good (R^2 = 0.995 ± 0.016, mean ± SD). We also evaluated our results by estimating instantaneous frequency by simply subtracting sequential points along the timeourse of the unwrapped phase:

$$d\phi_{k(t)} = \phi_{\mathrm{k(t+1)}} - \phi_{\mathrm{k(t)}}$$

$$\omega_{inst}(\mathrm{k,t}) = \frac{d\phi_{\mathrm{k(t)}}}{2\pi} * sr$$

However, due to occasional sharp discontinuities in the first derivative, this second method then requires the application of median filters over large temporal windows to attenuate the influence of fluctuations far outside of the bandpass range (see (Cohen, 2014; Samaha & Postle, 2015)). In our data sets, both methods yielded similar results.

Look-up-tables relating frequency and amplitude

To generate the look-up-tables (look-up-tables) that were used to relate changes in instantaneous frequency and amplitude, we used a wavelet decomposition based on a family of Morlet functions with center frequencies ranging from 3 to 20 Hz in 0.1 Hz steps. Using these wavelets, the amplitude at each frequency in this band was estimated and stored for use in the main analysis. To avoid biasing the results, the amplitude look-up-tables were calculated from a set of 6-second-long epochs drawn from an equal number of correct and incorrect trials separately for each subject and electrode (mean number of trials across subjects: 325 ± 36 SD). These spectra were also used to define peak alpha for each subject and EOI (10.3 Hz ± 1.1Hz SD across subjects in the 6 posterior electrodes of interest). The use of averaging many long epochs to estimate amplitude spectra (for our look-up-tables) is related to Welch's method(Welch, 1967). This method is common in spectral density estimation for achieving both 1) high frequency resolution and 2) low variance and stability in the estimate. Thus, this procedure produces stable amplitude spectra for each subject and electrode. In fact, within a subject the three contralateral channels we analyzed are correlated at 0.97 ± 0.02 SD, illustrating that our technique tends to converge on similar, stable spectra for neighboring channels. In contrast, the three contralateral channels show a much weaker correlation of 0.69 ± 0.09 SD between subjects, confirming that these spectra are phenotypic and subject specific.

To generate white noise look-up-tables, we used the built in white Gaussian noise (wgn) function in Matlab with parameter output power set to 1 dBw. We generated 6 second epochs of white noise separately for each subject using the number of trials in their dataset. Look-up-tables were then estimated by using a wavelet decomposition of these trials as described above. This process was repeated for 5000 iterations so we could assess the stability of resultant PaA estimates.

Shuffled look-up-tables used for statistical comparison were computed by pseudo-randomly shuffling the frequency axis (3:20 Hz in steps of 0.1) of each subject and electrode's original look-up-Table 2.5000 times.

Finally, to generate 1/f look-up-tables, we fit a two-term exponential to each subject and electrode's original look-up-table using Matlab's built in fit function and excluded the alpha bump (i.e. fit only amplitudes at frequencies below 5 and above 14 hz) in the fitting procedure.

Predicted alpha amplitude

We evaluated the hypothesis that changes in alpha amplitude and shifts in instantaneous frequency are interdependent by using each subject's amplitude spectra as a look-up-table to link these two metrics (as shown in Figure 2.1b). On every trial and timepoint, instantaneous frequency was used to index into this look-up-table, yielding a predicted amplitude value for each timepoint and trial. The alpha amplitude distribution is known to be a stable trait(Grandy et al., n.d.) – hence we are using each subject's phenotypic amplitude spectrum to generate single trial predicted alpha amplitude (PaA, Figure 2.2b). Single trial examples of PaA and amplitude are shown for 3 subjects (2, 13 and 15) on trials and electrodes 814, 623, 193 and 30, 26, 63, respectively (Figure 2.7b).

Correlations with observed alpha amplitude

We correlated PaA timecourses – computed by passing instantaneous frequency through the amplitude look-up-table – with empirically observed amplitude timecourses on a time-point by time-point basis. Note that these correlations emphasize the similarity of the timecourses as opposed to matching the exact scaling of the PaA with respect to the scale of the empirically observed data. Indeed, differences in the overall magnitude of PaA and the observed amplitude vary because a) wavelet transforms were used to estimate the look-up-tables while Hilbert transforms on bandpassed data were used to generate empirical estimates

of alpha amplitude and b) stable amplitude look-up-tables result from averaging many trials, and thus PaA reflect these average magnitudes as opposed to the single trial magnitudes for observed amplitude. We used wavelets to generate the look-up-tables so that we could increase the frequency resolution of our look-up-tables (i.e. smaller step sizes along the x-axis in Figure 2.1b). In Experiment 1, we computed correlations over 2,000 ms epochs centered on target presentation. In Experiment 2, we computed correlations over 4,000 ms epochs locked to an attentional cue that occurred 0.5 seconds into each trial.

Phase locking and phase bifurcation index

To make contact with previous papers, we also examined the relationship between alpha phase and behavioral performance. We first computed the intertrial phase locking index (PLI) by applying Hilbert transforms to data bandpassed around peak alpha as described previously. PLI was estimated from the complex values obtained from this Hilbert transform at time *t* over trials 1 to *k* using the formula:

$$PLI(\mathrm{t}) = \frac{1}{k}\sum_{1}^{k}\frac{C_{\mathrm{k(t)}}e^{\mathrm{i}\omega_{\mathrm{k(t)}}}}{\left|C_{\mathrm{k(t)}}e^{\mathrm{i}\omega_{\mathrm{k(t)}}}\right|}.$$

Where $Ce^{\mathrm{i}\omega}$ is the same complex representation of the data as outlined in the amplitude section above. This value ranges from 0 - 1 (no phase locking - perfect phase locking at any phase). Since stimulus onset was unpredictable, alpha phase should be randomly distributed pre-stimulus over all trials. Thus, we computed a phase bifurcation index from PLI to assess whether any observed phase locking occurred at the same or opposite phases between accuracy conditions (as described in (Busch et al., 2009; Dugue et al., 2011)). Bifurcation was computed over correct and incorrect trials at time t:

$$B(\mathrm{t}) = (PLI(\mathrm{t})_{\mathrm{correct}} - PLI(\mathrm{t})_{\mathrm{all}}) \times (PLI(\mathrm{t})_{\mathrm{incorrect}} - PLI(\mathrm{t})_{\mathrm{all}}).$$

Note that this value ranges from 1 (perfect phase locking in both conditions at opposite phases, leading to $PLI_{all} = 0$) to -1 (perfect phase locking in only one condition). Values close to zero

indicate random phase distributions for correct and incorrect trials (Figure 2.12, (Busch et al., 2009)).

Harmonic Oscillators - Amplitude and frequency are linked through oscillatory drive and local dampening

Here we derive an expression for amplitude in a target region (A_T) as a function of parameters of oscillators in the target and driving regions. We model voltage changes in time v(t) in the target region as a damped, driven harmonic oscillator with a second order differential equation of the form:

$$(1)\ mv(t)'' + cv(t)' + kv(t) = D(t)$$

Where $I(t)$ is sinusoidal driving force, let $D(t) = A_D cos(\omega_D t)$ without loss of generality (using sin to model the driving force yields identical results). The characteristic frequency in this target region (i.e. absent of driving force $D(t)$) depends on the parameters of this oscillator:

$$(2)\ \omega_T = \sqrt{k/m}$$

Using the method of undetermined coefficients, the steady state (particular) solution of (1) is

$$(3)\ v_{ss} = acos(\omega_D t) + bsin(\omega_D t)$$

Where amplitude in the target region (A_T) depends on coefficients a and b as follows

$$(4)\ A_T = \sqrt{a^2 + b^2}$$

To find expressions for a and b, and thus for A_T, we substitute v_{ss} in (2) for v in (1) to obtain

$$(5)\ (-am{\omega_D}^2 + bc\omega_D + ak)\cos(\omega_D t) + (-bm{\omega_D}^2 - ac\omega_D + bk)\sin(\omega_D t) = A_D cos(\omega_D t)$$

Equating terms with sin and cos yields the following system of equations:

$$(6)\ a(k - m{\omega_D}^2) + bc\omega_D = A_D$$
$$b(k - m{\omega_D}^2) - ac\omega_D = 0$$

Solving this system for a and b, we obtain

$$(7)\ a(k - m\omega_D{}^2)^2 + ac^2\omega_D{}^2 = A_D(k - m\omega_D{}^2)$$
$$a = A_D \frac{k - m\omega_D{}^2}{(k - m\omega_D{}^2)^2 + c^2\omega_D{}^2}$$
$$b(k - m\omega_D{}^2)^2 + bc^2\omega_D{}^2 = A_D c\omega_D$$
$$b = A_D \frac{c\omega_D}{(k - m\omega_D{}^2)^2 + c^2\omega_D{}^2}$$

Given $(k - m\omega_D{}^2)^2 + \omega_D{}^2c^2 \neq 0$. We then utilize the identity in (2) to write the system of equations in terms of ω_T

$$(8)\ a = A_D \frac{m(\omega_T{}^2 - \omega_D{}^2)}{m^2(\omega_T{}^2 - \omega_D{}^2)^2 + c^2\omega_D{}^2}$$
$$b = A_D \frac{c\omega_D}{m^2(\omega_T{}^2 - \omega_D{}^2)^2 + c^2\omega_D{}^2}$$

Finally, we can combine a and b using (4) to show that

$$(9)\ A_T = \sqrt{a^2 + b^2}$$
$$= \frac{A_D}{\sqrt{m^2(\omega_T{}^2 - \omega_D{}^2)^2 + c^2\omega_D{}^2}}$$

This demonstrates that A_T depends directly on ω_T. If there is no dampening, i.e. $c = 0$, maximal A_T is achieved as $\omega_D \rightarrow \omega_T$ (note that without dampening, A_T is infinite when $\omega_D = \omega_T$). In the case of dampening, $c > 0$, the effective characteristic frequency in the target region, ω_{eT} is bounded as follows: $\omega_{eT} \leq \sqrt{\omega_T{}^2 - \frac{c^2}{2m^2}}$ and maximal A_T is achieved as $\omega_D \rightarrow \omega_{eT}$. In both cases, amplitude in the target region will be maximal when that region is receiving ω_D close to its intrinsic frequency, and will fall off as $|\omega_D - \omega_{(e)T}|$ grows. This demonstrates that there are inherent dependencies between amplitude and frequency using the simplest possible model of a driven oscillation.

Data availability

EEG data and Matlab code supporting the frequency and predicted alpha amplitude findings of this study have been deposited in the open science framework with accessible at

https://osf.io/wkx5h/. Further data that support the findings of this study are available from the corresponding author upon reasonable request.

Acknowledgements:

We thank Sarah Fraley for help with data collection, and Eran Mukamel, Vy Vo, Bradley Voytek, Tommy Sprague, and Bradley Postle for useful discussions. Supported by NSDEG graduate fellowship to S.N., by HHMI international student fellowship and a Royal Thai Scholarship from the Ministry of Science and Technology, Thailand to S.I., and by NEI R21-EY024733, NEI R01-EY025872, and James S. McDonnell Foundation awards to J.T.S.

Contributions

S.N. and J.S. conceived the idea. S.N. carried out EEG experiment and analysis of data. R.S. provided feedback on time-frequency decomposition methods. S.I. provided data for analysis of relationship in Experiment 2. S.N and J.S. co-wrote the paper. All authors discussed the results and commented on the manuscript.

Competing interests

The authors declare no competing financial interests.

Chapter 2, in full, is a reprint of the material as it appears in: Nelli, S., Itthipuripat, S., Srinivasan, R., & Serences, J. T. (2017). Fluctuations in instantaneous frequency predict alpha amplitude during visual perception. *Nature communications*, *8*(1), 2071. The dissertation author was the primary investigator and author of this paper.

REFERENCES

Akam, T., & Kullmann, D. M. (2014). Oscillatory multiplexing of population codes for selective communication in the mammalian brain. *Nature Reviews. Neuroscience*, *15*(2), 111–22. http://doi.org/10.1038/nrn3668

Anderson, J. S., Carandini, M., Ferster, D., & Sherman, S. M. (2000). Orientation Tuning of Input Conductance , Excitation , and Inhibition in Cat Primary Visual Cortex Orientation Tuning of Input Conductance , Excitation , and Inhibition in Cat Primary Visual Cortex. *Journal of Neurophysiology*, *84*, 909–926.

Aronson, D. G., Ermentrout, G. B., & Kopell, N. (1990). Amplitude response of coupled oscillators. *Physica D: Nonlinear Phenomena*, *41*(3), 403–449. http://doi.org/10.1016/0167-2789(90)90007-C

Atallah, B. V., & Scanziani, M. (2009). Instantaneous Modulation of Gamma Oscillation Frequency by Balancing Excitation with Inhibition. *Neuron*, *62*(4), 566–577. http://doi.org/10.1016/j.neuron.2009.04.027

Azouz, R., & Gray, C. M. (2000). Dynamic spike threshold reveals a mechanism for synaptic coincidence detection in cortical neurons in vivo. *Proceedings of the National Academy of Sciences of the United States of America*, *97*(14), 8110–8115. http://doi.org/10.1073/pnas.130200797

Başar, E., Schurmann, M., Başar-Eroglu, C., & Karaka, S. (1997). Alpha oscillations in brain functioning : an integrative theory. *International Journal of Psychophysiology*, *26*. http://doi.org/10.1016/S0167-8760(97)00753-8

Benjamini, Y., & Hochberg, Y. (2016). Controlling the False Discovery Rate: A Practical and Powerful Approach to Multiple Testing. *Journal of the Royal Statistical Society*, *57*(1), 289–300.

Blatow, M., Rozov, A., Katona, I., Hormuzdi, S. G., Meyer, A. H., Whittington, M. A., … Monyer, H. (2003). A novel network of multipolar bursting interneurons generates theta frequency oscillations in neocortex. *Neuron*, *38*(5), 805–817. http://doi.org/10.1016/S0896-6273(03)00300-3

Boccaletti, S., Kurths, J., Osipov, G., Valladares, D. L., & Zhou, C. S. (2002). The synchronization of chaotic systems, *366*, 1–101.

Bosman, C. A., Schoffelen, J. M., Brunet, N., Oostenveld, R., Bastos, A. M., Womelsdorf, T., … Fries, P. (2012). Attentional Stimulus Selection through Selective Synchronization between Monkey Visual Areas. *Neuron*, *75*(5), 875–888. http://doi.org/10.1016/j.neuron.2012.06.037

Brunel, N., & Wang, X.-J. (2003). What Determines the Frequency of Fast Network Oscillations With Irregular Neural Discharges? I. Synaptic Dynamics and Excitation-Inhibition Balance. *Journal of Neurophysiology*, *90*(1), 415–430. http://doi.org/10.1152/jn.01095.2002

Busch, N., Dubois, J., & VanRullen, R. (2009). The phase of ongoing EEG oscillations predicts visual perception. *The Journal of Neuroscience : The Official Journal of the Society for Neuroscience*, *29*(24), 7869–7876. http://doi.org/10.1523/JNEUROSCI.0113-09.2009

Buzsáki, G., & Chrobak, J. J. (1995). Temporal structure in spatially organized neuronal ensembles: a role for interneuronal networks. *Current Opinion in Neurobiology*, *5*(4), 504–510. http://doi.org/10.1016/0959-4388(95)80012-3

Carandini, M., & Heeger, D. (2012). Normalization as a canonical neural computation. *Nature Reviews Neuroscience*, (November), 1–12. http://doi.org/10.1038/nrn3136

Cohen, M. X. (2014). Fluctuations in oscillation frequency control spike timing and coordinate neural networks. *The Journal of Neuroscience : The Official Journal of the Society for Neuroscience*, *34*(27), 8988–98. http://doi.org/10.1523/JNEUROSCI.0261-14.2014

Cravo, A. M., Rohenkohl, G., Wyart, V., & Nobre, A. C. (2013). Temporal expectation enhances contrast sensitivity by phase entrainment of low-frequency oscillations in visual cortex. *The Journal of Neuroscience : The Official Journal of the Society for Neuroscience*, *33*(9), 4002–10. http://doi.org/10.1523/JNEUROSCI.4675-12.2013

Draguhn, A., Buzsáki, G., Andreas, D., & Draguhn, A. (2004). Neuronal Oscillations in Cortical Networks. *Science*, *304*(June), 1926. http://doi.org/10.1126/science.1099745

Dugue, L., Marque, P., & VanRullen, R. (2011). The Phase of Ongoing Oscillations Mediates the Causal Relation between Brain Excitation and Visual Perception. *Journal of Neuroscience*, *31*(33), 11889–11893. http://doi.org/10.1523/JNEUROSCI.1161-11.2011

Elton, M., Winter, O., Heslenfeld, D., Loewy, D., Campbell, K., & Kok, A. (1997). Event-related potentials to tones in the absence and presence of sleep spindles. *Journal of Sleep Research*, *6*(2), 78–83. http://doi.org/10.1046/j.1365-2869.1997.00033.x

Foxe, J. J., Simpson, G. V, & Ahlfors, S. P. (1998). Parieto-occipital approximately 10 Hz activity reflects anticipatory state of visual attention mechanisms. *Neuroreport*, *9*(17), 3929–3933. http://doi.org/10.1097/00001756-199812010-00030

Fries, P. (2005). A mechanism for cognitive dynamics: Neuronal communication through neuronal coherence. *Trends in Cognitive Sciences*, *9*(10), 474–480. http://doi.org/10.1016/j.tics.2005.08.011

Fries, P. (2015). Rhythms for Cognition: Communication through Coherence. *Neuron*, *88*(1), 220–235. http://doi.org/10.1016/j.neuron.2015.09.034

Fries, P., Reynolds, J. H., Rorie, a E., & Desimone, R. (2001). Modulation of oscillatory neuronal synchronization by selective visual attention. *Science (New York, N.Y.)*, *291*(FEBRUARY), 1560–1563. http://doi.org/10.1126/science.1055465

Fries, P., Womelsdorf, T., Oostenveld, R., & Desimone, R. (2008). The effects of visual stimulation and selective visual attention on rhythmic neuronal synchronization in macaque area V4. *The Journal of Neuroscience : The Official Journal of the Society for Neuroscience*, *28*(18), 4823–4835. http://doi.org/10.1523/JNEUROSCI.4499-07.2008

Grandy, T. H., Werkle-Bergner, M., Chicherio, C., Schmiedek, F., Lövdén, M., & Lindenberger, U. (n.d.). Peak individual alpha frequency qualifies as a stable neurophysiological trait marker in healthy younger and older adults. http://doi.org/10.1111/psyp.12043

Gray, C. M., & Singer, W. (1989). Stimulus-specific neuronal oscillations in orientation columns of cat visual cortex. *Proceedings of the National Academy of Sciences of the United States of America*, *86*(5), 1698–1702. http://doi.org/10.1073/pnas.86.5.1698

Händel, B. F., Haarmeier, T., & Jensen, O. (2011). Alpha oscillations correlate with the successful inhibition of unattended stimuli. *Journal of Cognitive Neuroscience*, *23*(9), 2494–2502. http://doi.org/10.1162/jocn.2010.21557

Hasenstaub, A., Shu, Y., Haider, B., Kraushaar, U., Duque, A., & McCormick, D. A. (2005). Inhibitory postsynaptic potentials carry synchronized frequency information in active cortical networks. *Neuron*, *47*(3), 423–435. http://doi.org/10.1016/j.neuron.2005.06.016

Heeger, D. J. (1992). Normalization of cell responses in cat striate cortex. *Visual Neuroscience*. http://doi.org/10.1017/S0952523800009640

Heinze, H. J., Luck, S. J., Mangun, G. R., & Hillyard, S. A. (1990). Visual event-related potentials index focused attention within bilateral stimulus arrays. I. Evidence for early selection. *Electroencephalography and Clinical Neurophysiology*, *75*(6), 511–527. http://doi.org/10.1016/0013-4694(90)90138-A

Hickey, C., Van Zoest, W., & Theeuwes, J. (2010). The time course of exogenous and endogenous control of covert attention. *Experimental Brain Research*, *201*(4), 789–796. http://doi.org/10.1007/s00221-009-2094-9

Hutcheon, B., & Yarom, Y. (2000). Resonance, oscillation and the intrinsic frequency preferences of neurons. *Trends in Neuroscience*, *23*(5), 216–222. http://doi.org/10.1016/S0166-2236(00)01547-2

Isaacson, J. S., & Scanziani, M. (2011). How inhibition shapes cortical activity. *Neuron*, *72*(2), 231–243. http://doi.org/10.1016/j.neuron.2011.09.027

Itthipuripat, S., Cha, K., Rangsipat, N., & Serences, J. T. (2015). Value-based attentional capture influences context-dependent decision-making. *J Neurophysiol*, *114*(1), 560–569. http://doi.org/10.1152/jn.00343.2015

Itthipuripat, S., Ester, E. F., Deering, S., & Serences, J. T. (2014). Sensory Gain Outperforms Efficient Readout Mechanisms in Predicting Attention-Related Improvements in Behavior. *Journal of Neuroscience*, *34*(40), 13384–13398. http://doi.org/10.1523/JNEUROSCI.2277-14.2014

Izhikevich, E. M. (2001). Resonate-and-fire neurons. *Neural Networks*, *14*(Special Issue), 883–894.

Izhikevich, E. M. (2003). Simple model of spiking neurons. *IEEE Transactions on Neural Networks*, *14*(6), 1569–1572. http://doi.org/10.1109/TNN.2003.820440

Kayser, C., Montemurro, M. A., Logothetis, N. K., & Panzeri, S. (2009). Spike-Phase Coding Boosts and Stabilizes Information Carried by Spatial and Temporal Spike Patterns. *Neuron*, *61*(4), 597–608. http://doi.org/10.1016/j.neuron.2009.01.008

Kelly, S. P., Gomez-Ramirez, M., & Foxe, J. J. (2009). The strength of anticipatory spatial biasing predicts target discrimination at attended locations: A high-density EEG study. *European Journal of Neuroscience*, *30*(May), 2224–2234. http://doi.org/10.1111/j.1460-9568.2009.06980.x

Klimesch, W. (1996). Memory processes, brain oscillations and EEG synchronization. *International Journal of Psychophysiology*, *24*(1–2), 61–100. http://doi.org/10.1016/S0167-8760(96)00057-8

Klimesch, W., Doppelmayr, M., Röhm, D., Pöllhuber, D., & Stadler, W. (2000). Simultaneous desynchronization and synchronization of different alpha responses in the human electroencephalograph: A neglected paradox? *Neuroscience Letters*, *284*(1–2), 97–100. http://doi.org/10.1016/S0304-3940(00)00985-X

Klimesch, W., Sauseng, P., & Hanslmayr, S. (2007). EEG alpha oscillations: the inhibition-timing hypothesis. *Brain Research Reviews*, *53*(1), 63–88. http://doi.org/10.1016/j.brainresrev.2006.06.003

Lakatos, P., Karmos, G., Mehta, A. D. A. D., Ulbert, I., & Schroeder, C. E. C. E. C. E. (2008). Entrainment of neuronal oscillations as a mechanism of attentional selection. *Science (New York, N.Y.)*, *320*(5872), 110–3. http://doi.org/10.1126/science.1154735

Lakatos, P., O'Connell, M. N., Barczak, A., Mills, A., Javitt, D. C., & Schroeder, C. E. (2009). The Leading Sense: Supramodal Control of Neurophysiological Context by Attention. *Neuron*, *64*(3), 419–430. http://doi.org/10.1016/j.neuron.2009.10.014

Lopes da Silva, F. (2013). EEG and MEG: Relevance to neuroscience. *Neuron*, *80*(5), 1112–1128. http://doi.org/10.1016/j.neuron.2013.10.017

Lopes da Silva, F. H., Vos, J. E., Mooibroek, J., & van Rotterdam, A. (1980). Relative contributions of intracortical and thalamo-cortical processes in the generation of alpha rhythms, revealed by partial coherence analysis. *Electroencephalography and Clinical Neurophysiology*, *50*(5–6), 449–456. http://doi.org/10.1016/0013-4694(80)90011-5

Lowet, E., Roberts, M. J., Peter, A., Gips, B., & Weerd, P. De. (2016). Neuronal gamma-band synchronization regulated by instantaneous modulations of the oscillation frequency. *BioRxiv*.

Luck, S. J. (2012). Event-related potentials. *APA Handbook of Research Methods in Psychology*, *1*, 1–18.

Mangun, G. R., & Buck, L. A. (1998). Sustained visual spatial attention produces costs and benefits in response time and evoked neural activity. *Neuropsychologia*, *36*(3), 189–200. http://doi.org/10.1016/S0028-3932(97)00123-1

Mangun, G. R., & Hillyard, S. A. (1987). The spatial allocation of visual attention as indexed by event- related brain potentials. *Hum.Factors.*, *29*(2), 195–211.

Mangun, G. R., & Hillyard, S. A. (1988). Spatial gradients of visual attention: behavioral and electrophysiological evidence. *Electroencephalography and Clinical Neurophysiology*, *70*(5), 417–428. http://doi.org/10.1016/0013-4694(88)90019-3

Mann, E. O., & Mody, I. (2010). Control of hippocampal gamma oscillation frequency by tonic inhibition and excitation of interneurons. *Nature Neuroscience*, *13*(2), 205–12. http://doi.org/10.1038/nn.2464

Mathewson, K. E., Gratton, G., Fabiani, M., Beck, D. M., & Ro, T. (2009). To see or not to see: prestimulus alpha phase predicts visual awareness. *The Journal of Neuroscience : The Official Journal of the Society for Neuroscience*, *29*(9), 2725–2732. http://doi.org/10.1523/JNEUROSCI.3963-08.2009

Mazzoni, A., Panzeri, S., Logothetis, N. K., & Brunel, N. (2008). Encoding of naturalistic stimuli by local field potential spectra in networks of excitatory and inhibitory neurons. *PLoS Computational Biology*, *4*(12). http://doi.org/10.1371/journal.pcbi.1000239

Meeuwissen, E. B., Takashima, A., Fernández, G., & Jensen, O. (2011). Increase in posterior alpha activity during rehearsal predicts successful long-term memory formation of word sequences. *Human Brain Mapping*, *32*(12), 2045–2053. http://doi.org/10.1002/hbm.21167

Okun, M., & Lampl, I. (2008). Instantaneous correlation of excitation and inhibition during ongoing and sensory-evoked activities. *Nature Neuroscience*, *11*(5), 535–7. http://doi.org/10.1038/nn.2105

Pfurtscheller, G. (2001). Functional brain imaging based on ERD / ERS, *41*, 1257–1260.

Rihs, T. A., Michel, C. M., & Thut, G. (2007). Mechanisms of selective inhibition in visual spatial attention are indexed by ??-band EEG synchronization. *European Journal of Neuroscience*, *25*(2), 603–610. http://doi.org/10.1111/j.1460-9568.2007.05278.x

Rohenkohl, G., & Nobre, a. C. (2011). Alpha Oscillations Related to Anticipatory Attention Follow Temporal Expectations. *Journal of Neuroscience*, *31*(40), 14076–14084. http://doi.org/10.1523/JNEUROSCI.3387-11.2011

Saalmann, Yuri B., Pigarev, Ivan N., Vidyasagar, T. (2007). Neural Mechanisms of Visual Attention: How Top-Down Feedback Highlights Relevant Locations. *Science*, (June), 1612–1615.

Salinas, E., & Sejnowski, T. J. (2001). Correlated neuronal activity and the flow of neural information. *Nature Neuroscience*, *14*(7), 811–819. http://doi.org/10.1038/nn.2842

Samaha, J., & Postle, B. R. (2015). The speed of alpha-band oscillations predicts the temporal resolution of visual perception Jason Samaha and Bradley R. Postle. *Current Biology*, *25*, 2985–2990. http://doi.org/10.1016/j.cub.2015.10.007

Sauseng, P., Klimesch, W., Stadler, W., Schabus, M., Doppelmayr, M., Hanslmayr, S., … Birbaumer, N. (2005). A shift of visual spatial attention is selectively associated with human EEG alpha activity. *Eur J Neurosci*, *22*(11), 2917–2926. http://doi.org/EJN4482 [pii]\r10.1111/j.1460-9568.2005.04482.x

Shao, Z., & Burkhalter, A. (1996). Different balance of excitation and inhibition in forward and feedback circuits of rat visual cortex. *The Journal of Neuroscience : The Official Journal of the Society for Neuroscience*, *16*(22), 7353–7365.

Squires, N. K., Donchin, E., & Squires, K. C. (1977). Bisensory stimulation: Inferring decision-related processes from the P300 component. *Journal of Experimental Psychology: Human Perception and Performance*, *3*(2), 299–315. http://doi.org/10.1037//0096-1523.3.2.299

Thut, G., Nietezl, A., Brandt, S., & Pscual-Leone, A. (2006). -Band Electroencephalographic Activity over Occipital Cortex Indexes Visuospatial Attention Bias and Predicts Visual Target Detection. *Journal of Neuroscience*, *26*(37), 9494–9502. http://doi.org/10.1523/JNEUROSCI.0875-06.2006

van Vreeswijk, C., & Sompolinsky, H. (1996). Reproduced with permission of the copyright owner . Further reproduction prohibited without permission . *Science (New York, N.Y.)*, *274*, 1724–1726. http://doi.org/10.1126/science.274.5293.1724

VanRullen, R. (2016). How to evaluate phase differences between trial groups in ongoing electrophysiological signals. *Frontiers in Neuroscience*, *10*(SEP), 1–22. http://doi.org/10.3389/fnins.2016.00426

Vogels, T. P., Sprekeler, H., Zenke, F., Clopath, C., & Gerstner, W. (2011). Inhibitory plasticity balances excitation and inhibition in sensory pathways and memory networks. *Science (New York, N.Y.)*, *334*(6062), 1569–73. http://doi.org/10.1126/science.1211095

von Stein, a, Chiang, C., & König, P. (2000). Top-down processing mediated by interareal synchronization. *Proceedings of the National Academy of Sciences of the United States of America*, *97*(26), 14748–14753. http://doi.org/10.1073/pnas.97.26.14748

Voorhis, S., & Hillyard, S. a. (1977). Visual evoked potentials and selective attention to points in space. *Perception & Psychophysics*, *22*(1), 54–62. http://doi.org/10.3758/BF03206080

Wang, X. J. (2010). Neurophysiological and computational principles of cortical rhythms in cognition. *Physiological Reviews*, 1195–1268. http://doi.org/10.1152/physrev.00035.2008.

Wehr, M. S., & Zador, A. M. (2003). Balanced inhibition underlies tuning and sharpens spike timing in auditory cortex. *Nature*, *426*(6965), 442–6. http://doi.org/10.1038/nature02116

Welch, P. D. (1967). The Use of Fast Fourier Transform for the Estimation of Power Spectra: A Method Based on Time Averaging Over Short, Modified Periodograms. *IEEE Transactions on Audio and Electroacoustics*, *15*(2), 70–73. http://doi.org/10.1109/TAU.1967.1161901

Womelsdorf, T., Schoffelen, J.-M., Oostenveld, R., Singer, W., Desimone, R., Engel, A. K., & Fries, P. (2007). Modulation of neuronal interactions through neuronal synchronization. *Science (New York, N.Y.)*, *316*(5831), 1609–1612. http://doi.org/10.1126/science.1139597

Yamagishi, N., Callan, D. E., Anderson, S. J., & Kawato, M. (2008). Attentional changes in pre-stimulus oscillatory activity within early visual cortex are predictive of human visual performance. *Brain Research*, *1197*, 115–122. http://doi.org/10.1016/j.brainres.2007.12.063

Yordanova, J., Kolev, V., & Polich, J. (2001). P300 and alpha event-related desynchronization ~ERD! *Psychophysiology*, *38*, 143–152.

Chapter 3: The efficiency of visual processing depends on deviations of alpha rhythms from their endogenous peak frequency

Abstract

Findings concerning how the amplitude and frequency of alpha oscillations (8-12 Hz) impact the efficiency of visual processing make distinct predictions. Specifically, increased alpha amplitude at peak alpha frequency has been linked to cortical inhibition and impaired visual information processing (*tonic inhibition* hypothesis), while increases in peak frequency appear to improve perception by increasing the rate of visual information sampling (*perceptual sampling* hypothesis). As recent reports suggest that alpha amplitude and frequency are linked measurements that result from dynamic circuit interactions, we leveraged this interaction between top-down and bottom-up circuits to simultaneously examine these theories. Subjects (both sexes, N=52) performed a contrast change detection task while bottom-up neural activity was clamped at multiple alpha frequencies using a steady-state flickering stimulus. Two dissociable perceptual patterns emerged as a function of flicker frequency relative to each subject's endogenous peak alpha frequency. Clamping alpha at or above peak frequency impaired perceptual performance in one group of subjects, consistent with the tonic inhibition account, while entrainment at or above peak alpha enhanced performance in the second group. Interestingly, subjects adhering to the tonic inhibition account displayed naturally faster alpha oscillations that traversed the alpha state space less efficiently when clamped at higher frequencies, and vice versa. Thus, clamping neural circuits *away* from their natural alpha frequency leads to more efficient traversal, exposing the perceptual importance of the interaction between alpha drive and endogenous oscillations. This complex relationship also offers an explanation for seemingly disparate findings that alpha oscillations impair vs enhance visual perception.

Significance statement

Complex interactions between oscillations in top-down and bottom-up neural regions jointly impact both alpha amplitude and frequency as measured with scalp EEG. However, distinct predictions about how alpha oscillations impact perception have been postulated based on amplitude vs frequency. By clamping bottom-up circuits, we find evidence for both theories in distinct subjects. A particular subject's perceptual pattern appeared to depend on their peak frequency and the effect of alpha drive on the efficient state-space traversal of endogenous alpha oscillations. Thus, the interaction between alpha drive and each subject's natural, endogenous frequency determines the impact of alpha oscillations on visual perception.

Introduction

A dynamic balance between excitatory and inhibitory neural activity leads to brain rhythms such as the prominent set of oscillations in the alpha band (~7-12 Hz) that mediate visual information processing (Akam & Kullmann, 2014; Anderson, Carandini, Ferster, & Sherman, 2000; Atallah & Scanziani, 2009; Azouz & Gray, 2000; Brunel & Wang, 2003; Carandini & Heeger, 2012; Draguhn, Buzsáki, Andreas, & Draguhn, 2004; Pascal Fries, 2005, 2015; Heeger, 1992; Isaacson & Scanziani, 2011; Lopes da Silva, 2013; Mazzoni, Panzeri, Logothetis, & Brunel, 2008; Saalmann, Yuri B., Pigarev, Ivan N., Vidyasagar, 2007; Salinas & Sejnowski, 2001; van Vreeswijk & Sompolinsky, 1996). On one account, which we refer to as the *tonic inhibition* hypothesis, relatively sluggish increases in alpha amplitude are linked to the suppression of task-irrelevant visual information (For review see (Klimesch, Sauseng, & Hanslmayr, 2007)). For example, the high alpha amplitude typically observed during passive rest is quickly attenuated upon visual stimulation, task engagement, or the deployment of visuo-spatial attention, presumably due to a release from inhibition during active information processing (Bosman et al., 2012; Foxe, Simpson, & Ahlfors, 1998; P Fries, Reynolds, Rorie, & Desimone, 2001; Haegens, Handel, & Jensen, 2011; Kelly, Gomez-Ramirez, & Foxe, 2009;

Meeuwissen, Takashima, Fernández, & Jensen, 2011; Rihs, Michel, & Thut, 2007; Yamagishi, Callan, Anderson, & Kawato, 2008). Moreover, alpha amplitude is selectively higher over cortical areas that encode stimuli presented in unattended spatial locations, consistent with a link between alpha amplitude and the inhibition of irrelevant visual inputs (Sauseng et al., 2005).

A second account, which we term the *perceptual sampling* hypothesis, results from observations that faster alpha oscillations lead to higher perceptual acuity (Nelli, Itthipuripat, Srinivasan, & Serences, 2017; Samaha & Postle, 2015). Interestingly subjects who increase the frequency of their alpha oscillation via neurofeedback improve on working memory and cognitive tasks (Escolano, Aguilar, & Minguez, 2011; Zoefel, Huster, & Herrmann, 2011), and higher alpha frequencies lower two-flash fusion thresholds and higher detection rates between-subjects (Cecere, Rees, & Romei, 2015; Nelli et al., 2017; Samaha & Postle, 2015).The perceptual benefit associated with faster alpha rhythms is thought to arise from faster sampling of incoming visual information due to more rapid cycling between periods of inhibition and excitation as indexed by alpha phase (Busch, Dubois, & VanRullen, 2009; Busch & VanRullen, 2010; de Graaf et al., 2013; Mathewson et al., 2011; Spaak, de Lange, & Jensen, 2014; Zauner et al., 2012). This hypothesis that alpha frequency sets the rate at which the visual system samples and processes visual information provides an alternative to the purely inhibitory account of alpha espoused by the tonic inhibition account (Busch et al., 2009; Busch & VanRullen, 2010; Cecere et al., 2015; de Graaf et al., 2013; Foster & Awh, 2018; Landau & Fries, 2012; Mathewson et al., 2011; Palva & Palva, 2007; Samaha & Postle, 2015; Spaak et al., 2014; VanRullen, 2015; Zauner et al., 2012).

While previous reports have documented changes in alpha oscillations and behavior consistent with either the tonic inhibition or the perceptual sampling accounts, interpreting these findings is challenging because modulations in both alpha amplitude and frequency depend on complex interactions between top-down and bottom-up factors. For example, changes in top-

down demands such as expectation and attention modulate alpha amplitude and frequency in visual cortex, likely from circuit interactions with higher order driving regions that shift the excitatory/inhibitory balance (P Fries et al., 2001; Pascal Fries, Womelsdorf, Oostenveld, & Desimone, 2008; Klimesch, 1996; Klimesch et al., 2007; Nelli et al., 2017; Pfurtscheller, 2001; Rohenkohl & Nobre, 2011; Salinas & Sejnowski, 2001; Samaha & Postle, 2015; Shao & Burkhalter, 1996; von Stein, Chiang, & König, 2000). Consistent with these top-down effects, alpha current generators have been identified in infragranular cortical layers, a major source of feedback projections into visual cortex(Bollimunta, Chen, Schroeder, & Ding, 2008; Buffalo, Fries, Landman, Buschman, & Desimone, 2011; Felleman & Van Essen, 1991; Markov et al., 2014). Additionally, microstimulation of higher visual areas like V4 unidirectionally enhance alpha power in earlier areas like V1 (van Kerkoerle et al., 2014), consistent with causality MEG data suggesting that alpha oscillations propagate selectively from higher to lower-order areas along the cortical hierarchy (Michalareas et al., 2016). In addition to top-down influences, bottom-up factors such as simply opening one's eyes or presenting a salient stimulus also modulate the amplitude and phase/frequency of ongoing alpha oscillations (Lakatos et al., 2009; Rizzuto et al., 2003; Woertz, Pfurtscheller, & Klimesch, 2004). Thus, both top-down factors such as behavioral goals and bottom-up factors such as sensory stimulation interact to drive alpha oscillations as measured with scalp EEG (Nelli et al., 2017).

Here, we exploit the sensitivity of alpha oscillations to both top-down and bottom-up factors to determine the relative contributions of tonic inhibition and perceptual-sampling to visual perception. We recorded scalp EEG as subjects (N=52) viewed a flickering stimulus while performing an attentionally demanding change-detection task at fixation. The visual stimulus was flickered at multiple frequencies around the alpha band to 'clamp', or continually entrain, alpha rhythms in visual regions (from 6-13Hz; Figure 3.1A). Critically, the demanding change detection task allowed us to hold top-down attentional factors constant while we systematically

varied the frequency of the bottom-up stimulus drive. Importantly, we also recorded EEG during an independent rest period to estimate each subject's natural, endogenous peak alpha frequency. Thus, we were able to carefully characterize changes in behavior as a function of the offset between the driving frequency and each subject's endogenous peak alpha frequency (Figure 3.1B). If alpha oscillations primarily regulate perception via inhibitory processes associated with gradual changes in amplitude, then providing stimulus drive at each subject's peak alpha frequency should magnify suppression and negatively impact perception (Tonic Inhibition: Figure 3.1A, bottom left panel). However, if alpha oscillations primarily regulate perception via modulating the rate of perceptual sampling, then clamping rhythms above each subject's peak alpha frequency should systematically improve behavioral performance, and vice versa (Perceptual Sampling: Figure 3.1A, bottom right panel).

Materials & Methods

Participants

57 participants (33 in continuous version and 24 in trial-wise version, see below; 29 male) were recruited at the University of California San Diego and all data were collected at UCSD's Perception and Cognition Lab. All participants provided written informed consent in accordance with the Institutional Review Board at UCSD. Subjects were compensated $15 / hour for EEG. The age range of the subjects was 19-30 years old, and all participants had normal or corrected to normal vision. 5 participants (2 in continuous version, 3 in trial-wise version) were excluded due to having a negative sensitivity metric for one of the entrainment frequency conditions.

Apparatus and Stimuli

The experiment was implemented using Psychtoolbox in the MATLAB programming environment running on a Windows PC with the XP operating system. Subjects were positioned 60 cm from the display and stimuli were presented on a 15-inch CRT monitor with 1024 x 768 resolution and 120 Hz refresh rate. The output of the monitor was linearized in the stimulus presentation software.

Task and stimulus procedure

We flickered a centrally presented checkerboard at 8 frequencies encompassing the traditional alpha band (6.3, 7.1, 8, 9.2, 10, 10.9, 12 and 13.3 Hz; 25% Michaelson contrast and subtending 7.2 degrees visual angle Figure 3.1B). Subjects were instructed to maintain fixation on a black, centrally presented fixation dot, and the target was a dimming of this fixation dot for 16 ms at an unpredictable time. We determined a contrast threshold necessary to maintain roughly 75% hit rates for each subject in a short behavioral session before EEG data acquisition. We ran two versions of the task utilizing either “continuous” or “trial-wise” entrainment, described in detail below.

In the “continuous” entrainment version of the task, we continuously flickered a checkerboard at one frequency for an entire block consisting of 48 target presentations leading to a total of 96 presentations per frequency (two blocks per frequency, 16 total blocks). The flickering stimulus was up for a total of 151.8 seconds (2.53 minutes), and potential target times were selected randomly from 1.2 to 148.8 seconds into the block with the only stipulation that consecutive targets were separated by at least 1.2 seconds and at most 5 seconds. Subjects could respond at any time, and we ensured that consecutive blocks of trials did not occur at the same entrainment frequency and randomized frequency order between subjects.

In the “trial-wise” version, the entrainment frequency was chosen pseudo-randomly on each trial within a block, with 48 trials per block and 10 total blocks. Fixation contrast changes

only occurred on 2/3 of trials, leading to a total of 60 trials per frequency. We randomly chose target times to occur within 2208 – 2525 ms after the onset of the flickering stimulus to allow the entrained rhythm to reach a stable steady state before the target occurred (stimulus flickered for a total of 3000 ms). For the trial-wise version, the difference between the earliest and latest target times were fixed to be at least 95% of the total possible target onset time range (equal to 301 ms) to make sure target times were maximally unpredictable. Subjects could respond anytime during the trial or intertrial interval, which was chosen pseudorandomly on each trial from 1750 to 2250 ms.

Behavioral metrics

For the continuous entrainment task version, a response was considered a correct detection (a "hit") if it occurred from 84 – 1000 ms after a target while any response made outside this temporal window was considered a false alarm. This minimum RT of 84 seconds was also used in the trial-wise version of the experiment, although note that subjects could respond anytime during the ITI, which exceeded 1000 ms in the trial-wise version. An estimate of sensitivity (d') was calculated from hit and false alarm rates by: Z(hit rate) - Z(FA), while bias (criterion) was calculated as –0.5*(Z(hit rate) + Z(FA)).

EEG recording and preprocessing

All EEG recordings took place in a sound-attenuated and electromagnetically shielded room (ETS Lindgren, Cedar Park, TX). EEG and EOG were recorded with a Biosemi Active2 System (Amsterdam, The Netherlands) using a headcap with standard Biosemi 64 electrode layout. In addition to the 64 scalp electrodes, one reference electrode was placed on each mastoid (2 total), and 6 electrodes were placed around the eyes to identify and reject trials with blink and saccade artifacts. All EEG data were recorded at a sampling rate of 1024 Hz. Event

triggers were recorded in the EEG data file to precisely mark the time of each target presentation and the time of the subject's response.

After data collection, data from the scalp electrodes were re-referenced to the algebraic mean of the two mastoid electrodes. Then, the raw time series from each electrode was bandpass filtered between 0.25 to 55 Hz to attenuate eyeblinks, drift, and 60 Hz line noise. Data were either aligned to the nearest "on" frame of the flickering stimulus (for steady state visual evoked potential, or SSVEP, analyses) or to the target (event related potential, or ERP, analyses) before epoching. This was done because neural activity evoked by the SSVEP rely heavily on the phase of the stimulus, while ERP analyses depend only on the target time.

Peak endogenous frequency estimation

In addition to the main task, we recorded scalp EEG data in order to independently estimate each subject's endogenous peak alpha frequency. Subjects first completed half of the experimental blocks, which took approximately 20 minutes for both experiments (8 blocks for the continuous flicker, 5 blocks for the trial-wise flicker). Then, subjects were simply instructed to relax and fixate on a central fixation point for 3 minutes and then subsequently asked to close their eyes and relax for 3 minutes. We report peak frequency estimates from this latter, 3 minute eyes closed portion of the data due both precedent in the literature and higher signal-to-noise (SNR, see below) (Cohen, 2014; Samaha & Postle, 2015; Zauner et al., 2012). We computed spectra from raw, unfiltered data, which was epoched into 2000 clean (e.g. artifact free) 4 second intervals. Specifically, uV cutoffs were set to be more than 3 standard deviations from average, and cutoff ceilings and floors were set at 100 uV and 50 uV, respectively. Epochs were excluded from selection if they included more than 3 timepoints in any channel that exceeded this cutoff, and an entire channel was considered "bad" if more than 1.5% of total timepoints exceeded this cutoff (average channel/trial rejection counts were 9.7/28.2 and 9.4/20.4 for the continuous and trial-wise versions respectively). We extracted complex coefficients for these

2000 epochs at center frequencies from 2 to 20 Hz in steps of 0.1 Hz using overcomplete wavelets decomposition with 0.15 fractional bandwidth (equivalent to the bandwidth at full-width-half-max divided by the center frequency). We then estimated power at each frequency by squaring the absolute value of the complex coefficients for each epoch before averaging over all epochs (e.g., computing endogenous alpha power (Welch, 1967)). Peak alpha frequency was estimated from these spectra by extracting the frequency with maximal power within the range of 7 – 12.5 Hz. For each subject we discarded channels that did not have an apparent alpha bump, quantified by low SNR. Specifically, we computed the percent increase from the average power at the frequencies ±3 Hz from the estimated peak alpha frequency, and channels with a SNR value < 1 were input with a NaN. For eyes closed spectra, this lead to roughly 12.8 ± 13.8 SD out of 57 subjects with an NaN value per channel, while eyes open spectra had roughly 19.4 ± 12 SD out of 57 subjects that had a NaN value per channel, and this increase in number of subjects with no alpha bump in the eyes open condition was consistent across all electrodes ($t(63) = 16.8$, $p < 10^{-24}$) . Finally, in the main text we report peak alpha frequency as the mean endogenous frequency averaged across Oz and 4 surrounding electrodes as the peak alpha frequency (POz, Iz, O1 and O2; consistent with previous literature(Cohen & Gulbinaite, 2017)). For these 5 electrodes, an average of 7.2 ± 1.6 SD subjects had no peak frequency when estimated with eyes closed, compared with 16.6 ± 2.2 SD for eyes open ($t(4) = 15.7$, $p < 0.0001$).

Rhythmic Entrainment Source Separation (RESS) analysis

Although we briefly describe methods for this data here, source-localized RESS timecourses were extracted for single trials using exactly the procedure and Matlab scripts described in (Cohen & Gulbinaite, 2017). For each flicker frequency, the covariance matrix of the data at that frequency was computed (covariance at, or CA), as well as the covariance matrices ± 1Hz from the flicker frequency (covariance surround, or CS). We then found the

eigenvalues (e_{vals}) and eigenvectors (e_{vecs}) such that $CA*e_{vecs} = CS*e_{vecs}*e_{vals}$ using Matlab's builtin eig function. For each subject and frequency, we extracted the eigenvector with maximum eigenvalue as a scalp map for that entrainment frequency and entrainment frequency, which were used in two ways in the data. First, we obtained single trial RESS timecourses by filtering data at each timepoint and trial by that scalp map (e_{vec}*data). Second, PCA analyses were computed on data with the entrained scalp map projected out (described in PCA trajectory methods section).

Entrainment analyses

After preprocessing, task engaged RESS and raw data were subjected to wavelet decomposition to determine whether there was selective entrainment at the flicker frequencies. Data were averaged over all trials of each flicker frequency, and then complex coefficients were extracted using overcomplete wavelet decomposition with fractional-bandwidth of 0.1 at all of the possible entrainment frequencies due to the narrow spacing of the flicker frequencies. For analyses comparing entrainment between detected and undetected trials, we randomly sampled the minimum number of trials 100 times to balance between detected and undetected trial counts. 5 subjects had ≤ 1 trial in which the target went undetected trials for at least one of the entrainment frequencies, and thus these subjects were excluded from these specific statistical comparisons.

Behavioral Interpolation

We interpolated behavioral metrics for each subject to their peak alpha frequency as estimated during an eyes closed resting period. To do this, we chose to use a 1D shape-preserving piecewise cubic interpolation ("pchip") because this algorithm interpolates locally (instead of considering all of the data) without being subject to overshoots and without

introducing oscillations in the case that the data are not smooth(N. Fritsch & E. Carlson, 1980). Specifically, the pchip interpolating function p(X(j)) = Y(j), satisfies the following conditions:

1) p' is continuous.
2) p'(X(j)) is chosen so that p(x) respects monotonicity, meaning if the data is monotonic so is p(x).

We chose to interpolate from -1.5 to +1.5 Hz around each subject's endogenous peak frequency in steps of 0.5 Hz for all interpolation analyses.

Sinusoidal regression model

To quantify behavior aligned to peak alpha, we fit each behavioral metric separately for each subject using a model that included a linear and two sinusoidal regressors that were each one cycle defined over the 7 interpolated points (a sine and a cosine function). The cosine regressor reached a minimum at the peak frequency while the sine regressor was simply one orthogonal cycle (phase shifted by 90 degrees), thus forming a complete basis over the period defined by the interpolation range. We also included an intercept and a linear term in the model. We estimated beta (β) values for each regressor for each subject separately. To determine significance, we randomized the frequency axis 5000 times and estimated β for each of these iterations. We then performed t-tests against zero on both randomized and observed βs, and also computed P-values on the t-statistic for the difference between observed vs randomized βs.

Finally, our sinusoidal model appeared to capture the range of interpolated frequencies equally, as fit residuals were not impacted by whether the entrainment frequency was above, at or below peak alpha (One way repeated measures ANOVA on average residuals below, at, and above peak alpha: F(2,155)'s = 0.80, 2.19, 0.66, 1.04 with p's= 0.45, 0.12, 0.52, 0.36 for hits,

RTs, sensitivity and bias respectively; F(2,128)= 0.09 with p = 0.91 for false alarms as this was computed excluding 9 subjects that had no false alarms at ≥1 flicker frequency).

K-means Clustering

K-means clustering was performed on the matrix of sinusoidal beta values from regression models for all behavioral metrics. Thus, this resulted in a 52 subject by 10 feature matrix as input to MatLabs k-means algorithm with squared Euclidean distance as the distance metric for minimization. We iterated through the process 100 times, and on each iteration we re-initialized the centroid cluster positions five times to find a lower local minimum. The subject grouping with the lowest within-cluster sum of point-to-centroid distances was chosen out of these 100 iterations. To assess the best number of clusters, we repeated the above process using cluster sizes ranging from 1 to 6. Both the sum and mean of all within-cluster sum of point to centroid distances received the largest reduction from 1 to 2 clusters, compared with any number of clusters beyond 2 (Figure 3.6). Additionally, we computed silhouette statistics for our cluster assignments to assess goodness of fit. This metric compares the relative distance, in our case Euclidean, between each subject's point to other points in its assigned cluster to the distance to points in the next nearest cluster. Values close to one indicate that a given observation is a good fit for its cluster (Rousseeuw, 1987).

For each subject i, silhouette value s is defined as:

$$s(i) = \frac{b(i)-a(i)}{\max\{b(i),\ a(i)\}}$$

Where a(i) is the average distance between i and other data within the same cluster, and b(i) is the smallest average distance of i to all points in any other cluster. Finally, note that $-1 \leq s(i) \leq 1$. Silhouette values for 2 clusters were highest, with a sum of 20.03, and mean ± SE of 0.39 ± 0.02 (paired t-tests on silhouette values: t(51)'s = 3.4, 3.1, 2.6 and 3.9, with p's = 0.001, 0.003, 0.01 and 0.0003 for clusters from 3-6, respectively). For this reason, we chose to separate subjects into 2 clusters.

PCA trajectories

For each subject, we computed PCA trajectories on data that had the RESS scalp map projected out. Specifically, we did this by taking the remaining, non-SSVEP eigenvectors (e_{vecs}) and re-projected single trial electrode data (*data*) into this space: e_{vecs}*pinv(e_{vecs})*data, where pinv is the Moore-Penrose Pseuoinverse. We then filtered this data from -1 to +1 Hz around each subject's independently estimated peak alpha frequency using a third order zero-phase digital Butterworth filter. After concatenating trials and time, we correlated the electrode-by-time/trial matrix with itself and performed PCA on this electrode-by-electrode correlation matrix, known to give similar results as the covariance matrix (Baria, Maniscalco, & He, 2017). We then chose the first 10 principle components (PCs) that explained the most variance, and projected each timepoint and trial into the space formed by the span of these PCs. Finally, we calculated both velocity and Euclidean distance in this PC space, and averaged metrics and trajectories over either detected or undetected trials.

Behavioral control across a wide range of flicker frequencies

To ensure that any observed linear trends weren't part of a larger, overarching trend we ran a separate cohort of 27 subjects (16 male, age = 21.7 ± 3.1 SD) for continuous (768 trials, n= 15) or trial wise (672 trials, n=12) versions of the task in which all parameters were identical except that the flicker frequencies used were 0 (static), 1.5, 4, 6, 10, 15, 20 and 24 Hz .

Experiment-version differences

Because of the different structure of the tasks, there were some average differences in subject behavior. Sensitivity, Bias and false alarms rates were not significantly different between the two experiments (ranksum test, p values determined by comparison to 10,000 randomized iterations: z's = -1.86, 0.93 and 0.76 with p's 0.062, 0.34 and 0.45, respectively). RTs were increased in the trial-wise structure by definition, as we defined a relatively narrow (i.e.

~1000ms) time frame during which subjects had to respond due to the ambiguity of a response in the continuous structure, whereas subjects could respond within a much longer time frame for the trial wise version (2225-3042 ms depending on intertrial interval; 759.68 ± ms 245.1 SD vs 466.77 ± 59.6 SD ms; z = 4.76, $p<10^{-15}$). Finally hit rates were slightly higher during the continuous version of the task due to differences in the success in thresholding subjects at ~75% detection rates, as contrast thresholds were determined on a subject by subject basis in a behavioral session before the task (zvalue = -2.05, p = 0.036: Trial-wise hit rate = 66.4% ± 18.2% SD vs Continuous hit rate = 76.2% ± 13.1% SD). Finally, it appeared that average entrainment was significantly higher in the continuously entrained experiment, with SNR = 5.27 ±0.3 SE vs 2.7 ± 0.03 SE in the trial-wise version (2-way ANOVA, $F(1,51) = 106.5$, $p<10^{-13}$). Importantly, however, subject group had no interaction with k-means subject grouping (Two-way repeated measures ANOVA: Experiment X Subject-group interaction $F(1,51) = 0.58$, $p=0.45$). Thus, due to the lack of an interaction and the fact that there was significant entrainment in both experiments, we decided to collapse all data across experiment-entrainment type (paired t-tests of RESS SNR against 1: Continuous $7.9 \leq t(30)$'s ≤ 13.7, p's$<10^{-8}$; Trial-wise $4.3 \leq t(20)$'s ≤ 6.1, p's<0.001).

Results

Task Design and behavior

We flickered a centrally presented checkerboard at 8 frequencies encompassing the traditional alpha band (6.3, 7.1, 8, 9.2, 10, 10.9, 12 and 13.3 Hz; Figure 3.1B). The target was a 16 ms dimming of a black, centrally presented fixation dot for 16 ms on which subjects were instructed to maintain fixation. Each subject participated in a short behavioral session before EEG data acquisition to determine their contrast threshold, resulting in Hit rates = 72.27 ± 15.98, False Alarm rates = 4.69 ± 6.55%, and RTs = 585.06 ± 216.14ms during the task (mean ± SD).

From these measures we calculated sensitivity, an estimate of the ease with which a subjects' perceptual system can detect the target from noise, and bias, an estimate of the extent to which a subject's responses are biased to report a target. Signal sensitivity was relatively high while bias suggested relatively conservative response criteria, indicating subjects understood the task (Sensitivity: 2.94 ± 0.86 SD, Bias: 0.8 ± 0.43 SD)

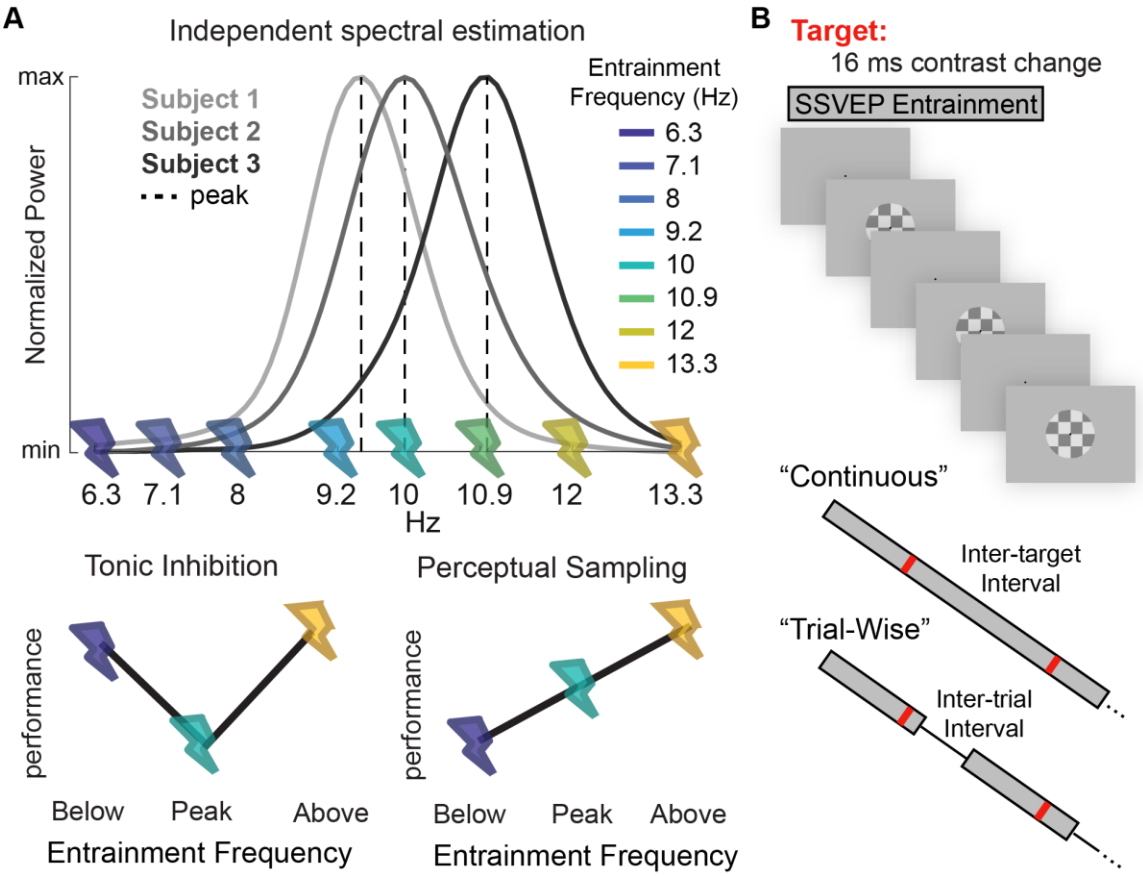

Figure 3.1: Study Motivation and Task Design. **A:** Three max normalized example power spectra are shown, and the peak alpha frequency of each individual subject is indicated with a dotted line. We used steady-state-visual evoked potentials (SSVEPs, indicated by lightning bolts) to test two hypotheses concerning the impact of alpha oscillations in visual cortex. Tonic inhibition (Hypothesis A) proposes that driving early visual alpha away from the resonant, endogenous peak frequency will positively impact perception. Perceptual Sampling (Hypothesis B) predicts that perceptual performance increases monotonically with increased early visual alpha frequencies. **B:** We flickered a centrally presented checkerboard at 8 different frequencies tiling the alpha band as subjects performed a contrast change detection task at fixation. Subjects were either presented with a continuously flickering checkerboard during which targets were separated by a variable inter-target interval ("Continuous"), or a checkerboard that was removed from the screen during a short inter-trial interval ("Trial-Wise").

Subjects completed two slightly different versions of the task, one in which we flickered the stimulus continuously ("continuous flickering") and one which employed a trial-by-trial structure ("Trial-wise flickering"). Although we designed the continuous version to optimize entrainment of the alpha rhythm, we also found significant entrainment in the trial-wise version and so we report results collapsed across these versions in the main text (Entrainment statistics reported in section below; version-specific parameters, along with behavioral and SSVEP statistics are reported in Materials and Methods).

Entrainment manipulation successfully clamps posterior alpha rhythms

Importantly, we first sought to confirm that brain rhythms were in fact driven at the intended frequency by our flickering stimulus, as, to our knowledge, there are few previous reports manipulating brain rhythms at similarly narrowly spaced frequencies within a frequency band. We employed a source-separation technique optimized to isolate entrained rhythms (RESS, or Rhythmic Entrainment Source Separation; see Methods; (Cohen & Gulbinaite, 2017)) to assess clamping of brain rhythms, but first validate its performance against traditional analysis techniques. To do this we calculated average RESS and electrode-based SSVEP amplitudes in a 2000 ms window surrounding target presentation (-1000 ms to +1000 ms) separately for each entrainment frequency, resulting resulted in a three-dimensional subject-by-entrained frequency-by-estimated frequency amplitude matrix (i.e. for 6.3 Hz stimulation trials, we estimated amplitude for all 8 alpha frequencies, for 7.1 Hz stimulation trials we estimated amplitude at all 8 frequencies, etc.). Importantly, the RESS scalp map allowed us to selectively project entrained alpha rhythms out of the data in order to investigate their impact on endogenous alpha oscillations in later analyses. Both electrode-based and RESS analyses confirmed successful entrainment of brain rhythms at each flicker frequency (Figure 3.2A; ME of stimulation in one way repeated measures ANOVA; RESS: $F(1,103) = 75.96$, $p < 10^{-10}$; Electrode: $F(1,103) = 48.67$, $p<10^{-8}$).

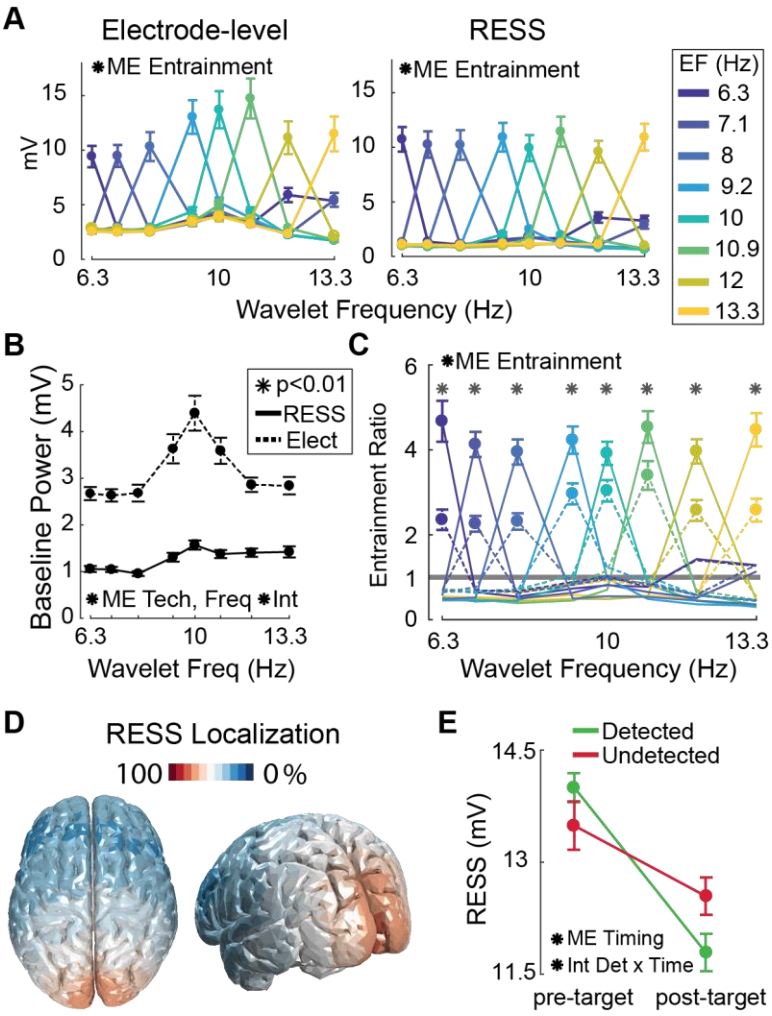

Figure 3.2: Entrainment of visual alpha oscillations. **A:** Successful clamping of alpha rhythms compared between electrode-based SSVEP and rhythmic entrainment source separation (RESS) methods. Plotted is average amplitudes within entrainment frequency, line color indicates entrainment frequency, errorbars indicate between-subject SEM, black stars indicate significance at p<0.01 using a one-way repeated measures ANOVA on entrainment; EF in legend = Entrainment Frequency. **B:** Amplitude estimates at non-entrained frequencies are larger using electrode-level (dotted black) compared with RESS data (black). Errorbars indicate SEM; black stars indicate significance at p<0.01 of two-way repeated measures ANOVA with technique and frequency as factors. **C:** Entrainment ratios calculated by dividing amplitude estimates at each entrained frequency by amplitude at non-entrained frequencies (Dotted lines = electrode-level, solid lines = RESS; black stars indicate significant main effect of entrainment for electrode-level and RESS. Errorbars indicate SEM; gray stars indicate within frequency paired t-tests at p<0.01. Gray line at entrainment ratio of one indicates the amplitude at a particular frequency was equal to the average of all other frequencies. **D:** Projection of topographic weights used to isolate the entrained rhythm using RESS, projection done using code from Cohen & Gulbinaite (2017). Red areas indicate high activation by the flickering stimuli averaged over all flicker frequencies. **E:** The amplitude of entrained rhythms decreases post-target, an effect greater on trials in which the target was correctly detected. Errorbars indicate SEM, black stars indicate significance at p<0.01 using two-way repeated measures ANOVA with time interval and detection as factors.

RESS better isolates entrained rhythms from endogenous alpha oscillations

Although both electrode-based and RESS methods selectively estimated SSVEP amplitudes relative to a baseline, this baseline was significantly contaminated by endogenous (i.e. non-entrained) alpha activity in traditional electrode-based estimates. Electrode-based amplitudes showed a baseline increase at non-entrained frequencies when compared with RESS estimates (Baseline plotted in Figure 3.2B; ME of technique: $F(1,51) = 216.25$, $p<10^{-15}$). Additionally, we found an increase in amplitude at 10 Hz, likely because the average endogenous alpha frequency was 10.08 ± 0.92 Hz across subjects (mean ± SD at electrode POz; ME of wavelet frequency: $F(7,357) = 13.6$, $p<10^{-14}$; Interaction between frequency and technique: $F(7,357) = 10.33$, $p<10^{-11}$; see Methods). This indicates a degree of nonselectivity such that electrode-based SSVEP amplitude estimates also include the brain processes that give rise to the endogenous alpha 'bump'.

To control for this non-selectivity we calculated entrainment ratios by dividing the amplitude at each combination of entrained and estimated frequencies (e.g. each cell of the 8 x 8 matrix produced by subjecting each of the entrainment trial types to wavelet decomposition at each frequency) by the average amplitude at all other combinations. Although entrainment at all frequencies was again significant using both methods (Figure 3.2C; one sided t-test that entrainment ratios > 1; Electrode entrainment ratios: $5.99 \leq t(51)s \leq 8.1$, $p \leq 10^{-7}$; RESS entrainment ratios: $7.9 \leq t(51)s \leq 11.2$, $p \leq 10^{-10}$), RESS indeed displayed higher entrainment ratios at each of the entrained frequencies (Figure 3.2C; Main effect of technique: $F(1,357) = 237.6$, $p <10^{-15}$; paired t-tests: $3.79 \leq t(51)'s \leq 9.8$, $p's \leq 0.0003$), and lower entrainment ratios away from entrained frequencies compared to the electrode-based analyses (paired t-test: $-7.1 \leq t(51)s \leq -2$, $p's \leq 0.044$). Finally, note, significant entrainment was also found at several flicker

frequency harmonics (for (entrainment, estimation) pairs: Electrode entrainment ratio t(51)'s for (6.3 Hz, 12 Hz) = 3.1 and (7 Hz, 13.3 Hz) = 2.6, p's = 0.0015 and 0.0062 respectively; RESS entrainment ratio t(51) for (6.3 Hz, 12 Hz) = 3.03, p=0.0019). Thus, we were able to isolate entrained alpha rhythms from endogenous alpha oscillations using a source decomposition technique.

Additionally, RESS spatial maps indicated maximal loadings over the back of the head, consistent with previous topographic characterizations of both SSVEPs and the endogenous alpha rhythm (Figure 3.2D shows average over all entrainment frequencies as the topographic size of the map was not modulated by entrainment frequency (One way ANOVA on number of electrodes with spatial filter loadings greater than a particular percentile: Main Effect of entrainment frequency F(7, 392)s = 1.7,1.2,1, 0.5, 1.3 with p's = 0.09, 0.31, 0.42, 0.78, 0.26 for 75, 80, 85, 90,and 95 percentiles respectively; p-values determined by comparing to a null distribution of F values obtained by running ANOVAs on counts after randomizing entrainment frequencies 1000 times).

Finally, prestimulus RESS amplitude (estimated from -1000:-500ms prestimulus to avoid stimulus evoked effects) was higher than poststimulus amplitude (500:1000ms post stimulus), and this effect was more pronounced when the stimulus was detected (averaged over all stimulation frequencies; ME of timing: $F(1,45) = 13.3$, $p<0.001$; Interaction between timing and detection: $F(1,45) = 15.2$, $p<0.001$). Thus, RESS amplitudes appeared to reflect attentional engagement, as seen in previous electrode-based reports (Morgan, Hansen, & Hillyard, 1996; Müller et al., 1998).

Behavioral performance as a linear function of entrainment frequency

We next determined whether there were purely linear modulations in behavior across entrainment frequency without considering each subject's alpha frequency. There were linear

trends in several behavioral metrics that indicated better performance with higher entrainment frequencies (Figure 3.3A; multiple linear regression βs/p's: Detection: 0.93/<10^{-8}; RT: -4.5/ <10^{-9} ; Sensitivity: 0.04/0.003; Bias: -0.008/0.2; FA: -0.09/0.28; we also report t-tests against zero on individually fit subject βs to be consistent with later analyses and due to the high degrees of freedom - 51 subjects and 8 frequencies: Detection: t(51) = 4.86, p =10^{-5}; RT: t(51) = -5.16, p <10^{-5}; Sensitivity: t(51) = 3.04, p =0.004; note RTs are only considered for trials on which the target was accurately detected, or 'hit' trials).

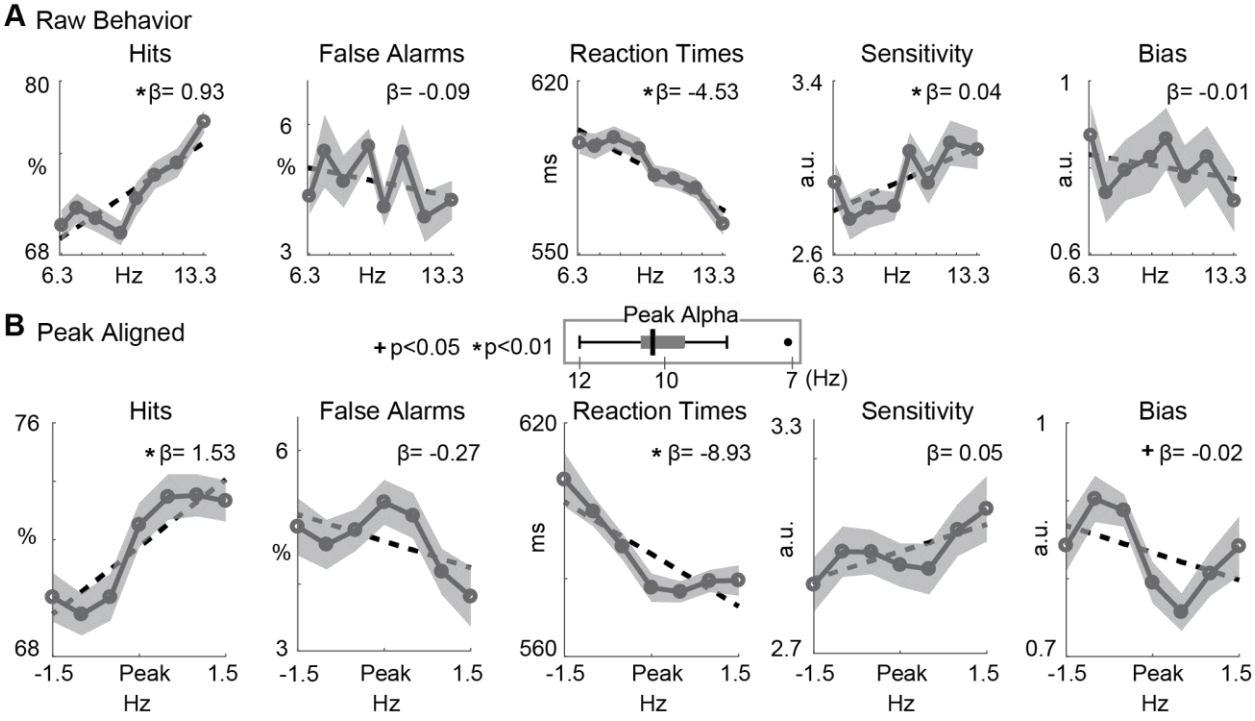

Figure 3.3: Linear trends in behavioral data. **A:** Average behavioral metrics within each stimulation condition are plotted, shaded areas indicate SEM. * indicates that linear regression β had a p-value <0.01 (left panel). **B:** Behavioral metrics for each subject were interpolated around each subject's respective peak alpha frequency (left panel). The linear relationship between each behavioral metric was assessed as in A, and beta values with a p<0.01 are indicated with *.

However, viewing the behavioral data without accounting for each subject's unique peak alpha frequency does not address the hypothesis that entrainment frequency modulates

behavior *with respect to* each subject's peak alpha frequency. Therefore, we first estimated each subject's peak alpha frequency during a separate block of EEG recordings in which subjects were not viewing the entrainment stimuli or performing any other task aside from fixation (Figure 3.3 inset: 10.1 ± 0.8 Hz mean ± SD; see Methods). Next, we interpolated behavioral data in a window from -1.5 Hz to +1.5 Hz centered on each subject's peak alpha frequency (See Methods for interpolation details). We found that while Hit rates and RTs still increased with entrainment frequency after aligning to peak alpha, sensitivity was no longer significantly modulated by entrainment and a modest decrease in bias emerged (Figure 3.3B; multiple linear regression βs/p's: Detection: 1.5/<10^{-6}; RT: -8.9/ <10^{-7} ; Sensitivity: 0.05/0.06; Bias: -0.02/0.038; FA: -0.27/0.06; due to the high degrees of freedom - 51 subjects and 8 frequencies – and to be consistent with later analyses, we also report t-tests against zero on individually fit subject βs; Detection: t(51) = 3.2, p =0.002; RT: t(51) = -3, p =0.004; Bias: t(51) = -1.1, p = 0.27). Thus, while perceptual performance appears to improve with stimulation frequency, the perceptual mechanisms, i.e. sensitivity vs bias, are not clear. Qualitatively, we note the source of ambiguity could be due to substantial non-linear modulations around peak alpha frequency.

Finally, we ran behavioral versions of the experiment with parameters identical except the stimulus was flickered at a wider range of frequencies to verify that these linear trends are specific to the alpha band (0 Hz, or static, 1.5, 4, 6, 10, 15, 20 and 24 Hz; see Methods). We then fit a regression line to the entrainment frequencies (excluding 0) as was done for the main task, and only found a marginally significant linear decrease in RTs across all stimulation frequencies, suggesting that entrainment within the alpha band engages distinct mechanisms from entrainment outside of the alpha band (Figure 3.4; Hits: β = 0.0004, p=0.57; False Alarms: β = -0.0006, p=0.13; RT: β = -0.64 ms, p=0.012; Sensitivity: β = 0.0068, p=0.16; Bias: β = 0.0031, p=0.19; additional statistics in Materials and Methods). Additionally, only hit rates were

reduced at 10 Hz compared with both 1.5 and 24 Hz, and entrainment at 10 Hz did not differ from entrainment at 4-15 Hz in any behavioral metric (t(26)s = -4.1, -3.9, p's=0, 0.0004), while RTs were slower and sensitivity reduced at 10 Hz compared with 20 and 24 Hz (Figure 3.4; RT t(26)s = 2.08, 3.9, p's= 0.04, 0.0004; Sensitivity t(26)s = -2.3, -3.8, p's = 0.03, 0; Post-hoc t-tests between 10 Hz and all other flicker frequencies: significant differences from 10 Hz are noted either below the x axis or next to the red dot indicating no stimulation; significance was assessed by randomizing frequency 5000 times). Finally, stimulation at 10 Hz resulted in fewer hits, more false alarms, slower RTs and reduced sensitivity compared with no entrainment (Post hoc t-tests: t(26)s = -3.3, 3.1, 8.1, -4.8 with p's = 0, 0.003, 0, 0). Together, this confirms that observed linear trends are specific to the alpha band.

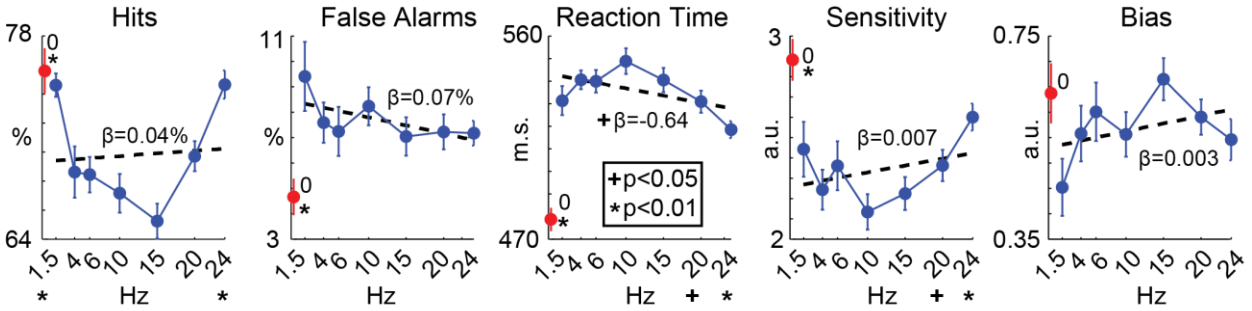

Figure 3.4: Behavioral trends over a larger frequency range. Mean Hit rates, False Alarm rates, Reaction times, Sensitivity and Bias are plotted, with error bars indicating SEM. Red dots indicate the no stimulation condition. βs and significance indicators from linear regressions are reported next to dotted regression lines. Significance for paired t-tests comparing behavior at 10 Hz and each other entrainment frequency are indicated next to the numerical label for relevant frequency.

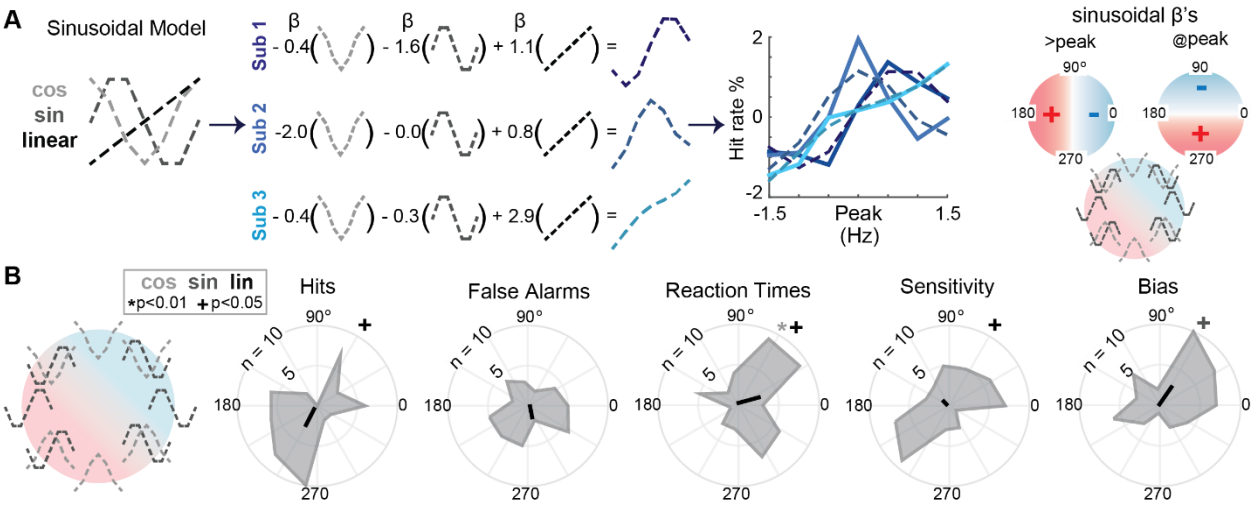

Figure 3.5: Sinusoidal modeling of behavioral data. **A:** Each subject's behavioral data was fit separately using two sinusoidal regressors (sine and cosine) and a linear regressor (left panel). Three example subjects are shown, with beta values for each regressor and the resultant fit (dotted blue lines, middle panels). True behavior (solid blue lines) are plotted alongside these fits. Right panel: these sinusoidal βs can be visualized on a polar plot. Red shaded regions indicate that entrainment at or above peak alpha results in increases in a particular behavioral metric. Blue shaded regions indicate decreases when subjects are clamped at or above peak alpha. Example regressors are plotted along the perimeter. **B:** The polar plot legend is reproduced (Left panel). Radial distance indicates the number of subjects for the gray shaded histograms (inner line is 5 subjects, outer line is 10). Black line indicates the mean vector over all subjects, where the outermost radial line labeled with n=10 is the maximal vector length. + indicates significance at 0.05 and * indicates significance at 0.01 computed based on t-tests against zero on βs for the regressor indicated by shading color (light gray is cosine, gray is sine, black is linear).

Sinusoidal modulations in behavior aligned to endogenous alpha frequency

Although we evaluated only linear trends in behavioral data as a first pass, a linear model is not sufficient to investigate the tonic inhibition hypothesis, and we qualitatively note prominent non-monotonic modulations around each subject's peak alpha frequency (Figure 3.4B). To quantify these non-linear modulations, we fit each behavioral metric separately for each subject using sine and cosine regressors to capture periodic modulations in the behavioral data, along with a regressor to capture the linear trend (Figure 3.5A; See Methods). We show three example subjects to illustrate how this model captured subject behavior (Figure 3.5A).

These sinusoidal beta values can be summarized using polar plots, and we provide a guide for how locations on these polar plots reflect the impact of entrainment at frequencies at or above a particular subject's peak alpha (Figure 3.5A Right Panel). First, RTs were significantly faster with entrainment at peak alpha as compared to above or below (Black vectors indicate mean over all subjects in Figure 3.5B; Note βs for the sinusoidal model are in z-score units; β_{cos} = 0.445 ± 0.16 SE, p=0.005). Second, bias marginally decreased with entrainment above peak alpha (β_{sin} = 0.38 ± 0.17 SE, p = 0.037). Finally, hit rates, RTs and sensitivity retained marginal linear effects in the sinusoidal model (β_{lin} = 0.41 ± 0.19 SE, p=0.033; β_{lin} = -0.64 ± 0.24 SE, p=0.012; β_{lin} = 0.46 ± 0.22 SE, p = 0.046). However, we note bimodal distributions apparent in sinusoidal βs (Figure 3.5B), implying substantial heterogeneity across subjects. This bimodal pattern motivated us to cluster subjects based on their pattern of behavioral results.

Distinct patterns in the impact of entrainment on subject behavior

Clustering apparent when circular histograms were plotted for the sinusoidal regressors indicated that there might be multiple sub-types of behavioral modulation in our experiment. To explore this possibility, we used an unsupervised k-means clustering algorithm to divide our subjects into groups based on beta weights from the sinusoidal model (see Methods). According to the "elbow method" and silhouette values, separation into 2 groups produced the most parsimonious account of the data (Figure 3.6; Silhouette values for 2 clusters were highest: t(51)'s = 3.4, 3.1, 2.6 and 3.9, with p's = 0.001, 0.003, 0.01 and 0.0003 for clusters from 3-6, respectively). This resulted in 21 subjects in Group 1 (white circles) and 31 subjects in Group 2 (gray circles; Figure 3.7; See Methods). For comparison purposes, we replot peak-aligned behavior separately for each group for comparison (Figure 3.7A Bottom Row).

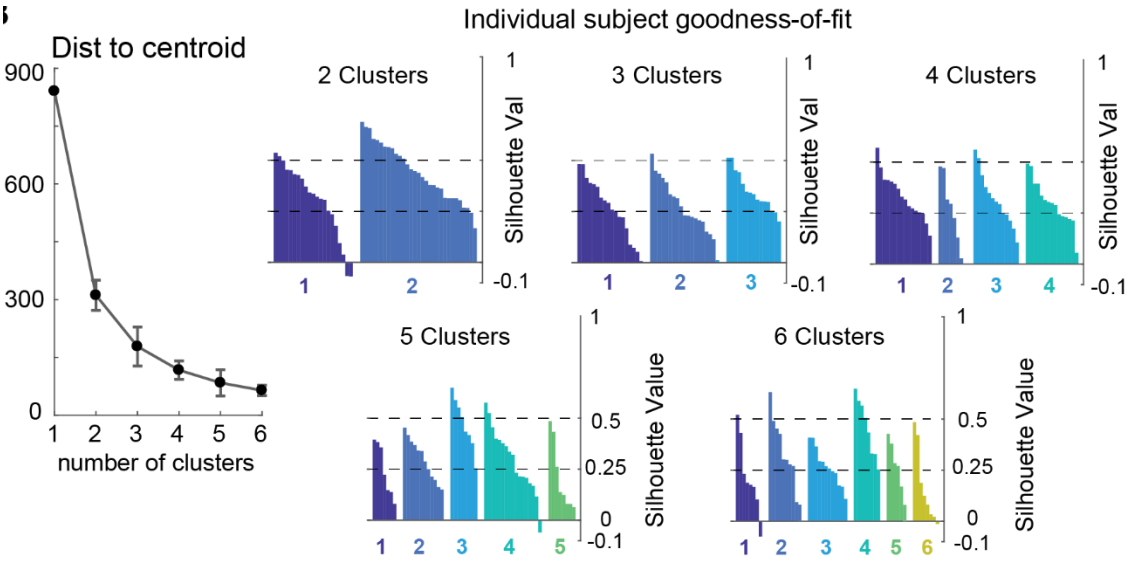

Figure 3.6: K-means cluster number determination. Left Panel: The mean distance of each point to the center of the cluster for different cluster numbers. Dots indicate mean, error bars indicate standard deviation over clusters (hence no bar for 1 cluster). Right Panel: Individual subject silhouette values were investigated as a goodness of fit measure. We plot from -0.1 to 1 on the x axis, and indicate 0.25 and 0.5 with dashed lines. Each bar indicates the silhouette value for one subject, and are colored differently according to cluster membership.

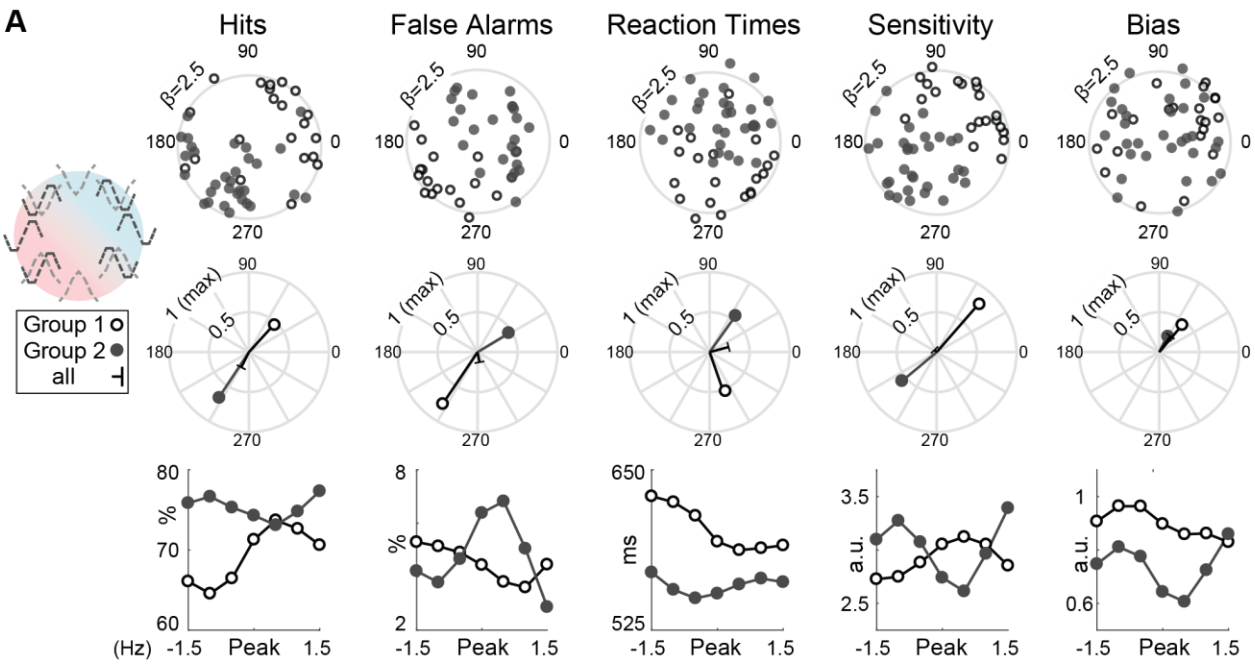

Figure 3.7: Behavioral groupings **A:** Polar plot interpretation guide (left panel) is plotted alongside single subject vectors (top row), where subjects are color coded according to their behavioral group (Group 1 is purple, Group 2 is green). The outermost ring indicates a sinusoidal ß vector length of 2.5 (i.e. combining both sinusoidal regressors). Middle row shows group average vectors for Group 1, Group 2 and all subjects (black), where the outermost radial ring is the maximal vector length. Bottom row shows the behavioral patterns separately for each subject group. Error bars indicate SEM.

These subject groups showed dissociable impacts of driving alpha at or above peak frequency on both hit rates, false alarms and sensitivity (Figure 3.7A). Subjects in Group 1 had higher false alarm rates and reduced sensitivity when entrained at peak alpha as compared to away from peak alpha (False Alarms β_{cos} =0.59, p=0.003; Sensitivity: β_{cos} =1.03, p=0.0008), as well as lower hit rates, more false alarms and reduced sensitivity when entrained above as compared with below peak alpha (Detection β_{sin} = 0.70, p = 0.028; RT: β_{sin} =-0.93, p=0.001; False Alarms β_{sin} =-1.2, $p<10^{-15}$; Sensitivity: β_{sin} =1.18, $p<10^{-15}$). Thus, perceptual performance is relatively impaired when subjects in Group 1 are entrained at or above their peak alpha frequency, in line with the tonic inhibition hypothesis. On the other hand, Group 2 showed higher sensitivity at peak alpha, contributed to by both higher detection and lower false alarm rates

(Detection β_{cos}= -0.65, p=0.003; False Alarms: β_{cos}=0.59, p=0.003; Sensitivity β_{cos}= -0.71, $p<10^{-15}$). Additionally, subjects in Group 2 had higher hit rates, higher sensitivity, and faster RTs when entrained above peak alpha, parsimonious with the perceptual sampling account (Detection β_{sin} = -0.93, $p <10^{-15}$; RT: β_{sin} =0.83, p=0.0004; Sensitivity: β_{sin} = -0.63, p=0.0016). Thus, when alpha oscillations are clamped at or above each subjects peak endogenous frequency, subjects in Group 1 perform relatively worse while performance is actually enhanced in Group 2.

Finally, note that these subject groups did not differ on their levels of alpha entrainment (RESS entrainment ratios for Group 1 = 4.18 ± 0.25 and Group 2 = 4.32 ± 0.39 SE for; two-way ANOVA on RESS entrainment ratios with Subject group and Experiment-version as factors: main effect of subject group: $F(1,51) <10^{-4}$, p=0.99). Finally, the behavioral groupings had no association with which experiment type the subject participated in (i.e. the blocked or trial-wise frequency manipulation experiments, Experiment-by-subject group interaction in two way ANOVA: F(1,51) = 0.58, p=0.45; $\chi^2(1, 51) = 0.008$, p = 0.78, significance based on 10,000 randomized subject groupings).

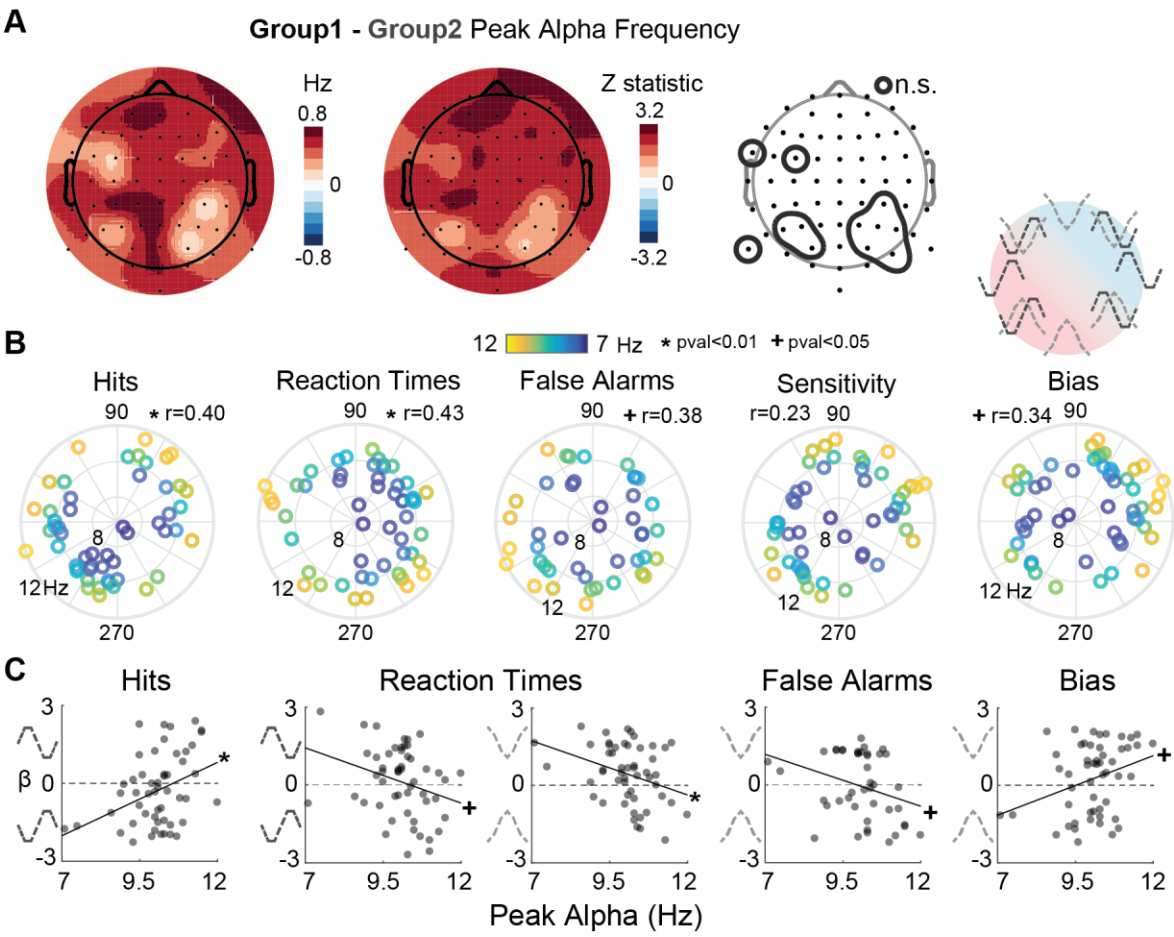

Figure 3.8: Relationship between behavior and peak alpha frequency **A:** Behavioral group, as assigned based on patterns in behavioral performance, was associated with peak alpha frequency, with Group 1 showing higher peak alpha frequencies over nearly all electrodes (52/64, top scalp map). The bottom scalp map shows z statistics for each electrode, electrode areas circled in white were not significant after 10,000 randomizations and FDRr correction at 0.05. **B:** Circular-linear correlations were computed for each behavioral metric between single subject sinusoidal vectors and their peak alpha frequency. Each circle is a single subject where the distance from the center of the polar plot is determined by the peak alpha frequency (which is also indicated by the color of each dot). Rho correlation values that were significant at p<0.01 are accompanied by *, while those significant at 0.05 have +. **C:** βs vs peak alpha frequencies are plotted for regressors and behavioral metrics, Rho correlation values significant at p<0.01 are accompanied by *, while those significant at 0.05 have +. Dotted line at 0 denotes where βs switch from negative to positive sign. Dotted regressors are provided along the y-axis for guidance.

Behavioral groupings are linked to the frequency of the endogenous alpha rhythm

We hypothesized that differences in endogenous alpha oscillations may underlie the observed dissociable patterns in behavior. To test for this we compared peak alpha power and

frequency as estimated from the independent resting session (For both power and frequency we computed group level differences at each electrode using a Wilcoxon ranksum test due to an unequal number of subjects in each group, and compared the observed z-statistic to z-statistics obtained from 10,000 randomized group assignments; See Methods). Importantly, note spectral data is independent of the data used to group subjects, as group assignment was based solely on behavioral data.

We found no difference between the power, or *amount,* of resting alpha between Group 1 and Group 2 in any electrode (p's ≥ 0.28, $-0.67 \leq z\text{'s} \leq 1.15$). However, there was a marked difference in peak alpha frequency between the groups: subjects in Group 1 had an average peak alpha frequency of 10.53 Hz compared with 10.02 Hz for Group 2 over all channels. All 64 electrodes showed higher peak alpha frequencies in Group 1 compared with Group 2, and this elevation reached significance in 52 electrodes (significant frequency differences after FDR correction at 0.05 ranged from 0.303-0.764 Hz; $1.8 \leq z\text{'s} \leq 2.92$ with $0.0015 \leq p\text{'s} \leq 0.04$ as determined by comparing observed z statistics to 10,000 randomizations of group membership; all frequency differences ≥ 0.1 Hz).

Thus, subjects that performed worse when clamped at or above their peak alpha frequency had naturally faster endogenous alpha oscillations (Group 1), while subjects that benefit behaviorally from clamping alpha at or above their peak frequency had slower endogenous alpha oscillations (Group 2).

Sinusoidal patterns in behavior resulting from clamping alpha are predicted by endogenous alpha frequency

We next investigate whether the association between behavior and peak alpha frequency holds in a more continuous manner. To that end, we computed circular-linear correlations between peak alpha frequency and the angle of each subject's sinusoidal regressor

($\tan^{-1}\frac{\beta sin}{\beta cos}$). We found that each subject's peak alpha frequency was associated with their sinusoidal pattern in hit rates, RTs, bias and false alarms (Hit Rate: *r* = 0.404, p = 0.01; RT: *r* =0.425, p= 0.006; Bias: *r* = 0.34, p=0.048; False Alarms: *r* =0.382, p=0.038; p-values based on a comparison to a null-distribution of correlations obtained by randomizing peak alpha frequency 10,000 times). Interestingly, no significant correlations were seen between peak alpha and the linear trend term (p's > 0.3 for all behavioral metrics). We further decomposed these sinusoidal patterns for each behavioral metric. First, we found that the sine regressor that peaked away from peak alpha summarized the relationship between hit rates and peak alpha (Figure 3.8C; *r* = 3.8, p = 0.003), while the cosine regressor that peaked at peak alpha dominated the relationship between peak alpha frequency and both bias and false alarms (Bias: *r* = 0.31, p =0.02; false alarms: *r* = -0.31, p = 0.033). Finally, RTs showed both sine and cosine correlations with peak alpha (cos: *r* = -0.34, p = 0.01; sin: *r* = -0.29, p =0.03). Finally, it is of note that the regressor was essentially flipped between subjects with high and low frequencies for each of these correlations, indicated by β estimates of opposite signs.

Thus, we confirm that there is a fine-grained relationship between perceptual performance and peak alpha frequency consistent with the previously observed differences between behavioral groups. Specifically, we again found that subjects with high endogenous alpha frequencies were concentrated in the portion of the sinusoidal space associated with worse performance when entrained at or above peak alpha, while subjects with low endogenous alpha frequencies showed the opposite perceptual patterns.

State space velocity is modulated by interactions between endogenous and entrained frequency

So far we have described how the perceptual impact of driving alpha rhythms is linked to the endogenous alpha rhythm. Thus, we next explore the possibility that the impact of this interaction between entrained and endogenous frequency on behavior is due to the dynamical

state of endogenous alpha at different entrainment frequencies. To test this, we projected out the RESS scalp maps to remove the entrained alpha signal and performed PCA on the isolated endogenous alpha oscillation (EEG data filtered ± 1Hz around each subject's peak alpha frequency with a 3rd order zero-phase digital Butterworth filter; See Methods). We then selected the components that explained the most variance to form a state space onto which we projected single timepoints of endogenous alpha data from both correct and incorrect trials. We verified all analyses reported below using the first 1-10 components that explained the most variance to ensure any observed effects were robust to the dimensionality of the state space (Figure 3.9A right panel shows the percent variance explained for these PC choices; analysis strategy is based on prior work from (Baria et al., 2017), also see Methods).

When single subject trajectories were plotted, we qualitatively observed that trajectories appeared to move a greater distance from the time of target onset to the time that a response was made on trials on which the target was detected. In contrast, there was little deviation from this pre-target region on undetected trials, with the location in state space at response indistinguishable from that at target onset (Figure 3.9A). To quantify these differences, we calculated the Euclidean distance between state space location at the time of target presentation and each timepoint on both detected and undetected trials, and found both reduced pre-target and greater post-target distances on correct as compared to incorrect trials (Figure 3.9B; switch from negative to positive t-values occurs at 160 ms post-target; timepoints where p survives FDR correction at 0.01: negative t(54s)= from -2.68 to -4.9; positive t(54)s from 2.75 to 8.78). Indeed, movement in the state space was slower before the target but faster after the target on detected compared with undetected trials (based on average velocities for the 500 ms before and after target presentation: pretarget $t(54) = -6.34$, $p < 10^{-7}$; postarget $t(54) = 6.30$, $p < 10^{-7}$). Thus, it appears that a stable pre-target location in the state space and

subsequent high velocity movement away from this location characterizes the dynamic trajectory of endogenous alpha oscillations when the target was correctly detected.

Given that subjects with high peak alpha frequencies performed worse when clamped at or above peak alpha, we next investigated if post-target state-space velocity was slower when subjects with higher peak frequencies were clamped at higher alpha frequencies (and vice versa for low alpha frequency subjects; 500 ms window indicated in Figure 3.9B, gray shaded area). Interestingly, peak alpha and entrainment frequency interacted to impact state-space velocity on detected but not on undetected trials (Figure 3.9C right and bottom panels; linear mixed effects model that included entrainment frequency, peak alpha frequency, and an interaction term between the two factors as fixed effects, and subject as random effects: βs range from -0.003 to -0.006 from PC 1 to 10; -3.65 ≤ t(436)s < -2.4, p's ≤0.007, significance determined from 5000 randomizations of peak alpha frequency; See Methods). We median split subjects into high and low alpha frequencies to visualize this interaction, and observed that movement in the state space is slower when alpha oscillations are entrained at lower frequencies for subjects with naturally low peak alpha frequencies, while movement was slower for subjects with high peak alpha frequencies when alpha rhythms are entrained at higher frequencies (Figure 3.9C Top Left Panel). Finally, because the pairwise correlation matrix can be impacted by phase locking, we confirmed that this interaction could not be simply accounted for by the degree of phase locking or the ERP in the same 500 ms post-target window (PLI: t(436)'s = -0.94, -1.48, p's = 0.25, 0.08; ERP: t(420)s = -1, 1.1, p's = 0.16, 0.13; significance determined from 5000 randomizations of peak alpha frequency; PLI and ERP predicted using linear mixed effects model with included entrainment frequency, peak alpha frequency, and an interaction term between the two factors as fixed effects, and subject as random effects).

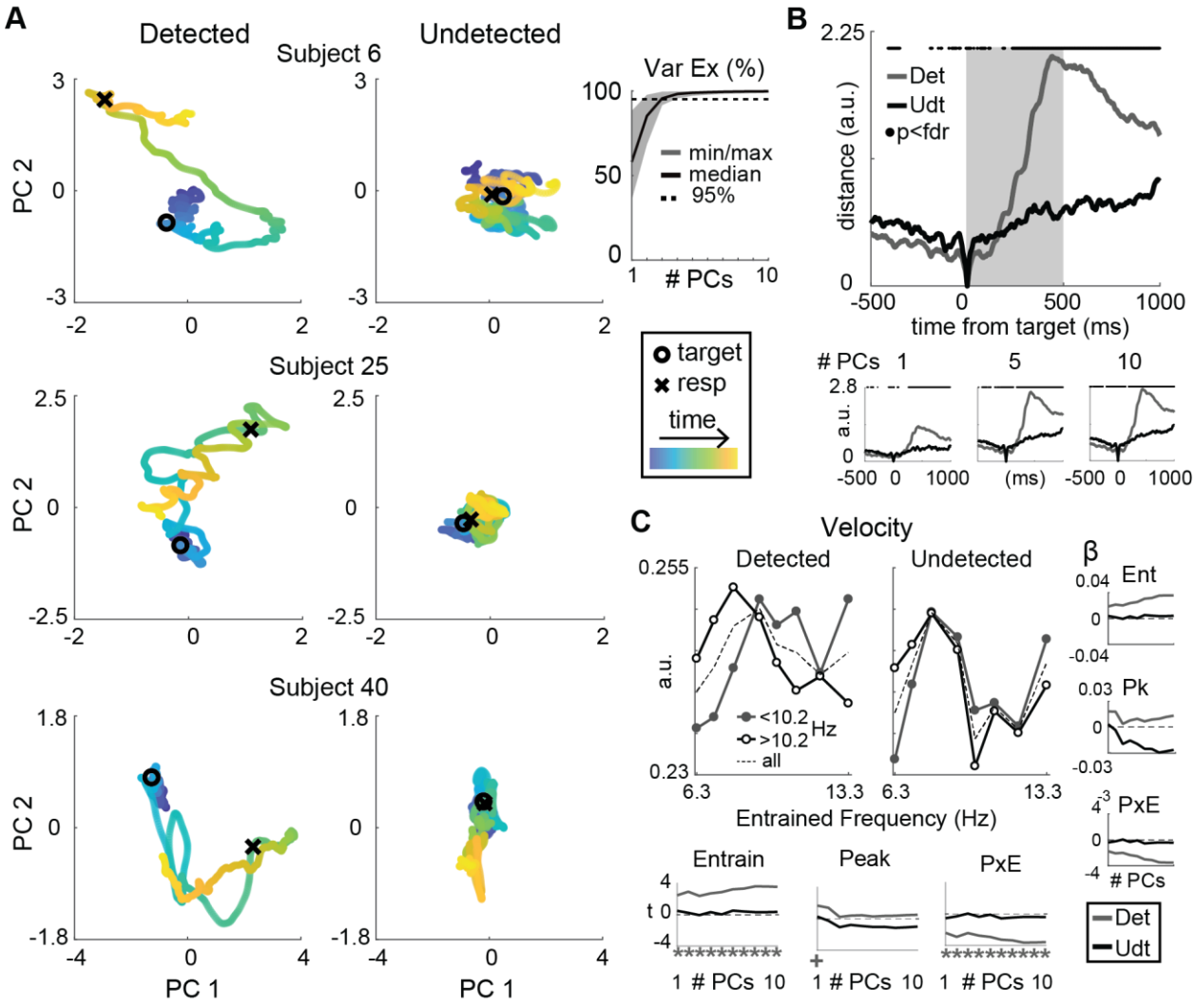

Figure 3.9: Endogenous alpha state space. **A**: Each row shows PCA trajectories for an example subject on detected (left panels) and undetected (right panels) trials. Black circles denote target onset, black X denotes average reaction time, purple timepoints start 500ms pre-target and yellow timepoints end 1000ms post-target. Variance explained is plotted for all subjects as a function of the number of principle components (Top right panel; shaded area indicates minimum to maximum across subjects). **B**: Top: Euclidean distance from the target location in the two-dimensional PC space plotted for detected and undetected trials. Black dots indicate timepoints with t-statistics that remained significant after comparison with 5000 t-statistics computed from randomized condition labels and FDR correction at p<0.01. Gray shaded rectangle indicates timepoints used for analysis in C. Bottom: example distances computed in 1, 5 and 10 dimensional state spaces are also plotted, significance computed and plotted identically as for top panel. **C:** Velocity in a 500ms post-target epoch on trials in which the target was detected (left panel) and on trials when it was not (right panel). Subjects were median split based on peak alpha frequency to display the significant interaction between entrained frequency and peak alpha frequency. β (right column) and t-values (bottom row) from linear mixed effects models fit separately for detected and undetected velocities. The x-axis displays models fit separately for PCs 1-10; significance indicated by * for p<0.01 and + for p<0.05 determined from 5000 randomizations of velocity between subjects.

Discussion

Alpha oscillations have long been associated with visual attention and perception. However, the precise mechanisms of their impact on visual information processing are a topic of much debate, in part because distinct theoretical frameworks have been built on observations concerning changes in alpha power and changes in alpha frequency. Results showing that high alpha power impairs behavioral performance have led to the tonic inhibition hypothesis, which holds that the alpha oscillations inhibit visual information processing. On the other hand, results showing that faster alpha oscillations lead to enhanced behavioral performance have led to the perceptual sampling hypothesis, which holds that more rapid fluctuations between periods of excitation and inhibition increases the effective sampling rate of the visual system.

We did find evidence across some, but not all, behavioral metrics for a monotonic improvement in visual perception with increasing entrainment frequencies, consistent with the perceptual sampling account. However, aligning behavioral metrics to each subject's peak alpha frequency revealed sinusoidal patterns in behavioral performance that suggest a more complex relationship between alpha drive and the efficiency of information processing. Indeed, clamping posterior alpha rhythms resulted in two distinct patterns of behavioral responses with respect to endogenous, peak alpha frequency. One group of subjects displayed impaired performance when clamped at or above their peak alpha frequency, in line with the tonic inhibition account and inconsistent with the perceptual sampling hypothesis. In contrast, the other group of subjects displayed enhanced performance when clamped at or above their peak alpha frequency, consistent with both the perceptual sampling hypothesis and with perceptual *enhancement* at peak alpha.

Critically, while the separation of subjects into two groups was based solely on their behavioral data, subject group was systematically associated with each subject's endogenous alpha rhythm. We found that subjects with behavioral patterns more closely adhering to the tonic inhibition hypothesis (impaired behavior at or above peak alpha) had naturally *faster* alpha rhythms, while subjects adhering closer to the perceptual sampling account (enhanced behavior at or above peak alpha) had naturally *slower* alpha rhythms. Furthermore, this relationship between behavior and endogenous alpha held up in a continuous manner such that each clamping alpha at or above peak frequency resulted in worse performance for subjects with higher endogenous frequencies, more parsimonious with the tonic inhibition account, while the opposite pattern was seen for subjects with lower endogenous frequencies. Thus, individual subjects' endogenous alpha frequency determined the perceptual impact of alpha drive. Interestingly, no significant correlations were seen between peak alpha and the linear trend term, suggesting that sinusoidal but not linear perceptual patterns in response to alpha drive are associated with peak alpha frequency.

We then investigated whether these differential behavioral responses observed in subjects with high vs low alpha frequencies could be due to the dynamical state of the endogenous alpha rhythm under alpha drive. First, increased state space velocity was associated with target detection, suggesting rapid changes in the state of endogenous alpha are key to efficient perceptual performance. This fits with theoretical models that emphasize transient dynamics through neural state spaces rather than arrival or staying at a stable state, as the information present in these trajectories are robust to initial state and naturally generate a representation of incoming stimuli in the context of previous ones (Baria et al., 2017; Buonomano & Maass, 2009; Maass, Natschlager, & Markram, 2002; Misha, Ramon, & Gilles, 2008). Slow cortical activity trajectories during conscious but not unconscious perception have also been found to be fast evolving (Baria et al., 2017), a result we extend to the alpha band

here. Importantly, we show that efficient traversal of endogenous alpha oscillations is perceptually beneficial, even when the visual system is being clamped at a particular frequency. Additionally, each subject's natural endogenous frequency interacted with the driving frequency to impact state-space velocity. Specifically, subjects with high endogenous alpha frequencies traversed their alpha state space less efficiently when clamped at high frequencies. Conversely, subjects with low endogenous alpha frequencies traversed their alpha state space more efficiently when clamped at high frequencies. This suggests that driving neural circuits at alpha frequencies distinct from the dominant, natural state of the alpha oscillation may be perceptually beneficial because it aids in the efficient traversal through the state space, which is in turn necessary for visual perceptual.

To summarize, we find different subjects show perceptual patterns consistent with both accounts of the alpha oscillation. Specifically, when natural, endogenous alpha oscillations are fast, driving these circuits even faster is not perceptually beneficial. In contrast, if endogenous alpha oscillations are slow, driving early visual circuits at a faster frequency does benefit perception. Finally, our results that clamping alpha *away* from the endogenous frequency results in more efficient, transient dynamics suggests that decoupling from the dominant alpha oscillation but staying within the bounds of the alpha band is key for perception. This central tendency is striking, as it suggests the middle of the alpha band as an optimal dynamical range for the neural circuits involved in alpha oscillations and their impact on visual perception. The existence of an optimal dynamical range for human visual information processing and transfer may be conceivable. Specifically, large scale anatomical wiring of the visual system is relatively stereotyped between subjects (Felleman & Van Essen, 1991; Takemura et al., 2016; D. C. B. T.-P. in B. R. Van Essen, 2005; D. C. Van Essen & Maunsell, 1983), and the size of such networks is known to play a key role in the temporal dynamics of information propagation (Buzsáki, 2006; Draguhn et al., 2004).

Finally, future studies are necessary to establish why peak alpha frequency, generally viewed as a stable trait, has such striking differential impacts on perception under alpha drive. Are alpha oscillations inherently different processes in subjects with fast and slow rhythms? Or does each subject have multiple steady-states for endogenous alpha oscillations, the most dominant of which we call the endogenous rhythm, such that switching between fast and slow dynamical states is key for perception? Studies without alpha entrainment in which subjects switch between rest and task engagement would be necessary to answer whether these differential dynamical alpha states exist either within or between individual subjects.

Together, we found that driving early visual circuits processing a relevant visual stimulus in the alpha band interacts with the endogenous rhythm to impact perception. This interaction depends on each subject's particular alpha frequency, suggesting knowledge of the endogenous alpha rhythms could have implications for the optimization of visual information processing through both brain stimulation and the presentation of information. Additionally, we note that the observed between-subject differences in the interaction between driven and endogenous alpha frequency could account for the discrepancies between empirical findings supporting tonic inhibition vs perceptual sampling accounts.

Chapter 3, in full, is in preparation for publication of the material at it currently appears in: Nelli S, Serences J. (2019). The efficiency of visual processing depends on deviations of alpha rhythms from their endogenous peak frequency. *In Prep*. The dissertation author was the primary investigator and author of this paper.

REFERENCES

Akam, T., & Kullmann, D. M. (2014). Oscillatory multiplexing of population codes for selective communication in the mammalian brain. *Nature Reviews. Neuroscience*, *15*(2), 111–22. http://doi.org/10.1038/nrn3668

Anderson, J. S., Carandini, M., Ferster, D., & Sherman, S. M. (2000). Orientation Tuning of Input Conductance , Excitation , and Inhibition in Cat Primary Visual Cortex Orientation Tuning of Input Conductance , Excitation , and Inhibition in Cat Primary Visual Cortex. *Journal of Neurophysiology*, *84*, 909–926.

Atallah, B. V., & Scanziani, M. (2009). Instantaneous Modulation of Gamma Oscillation Frequency by Balancing Excitation with Inhibition. *Neuron*, *62*(4), 566–577. http://doi.org/10.1016/j.neuron.2009.04.027

Azouz, R., & Gray, C. M. (2000). Dynamic spike threshold reveals a mechanism for synaptic coincidence detection in cortical neurons in vivo. *Proceedings of the National Academy of Sciences of the United States of America*, *97*(14), 8110–8115. http://doi.org/10.1073/pnas.130200797

Baria, A. T., Maniscalco, B., & He, B. J. (2017). Initial-state-dependent, robust, transient neural dynamics encode conscious visual perception. *PLoS Computational Biology*, *13*(11), 1–29. http://doi.org/10.1371/journal.pcbi.1005806

Bollimunta, A., Chen, Y., Schroeder, C. E., & Ding, M. (2008). Neuronal Mechanisms of Cortical Alpha Oscillations in Awake-Behaving Macaques. *Journal of Neuroscience*, *28*(40), 9976–9988. http://doi.org/10.1523/JNEUROSCI.2699-08.2008

Bosman, C. A., Schoffelen, J. M., Brunet, N., Oostenveld, R., Bastos, A. M., Womelsdorf, T., … Fries, P. (2012). Attentional Stimulus Selection through Selective Synchronization between Monkey Visual Areas. *Neuron*, *75*(5), 875–888. http://doi.org/10.1016/j.neuron.2012.06.037

Brunel, N., & Wang, X.-J. (2003). What Determines the Frequency of Fast Network Oscillations With Irregular Neural Discharges? I. Synaptic Dynamics and Excitation-Inhibition Balance. *Journal of Neurophysiology*, *90*(1), 415–430. http://doi.org/10.1152/jn.01095.2002

Buffalo, E. A., Fries, P., Landman, R., Buschman, T. J., & Desimone, R. (2011). Laminar differences in gamma and alpha coherence in the ventral stream. *Proceedings of the National Academy of Sciences*, *108*(27), 11262 LP-11267. Retrieved from http://www.pnas.org/content/108/27/11262.abstract

Buonomano, D. V., & Maass, W. (2009). State-dependent computations: Spatiotemporal processing in cortical networks. *Nature Reviews Neuroscience*, *10*(2), 113–125. http://doi.org/10.1038/nrn2558

Busch, N., Dubois, J., & VanRullen, R. (2009). The phase of ongoing EEG oscillations predicts visual perception. *The Journal of Neuroscience : The Official Journal of the Society for Neuroscience*, *29*(24), 7869–7876. http://doi.org/10.1523/JNEUROSCI.0113-09.2009

Busch, N., & VanRullen, R. (2010). Spontaneous EEG oscillations reveal periodic sampling of visual attention. *Proceedings of the National Academy of Sciences*, *107*(37), 16048–16053. http://doi.org/10.1073/pnas.1004801107

Buzsáki, G. C. N. (2006). *Rhythms of the brain*. *Rhythms of the Brain*. http://doi.org/10.1093/acprof:oso/9780195301069.001.0001

Carandini, M., & Heeger, D. (2012). Normalization as a canonical neural computation. *Nature Reviews Neuroscience*, (November), 1–12. http://doi.org/10.1038/nrn3136

Cecere, R., Rees, G., & Romei, V. (2015). Individual differences in alpha frequency drive crossmodal illusory perception. *Current Biology*, *25*(2), 231–235. http://doi.org/10.1016/j.cub.2014.11.034

Cohen, M. X. (2014). Fluctuations in oscillation frequency control spike timing and coordinate neural networks. *The Journal of Neuroscience : The Official Journal of the Society for Neuroscience*, *34*(27), 8988–98. http://doi.org/10.1523/JNEUROSCI.0261-14.2014

Cohen, M. X., & Gulbinaite, R. (2017). Rhythmic entrainment source separation : Optimizing analyses of neural responses to rhythmic sensory stimulation " S " R -1 SW = λ W. *NeuroImage*, *147*(December 2016), 43–56. http://doi.org/10.1016/j.neuroimage.2016.11.036

de Graaf, T. A., Gross, J., Paterson, G., Rusch, T., Sack, A. T., & Thut, G. (2013). Alpha-Band Rhythms in Visual Task Performance: Phase-Locking by Rhythmic Sensory Stimulation. *PLoS ONE*, *8*(3), 29–32. http://doi.org/10.1371/journal.pone.0060035

Draguhn, A., Buzsáki, G., Andreas, D., & Draguhn, A. (2004). Neuronal Oscillations in Cortical Networks. *Science*, *304*(June), 1926. http://doi.org/10.1126/science.1099745

Escolano, C., Aguilar, M., & Minguez, J. (2011). EEG-based upper alpha neurofeedback training improves working memory performance. *Proceedings of the Annual International Conference of the IEEE Engineering in Medicine and Biology Society, EMBS*, 2327–2330. http://doi.org/10.1109/IEMBS.2011.6090651

Felleman, D. J., & Van Essen, D. C. (1991). Distributed hierarchical processing in the primate cerebral cortex. *Cerebral Cortex (New York, N.Y. : 1991)*, *1*(1), 1–47.

Foster, A. J. J., & Awh, E. (2018). The role of alpha oscillations in spatial attention: Limited evidence for a suppression account. *Current Opinion in Psychology*. http://doi.org/10.1016/j.copsyc.2018.11.001

Foxe, J. J., Simpson, G. V, & Ahlfors, S. P. (1998). Parieto-occipital approximately 10 Hz activity reflects anticipatory state of visual attention mechanisms. *Neuroreport*, *9*(17), 3929–3933. http://doi.org/10.1097/00001756-199812010-00030

Fries, P. (2005). A mechanism for cognitive dynamics: Neuronal communication through neuronal coherence. *Trends in Cognitive Sciences*, *9*(10), 474–480. http://doi.org/10.1016/j.tics.2005.08.011

Fries, P. (2015). Rhythms for Cognition: Communication through Coherence. *Neuron*, *88*(1), 220–235. http://doi.org/10.1016/j.neuron.2015.09.034

Fries, P., Reynolds, J. H., Rorie, a E., & Desimone, R. (2001). Modulation of oscillatory neuronal synchronization by selective visual attention. *Science (New York, N.Y.)*, *291*(FEBRUARY), 1560–1563. http://doi.org/10.1126/science.1055465

Fries, P., Womelsdorf, T., Oostenveld, R., & Desimone, R. (2008). The effects of visual stimulation and selective visual attention on rhythmic neuronal synchronization in macaque area V4. *The Journal of Neuroscience : The Official Journal of the Society for Neuroscience*, *28*(18), 4823–4835. http://doi.org/10.1523/JNEUROSCI.4499-07.2008

Haegens, S., Handel, B. F., & Jensen, O. (2011). Top-Down Controlled Alpha Band Activity in

Somatosensory Areas Determines Behavioral Performance in a Discrimination Task. *Journal of Neuroscience*, *31*(14), 5197–5204. http://doi.org/10.1523/JNEUROSCI.5199-10.2011

Heeger, D. J. (1992). Normalization of cell responses in cat striate cortex. *Visual Neuroscience*. http://doi.org/10.1017/S0952523800009640

Isaacson, J. S., & Scanziani, M. (2011). How inhibition shapes cortical activity. *Neuron*, *72*(2), 231–243. http://doi.org/10.1016/j.neuron.2011.09.027

Kelly, S. P., Gomez-Ramirez, M., & Foxe, J. J. (2009). The strength of anticipatory spatial biasing predicts target discrimination at attended locations: A high-density EEG study. *European Journal of Neuroscience*, *30*(May), 2224–2234. http://doi.org/10.1111/j.1460-9568.2009.06980.x

Klimesch, W. (1996). Memory processes, brain oscillations and EEG synchronization. *International Journal of Psychophysiology*, *24*(1–2), 61–100. http://doi.org/10.1016/S0167-8760(96)00057-8

Klimesch, W., Sauseng, P., & Hanslmayr, S. (2007). EEG alpha oscillations: the inhibition-timing hypothesis. *Brain Research Reviews*, *53*(1), 63–88. http://doi.org/10.1016/j.brainresrev.2006.06.003

Lakatos, P., O'Connell, M. N., Barczak, A., Mills, A., Javitt, D. C., & Schroeder, C. E. (2009). The Leading Sense: Supramodal Control of Neurophysiological Context by Attention. *Neuron*, *64*(3), 419–430. http://doi.org/10.1016/j.neuron.2009.10.014

Landau, A. N., & Fries, P. (2012). Attention samples stimuli rhythmically. *Current Biology*, *22*(11), 1000–1004. http://doi.org/10.1016/j.cub.2012.03.054

Lopes da Silva, F. (2013). EEG and MEG: Relevance to neuroscience. *Neuron*, *80*(5), 1112–1128. http://doi.org/10.1016/j.neuron.2013.10.017

Maass, W., Natschlager, T., & Markram, H. (2002). Real-time computing without stable states: a new framework for neural computation based on perturbations. *Neural Computation*, *14*(11), 2531–2560. http://doi.org/10.1162/089976602760407955

Markov, N. T., Vezoli, J., Chameau, P., Falchier, A., Quilodran, R., Huissoud, C., … Kennedy, H. (2014). Anatomy of hierarchy: feedforward and feedback pathways in macaque visual cortex. *The Journal of Comparative Neurology*, *522*(1), 225–259. http://doi.org/10.1002/cne.23458

Mathewson, K. E., Lleras, A., Beck, D. M., Fabiani, M., Ro, T., & Gratton, G. (2011). Pulsed out of awareness: EEG alpha oscillations represent a pulsed-inhibition of ongoing cortical processing. *Frontiers in Psychology*, *2*(MAY), 1–15. http://doi.org/10.3389/fpsyg.2011.00099

Mazzoni, A., Panzeri, S., Logothetis, N. K., & Brunel, N. (2008). Encoding of naturalistic stimuli by local field potential spectra in networks of excitatory and inhibitory neurons. *PLoS Computational Biology*, *4*(12). http://doi.org/10.1371/journal.pcbi.1000239

Meeuwissen, E. B., Takashima, A., Fernández, G., & Jensen, O. (2011). Increase in posterior alpha activity during rehearsal predicts successful long-term memory formation of word sequences. *Human Brain Mapping*, *32*(12), 2045–2053. http://doi.org/10.1002/hbm.21167

Michalareas, G., Vezoli, J., van Pelt, S., Schoffelen, J.-M., Kennedy, H., & Fries, P. (2016).

Alpha-Beta and Gamma Rhythms Subserve Feedback and Feedforward Influences among Human Visual Cortical Areas. *Neuron*, *89*(2), 384–397. http://doi.org/10.1016/j.neuron.2015.12.018

Misha, R., Ramon, H., & Gilles, L. (2008). Transient dynamics for neural processing. *Science*, *321*(5885), 48–50. Retrieved from http://www.ncbi.nlm.nih.gov/pubmed/18599763

Morgan, S. T., Hansen, J. C., & Hillyard, S. A. (1996). Selective attention to stimulus location modulates the steady-state visual evoked potential. *Proceedings of the National Academy of Sciences*, *93*(10), 4770 LP-4774. Retrieved from http://www.pnas.org/content/93/10/4770.abstract

Müller, M. M., Picton, T. W., Valdes-Sosa, P., Riera, J., Teder-Sälejärvi, W. A., & Hillyard, S. A. (1998). Effects of spatial selective attention on the steady-state visual evoked potential in the 20–28 Hz range. *Cognitive Brain Research*, *6*(4), 249–261. http://doi.org/https://doi.org/10.1016/S0926-6410(97)00036-0

N. Fritsch, F., & E. Carlson, R. (1980). *Monotone Piecewise Cubic Interpolation*. *SIAM J.~Numer.~Anal.* (Vol. 17). http://doi.org/10.1137/0717021

Nelli, S., Itthipuripat, S., Srinivasan, R., & Serences, J. T. (2017). Fluctuations in instantaneous frequency predict alpha amplitude during visual perception. *Nature Communications*, *8*(1). http://doi.org/10.1038/s41467-017-02176-x

Palva, S., & Palva, J. M. (2007). New vistas for alpha-frequency band oscillations. *Trends in Neurosciences*, *30*(4), 150–158. http://doi.org/10.1016/j.tins.2007.02.001

Pfurtscheller, G. (2001). Functional brain imaging based on ERD / ERS, *41*, 1257–1260.

Rihs, T. A., Michel, C. M., & Thut, G. (2007). Mechanisms of selective inhibition in visual spatial attention are indexed by ??-band EEG synchronization. *European Journal of Neuroscience*, *25*(2), 603–610. http://doi.org/10.1111/j.1460-9568.2007.05278.x

Rizzuto, D. S., Madsen, J. R., Bromfield, E. B., Schulze-bonhage, A., Seelig, D., Aschenbrenner-scheibe, R., & Kahana, M. J. (2003). Reset of human neocortical oscillations during a working memory task. *Proceedings of the National Academy of Sciences*, (21). http://doi.org/10.1073/pnas.0732061100

Rohenkohl, G., & Nobre, a. C. (2011). Alpha Oscillations Related to Anticipatory Attention Follow Temporal Expectations. *Journal of Neuroscience*, *31*(40), 14076–14084. http://doi.org/10.1523/JNEUROSCI.3387-11.2011

Rousseeuw, P. J. (1987). Silhouettes : a graphical aid to the interpretation and validation of cluster analysis, *20*, 53–65.

Saalmann, Yuri B., Pigarev, Ivan N., Vidyasagar, T. (2007). Neural Mechanisms of Visual Attention: How Top-Down Feedback Highlights Relevant Locations. *Science*, (June), 1612–1615.

Salinas, E., & Sejnowski, T. J. (2001). Correlated neuronal activity and the flow of neural information. *Nature Neuroscience*, *14*(7), 811–819. http://doi.org/10.1038/nn.2842

Samaha, J., & Postle, B. R. (2015). The speed of alpha-band oscillations predicts the temporal resolution of visual perception Jason Samaha and Bradley R. Postle. *Current Biology*, *25*, 2985–2990. http://doi.org/10.1016/j.cub.2015.10.007

Sauseng, P., Klimesch, W., Stadler, W., Schabus, M., Doppelmayr, M., Hanslmayr, S., … Birbaumer, N. (2005). A shift of visual spatial attention is selectively associated with human EEG alpha activity. *Eur J Neurosci*, *22*(11), 2917–2926. http://doi.org/EJN4482 [pii]\r10.1111/j.1460-9568.2005.04482.x

Shao, Z., & Burkhalter, A. (1996). Different balance of excitation and inhibition in forward and feedback circuits of rat visual cortex. *The Journal of Neuroscience : The Official Journal of the Society for Neuroscience*, *16*(22), 7353–7365.

Spaak, E., de Lange, F. P., & Jensen, O. (2014). Local Entrainment of Alpha Oscillations by Visual Stimuli Causes Cyclic Modulation of Perception. *Journal of Neuroscience*, *34*(10), 3536–3544. http://doi.org/10.1523/JNEUROSCI.4385-13.2014

Takemura, H., Rokem, A., Winawer, J., Yeatman, J. D., Wandell, B. A., & Pestilli, F. (2016). A Major Human White Matter Pathway Between Dorsal and Ventral Visual Cortex. *Cerebral Cortex*, *26*(5), 2205–2214. Retrieved from http://dx.doi.org/10.1093/cercor/bhv064

Van Essen, D. C. B. T.-P. in B. R. (2005). Corticocortical and thalamocortical information flow in the primate visual system. In *Cortical Function: a View from the Thalamus* (Vol. 149, pp. 173–185). Elsevier. http://doi.org/https://doi.org/10.1016/S0079-6123(05)49013-5

Van Essen, D. C., & Maunsell, J. H. R. (1983). Hierarchical organization and functional streams in the visual cortex. *Trends in Neurosciences*, *6*, 370–375. http://doi.org/https://doi.org/10.1016/0166-2236(83)90167-4

van Kerkoerle, T., Self, M. W., Dagnino, B., Gariel-Mathis, M.-A., Poort, J., van der Togt, C., & Roelfsema, P. R. (2014). Alpha and gamma oscillations characterize feedback and feedforward processing in monkey visual cortex. *Proceedings of the National Academy of Sciences*, *111*(40), 14332 LP-14341. Retrieved from http://www.pnas.org/content/111/40/14332.abstract

van Vreeswijk, C., & Sompolinsky, H. (1996). Reproduced with permission of the copyright owner . Further reproduction prohibited without permission . *Science (New York, N.Y.)*, *274*, 1724–1726. http://doi.org/10.1126/science.274.5293.1724

VanRullen, R. (2015). Perceptual Rhythms.

von Stein, a, Chiang, C., & König, P. (2000). Top-down processing mediated by interareal synchronization. *Proceedings of the National Academy of Sciences of the United States of America*, *97*(26), 14748–14753. http://doi.org/10.1073/pnas.97.26.14748

Welch, P. D. (1967). The Use of Fast Fourier Transform for the Estimation of Power Spectra: A Method Based on Time Averaging Over Short, Modified Periodograms. *IEEE Transactions on Audio and Electroacoustics*, *15*(2), 70–73. http://doi.org/10.1109/TAU.1967.1161901

Woertz, M., Pfurtscheller, G., & Klimesch, W. (2004). Alpha power dependent light stimulation: Dynamics of event-related (de)synchronization in human electroencephalogram. *Cognitive Brain Research*, *20*(2), 256–260. http://doi.org/10.1016/j.cogbrainres.2004.03.014

Yamagishi, N., Callan, D. E., Anderson, S. J., & Kawato, M. (2008). Attentional changes in pre-stimulus oscillatory activity within early visual cortex are predictive of human visual performance. *Brain Research*, *1197*, 115–122. http://doi.org/10.1016/j.brainres.2007.12.063

Zauner, A., Fellinger, R., Gross, J., Hanslmayr, S., Shapiro, K., Gruber, W., … Klimesch, W. (2012). Alpha entrainment is responsible for the attentional blink phenomenon.

NeuroImage, *63*(2), 674–686. http://doi.org/10.1016/j.neuroimage.2012.06.075

Zoefel, B., Huster, R. J., & Herrmann, C. S. (2011). Neurofeedback training of the upper alpha frequency band in EEG improves cognitive performance. *NeuroImage*, *54*(2), 1427–31. http://doi.org/10.1016/j.neuroimage.2010.08.078

CONCLUSION

The alpha oscillation, a prominent (~8-12 Hz) oscillation maximal in visual regions, seems to determine how perception waxes and wanes in time. Nearly a century of research has linked modulations in the amplitude or phase/frequency of ongoing alpha oscillations with modulations in behavior (Başar, 2012). Observations concerning alpha amplitude has led to the tonic inhibition theory that relatively slow changes in alpha amplitude lead to a release from inhibition (Klimesch, Sauseng, & Hanslmayr, 2007). Alternatively, observations concerning alpha phase and frequency have contributed to the phasic inhibition account that more rapid, cycle-by-cycle changes in alpha phase determine the efficiency of visual information processing (Samaha & Postle, 2015). However, how tonic and phasic inhibition are related through the top-down mechanisms that drive alpha oscillations has not been fully explored. The three chapters in this thesis aimed to address these outstanding questions about the role of alpha oscillations in human vision. Specifically, I propose that each subject's phenotypic alpha characteristics result from the attractor cycle of an underlying dynamical system. Thus, instead of representing distinct processes, measurements of alpha amplitude, phase and frequency are likely simply byproducts of the alpha dynamical state at that specific moment. In this thesis, I use mathematical analysis and empirical data to challenge core assumptions underlying current theories of the role that alpha oscillations play in regulating cortical information processing. We then propose a more parsimonious and unified theoretical framework in which alpha frequency, phase and amplitude should not be viewed as independent metrics to be correlated with behavior, but instead as the result of a common dynamical system that impacts visual perception.

In Chapter 1, I addressed the question of whether visual perception, attentional selection, and the short-term retention of information wax and wane in the alpha range using a classic partial report paradigm (Sperling, 1960). Interestingly, we found that cued recall was linked to with higher phase locking at theta frequencies, while neighbor recall was associated

with higher phase locking and power at alpha frequencies. This suggests that the mechanisms underlying high fidelity attentional selection of perceived items operates at theta frequencies, while those underlying responses for nearby but uncued letters operate at alpha frequencies. As alpha-band behavioral rhythmicity decreased with memory delay, we hypothesize that alpha rhythmic behavioral mechanisms underlie spatial imprecision in attentional selection, which has a cascading effect on subjects ability to distinguish uncued from cued letters in the iconic representation. Imprecise attentional selection shows elevated alpha rhythmicity as measured through both amplitude and phase locking metrics, indicating similar behavioral impacts of both the tonic and phasic inhibition accounts.

In Chapter 2, I addressed how endogenous fluctuations in alpha frequency and amplitude interact to impact early visual information processing. We record electroencephalography in human subjects and show that both alpha amplitude and instantaneous frequency predict behavioral performance in the same visual discrimination task. Consistent with a model of coupled oscillators, we show that fluctuations in instantaneous frequency predict alpha amplitude on a single trial basis, empirically demonstrating that these metrics are not independent. This interdependence suggests that changes in amplitude and instantaneous frequency reflect a common change in the excitatory and inhibitory neural activity that regulates alpha oscillations and visual information processing. Within this updated framework, I hypothesize that shifts in frequency and phase may be the mechanism by which local populations desynchronize from the inhibitory alpha rhythm to process incoming stimuli, thereby resulting in reductions of alpha amplitude as measured at the scalp. This would link the observations about alpha phase, frequency and amplitude into a parsimonious framework.

In Chapter 3, I aimed to determine if the entrainment of alpha rhythms in early visual populations interact with the endogenous alpha oscillation to impact behavior. We found that whether activity at a subject's peak alpha frequency impairs or enhances perceptual performance depends on each subject's intrinsic peak alpha frequency. Specifically, when the

oscillatory frequency set by top-down mechanisms is already fast, entraining stimulus-driven circuits even faster is not perceptually beneficial. In contrast, if the endogenous oscillatory frequency is slow, entraining these early circuits at a faster frequency does in fact benefit perception. This is striking, as it suggests the existence of an optimal dynamical range for the neural circuits involved in alpha oscillations. First, given that the anatomical characteristics of networks play a key role in determining information propagation times(G. C. N. Buzsáki, 2006; G. Buzsáki & Chrobak, 1995; Draguhn, Buzsáki, Andreas, & Draguhn, 2004), this optimal dynamical range may reflect stereotypy in anatomical pathways (perhaps conserved through evolution) between subjects. Interestingly, task-driven, rapid traversal through the alpha state space is perceptually beneficial, and the speed of this traversal is impacted by the interaction between driven and endogenous alpha frequency. The precise dynamical organization underlying this result need further explanation. Specifically, it is possible that each subject may have multiple dissociable steady-attractor states for endogenous alpha rhythms, as, it has been observed that the same macroscopic field potential can be brought about by various intrinsic cellular and network mechanisms, meaning the resonance and perturbation properties of two oscillations nominally in the alpha band can actually be quite different (G. C. N. Buzsáki, 2006). Conversely, our findings could reflect a phenotypic, between-subjects difference in the dynamical alpha system. Together, the impact of alpha oscillations on perception depends on circuit interactions with top-down driving oscillators, and we find that optimal oscillatory drive for visual perception depends intimately on each subjects particular dynamical system and resultant peak alpha frequency. This oscillatory drive appears to impact the efficient traversal of endogenous oscillations through the alpha state space.

In sum, I find an interaction between behavioral rhythmicity and perceptual fidelity (C1), of a link between alpha amplitude and frequency (C2), and a dependence of the perceptual impact of alpha drive on the natural alpha oscillation (C3). These results suggest an intimate dependence on the underlying dynamical system, offering the explanation that seemingly

disparate previous findings that alpha oscillations can both impair and enhance perceptual performance could actually be due to incomplete characterization of each subject's individual dynamical system.

We note that the dynamical system governing alpha oscillations is extremely complex and widespread, involving interactions with higher-order driving regions. Thus, the posterior alpha oscillation responds not only to incoming visual information but also to top-down cognitive factors such as shifts in attention. Further dynamical and state-space analyses should be done to consider alpha oscillations as attractor states, as outlined in the introduction, instead of quantifying certain aspects such as phase, frequency and amplitude and correlating these specific aspects with behavior. Indeed, this thesis opens the possibility that there are distinct alpha dynamical states that differ in their impact on visual perception, and that driving visual cortex at specific alpha frequencies can modulate this impact. Further exciting directions include: 1) whether cognitive factors such as task switching can induce top down factors to endogenously drive posterior rhythms, and whether this interaction modulates the perceptual impact of alpha oscillations in a similar way that we see in C3; 2) whether the amplitude spectrum reflects different alpha oscillations in independent circuits that sometimes interact, or whether it reflects one large circuit governing the alpha oscillation that sometimes changes its properties to impact visual perception; 3) whether it is portions of the alpha phase plane, or the attractor state itself that impacts visual perception.

Finally, these results suggest that different dynamical alpha states can both enhance and impair visual information processing. I propose that confusion in the literature concerning alpha oscillations has arisen because it is simply an ill-posed problem to characterize this space from simply measuring one oscillatory metric, such as power, phase or frequency. As the question of whether these macroscopic oscillations obey harmonic, relaxation, or some more complex oscillatory behavior, and whether this is modulated by brain region, is still outstanding(G. C. N. Buzsáki, 2006), it is our suggestion for experimenters to use each subjects

individual amplitude to frequency mapping (the amplitude spectra) as an empirical starting point for determining the coupling properties of rhythmic networks in each particular case.

REFERENCES

Başar, E. (2012). A review of alpha activity in integrative brain function: Fundamental physiology, sensory coding, cognition and pathology. *International Journal of Psychophysiology*, *86*(1), 1–24. http://doi.org/10.1016/j.ijpsycho.2012.07.002

Buzsáki, G. C. N. (2006). *Rhythms of the brain*. *Rhythms of the Brain*. http://doi.org/10.1093/acprof:oso/9780195301069.001.0001

Buzsáki, G., & Chrobak, J. J. (1995). Temporal structure in spatially organized neuronal ensembles: a role for interneuronal networks. *Current Opinion in Neurobiology*, *5*(4), 504–510. http://doi.org/10.1016/0959-4388(95)80012-3

Draguhn, A., Buzsáki, G., Andreas, D., & Draguhn, A. (2004). Neuronal Oscillations in Cortical Networks. *Science*, *304*(June), 1926. http://doi.org/10.1126/science.1099745

Klimesch, W., Sauseng, P., & Hanslmayr, S. (2007). EEG alpha oscillations: the inhibition-timing hypothesis. *Brain Research Reviews*, *53*(1), 63–88. http://doi.org/10.1016/j.brainresrev.2006.06.003

Samaha, J., & Postle, B. R. (2015). The speed of alpha-band oscillations predicts the temporal resolution of visual perception Jason Samaha and Bradley R. Postle. *Current Biology*, *25*, 2985–2990. http://doi.org/10.1016/j.cub.2015.10.007

Sperling, G. (1960). The information available in brief visual presentations. *Psychological Monographs*.